

The Fate of Nutrients in Two Coastal Freshwater Systems

Dissertation

Presented in Partial Fulfillment of the Requirements for the Degree of Doctor of  
Philosophy to the Graduate School of The Ohio State University

By

Deon Hanley Knights

Graduate Program in Earth Sciences

The Ohio State University

2020

Dissertation Committee

Audrey H. Sawyer, Advisor

Joachim B. Moortgat

Derek E. Sawyer

Rachel S. Gabor

Copyright by  
Deon Hanley Knights  
2020

## **Abstract**

Human activities including fertilizer application and fossil fuel burning have increased nutrient concentrations in coastal waters. Nutrient inputs can be difficult to constrain at the coastal interface where multiple waters mix, including river water, groundwater, and lake or ocean water. At coastal interfaces, rivers distribute their nutrient loads across delta wetlands, where processes like anaerobic respiration and plant uptake may reduce nutrient concentrations. Beneath the coast, groundwater also carries nutrients offshore, where biogeochemical reactions alter the nutrient chemistry and discharge rates are difficult to measure. I aim to improve the assessment of nutrient loads to coastal waters in these challenging environments through two case studies. First, I estimate groundwater discharge, a previously unaccounted source of nutrients, to the United States Great Lakes coast using high-resolution geospatial analysis. By integrating land use data, I also identify areas of the coast that are vulnerable to high nutrient loads from groundwater. My analysis shows that almost one-third of Lake Erie's United States coastline is vulnerable to contamination from groundwater nutrient sources. By collecting field measurements at a vulnerable beach site, I show that the nitrogen load from groundwater exceeds 1 gram/day/meter of coastline, which constitutes a small but non-negligible source to Lake Erie. In the second case study, I use benthic chambers to measure nitrogen removal rates in a coastal wetland in Wax Lake Delta, Louisiana.

Results suggest that summertime nitrate removal kinetics are highly correlated with a widely available remotely-sensed vegetation index (NDVI). Heavily vegetated, submerged levees at intermediate elevations in the delta are thus predicted to be the most reactive habitats. Though less reactive, larger channels primarily on the eastern half of the delta may contribute most to nitrate removal, as they receive the greatest mass fluxes of nitrate. Numerical simulations of reactive nitrate transport in Wax Lake Delta and six synthetic deltas suggest that nitrate removal may be intrinsically limited in river-dominated deltas to a small fraction of the incoming nitrate load. Removal increases with delta topset gradient, and smaller, high-sitting deltas remove more nitrate than larger, low-lying deltas. From a management standpoint, nitrate removal efficiency can be improved by designing river diversions to build steeper deltas. Steeper deltas are created by accessing coarser sediments in river diversion projects. However, manmade deltas alone cannot remove most nitrate discharging to the sea. Policy that addresses the nitrate load upstream is necessary to further reduce coastal nitrate loading.

## **Acknowledgments**

I thank my advisor, thesis committee, and research group members for their input and advice during my research. I also thank my honorary co-advisors, Rebecca Barnes, and Doug Edmonds for all of their insight and suggestions over the past six years. My entire family provided me with fundamental support throughout this whole process. I want to especially thank my wife, Mary Knights, my parents, Dianne Baptiste and Handley Knights and my sister, Deliece Knights for their priceless contributions to this project. Many friends and lab mates assisted me with field sampling and lab experiments, including Corey Wallace, Kelsey Snodgrass, Amelia Nelson, Savannah Scott, Kevin Parks, Alexander Brown, Yaoquan Zhou, Trevor Browning, Kerri Dobson, Melisa Diaz, Nlingi Habana, Joshua Ninke and Chis Hulse. I thank Sue Welch and Kathy Welch who provided me with valuable lab resources and support with chemical analysis. Lienne Sethna, Connor Gallagher, Megan Mave, Laura Miller and Carissa Hipsher assisted with collecting samples from Lake Erie, and I thank Ron Huffman for providing access to that field site. Elizabeth Olliver provided valuable insight on Wax Lake Delta over the years. This research was supported by the National Science Foundation through award EAR-1446724, grants from the Geologic Society of America and International Association of GeoChemistry, and a grant through the Ohio Water Resources Center.

## Vita

- 2012.....B.S. Geology, University of Delaware
- 2016.....M.S. Earth Sciences, The Ohio State University
- 2016 to present.....Graduate Research Associate, School of Earth Sciences, The Ohio  
State University
- 2012.....B.S. Geology, University of Delaware
- 2016.....M.S. Earth Sciences, The Ohio State University
- 2016 to present.....Graduate Research Associate, School of Earth Sciences,  
The Ohio State University

## Publications

- Knights, D., K.C. Parks, A.H. Sawyer, C.H. David, T.N. Browning, K.M. Danner, and  
C.D. Wallace, (2017), Direct groundwater discharge and vulnerability to hidden  
nutrient loads along the Great Lakes coast of the United States, *Journal of  
Hydrology*, 554, doi:10.1016/j.jhydrol.2017.09.001.
- Knights, D., A.H. Sawyer, R.T. Barnes, C. Musial, and S. Bray (2017), Tidal controls on  
riverbed denitrification along a tidal freshwater zone, *Water Resources Research*,  
53, doi: 10.1002/2016WRD19405.

Musial, C., A.H. Sawyer, R.T. Barnes, S. Bray, and D. Knights (2015), Surface water-groundwater exchange dynamics in a tidal freshwater zone, *Hydrological Processes*, 30(5), doi:10.1002/hyp.10623.

Sawyer, A.H., D.A. Edmonds, and D. Knights (2015), Surface water-groundwater connectivity in deltaic distributary channel networks, *Geophysical Research Letters*, 42, doi:10.1002/2015GL0666156.

#### Fields of Study

Major Field: Earth Sciences

## Table of Contents

Abstract.....	iii
Acknowledgments.....	v
Vita.....	vi
List of Tables .....	x
List of Figures .....	xi
Chapter 1. Introduction .....	1
1.1. Motivation.....	1
1.2. Thesis Organization .....	5
Chapter 2. Direct groundwater discharge and vulnerability to hidden nutrient loads along the Great Lakes coast of the United States .....	7
2.1. Introduction.....	7
2.2. Methods.....	9
2.3. Great Lakes Analysis .....	16
2.4. Field Study of a vulnerable beach.....	20
2.5. Considerations for assessing vulnerability.....	31
2.6. Conclusion .....	33
Chapter 3. Nutrient Removal across Ecogeomorphic Zones in Wax Lake Delta Louisiana, (USA).....	35
3.1. Introduction.....	35
3.2. Methods.....	39
3.3. Results.....	50
3.4. Discussion .....	58
3.5. Conclusion .....	65
Chapter 4. The Relationship between Delta Form and Nitrate Removal Function: Computer Modeling Experiments.....	67
4.1. Introduction.....	67

4.2. Methods.....	71
4.3. Results.....	78
4.4. Discussion.....	86
4.5. Conclusion.....	93
Chapter 5. Summary.....	95
5.1. Synthesis.....	95
5.2. Key Findings and Future Work.....	95
Reference.....	99
Appendix A. Wax Lake Delta Field Supplement.....	133
Appendix B. Python and R Codes.....	135

## List of Tables

Table 2.1. Water budget statistics for the Great Lakes .....	18
Table 3.1. Summary of input parameters and results for two upscaling methods .....	62
Table 3.2. Removal rate in this Wax Lake Compared to other coastal wetlands .....	64
Table 4.1. Nitrate removal and ecogeomorphic area for six synthetic deltas .....	91
Table A.1. Chemistry data for Wax Lake Delra .....	131

## List of Figures

Figure 1.1. Nutrient are transported through multiple pathways .....	4
Figure 2.1. Location of Lake Erie Study Site .....	11
Figure 2.2. Average seepage rates .....	14
Figure 2.3. Map of direct groundwater discharge for US Great Lakes.....	17
Figure 2.4. Comparison of direct groundwater discharge.....	19
Figure 2.5. Vulnerability of Great Lakes to contamination .....	22
Figure 2.6. Seepage rates decrease from shore .....	25
Figure 2.7. Nutrient concentration in water compared to chloride .....	29
Figure 2.8. Nutrient concentration offshore.....	30
Figure 3.1. Location of field site.....	38
Figure 3.2. Examples of field chemistry .....	43
Figure 3.3. Examples of chamber results.....	45
Figure 3.4. Ambient nitrate and chloride .....	50
Figure 3.5. Concentration effects on removal.....	52
Figure 3.6. Scatter plots of predicted and observed removal.....	54
Figure 3.7. Upscaled nitrate removal maps .....	56
Figure 4.1. Reactive transport model and field sites.....	72
Figure 4.2. Topography of synthetic deltas .....	75

Figure 4.3. Modeled nitrate concentration on Wax Lake .....	79
Figure 4.4. Validated hydrodynamic model results .....	80
Figure 4.5. Transfer velocity of Wax Lake Delta .....	82
Figure 4.6. Maps of nitrate concentration for synthetic deltas .....	84
Figure 4.7. Mass transfer velocity for synthetic deltas .....	85
Figure 4.8. Removal versus delta geometrics .....	86
Figure 4.9. Ecogeomorphic zones on synthetic deltas .....	87
Figure A.1. Benthic Chamber .....	133

## **Chapter 1. Introduction**

### 1.1. Motivation

Coastal areas are home to diverse ecosystems, valuable industries, and some of the world's largest metropolitan centers. They provide important economic and environmental resources such as water, fisheries, wildlife habitats, and tourism attractions. For example, in the United States, coastal fisheries are a 5.6 billion-dollar industry (National Marine Fisheries Service, 2020). Hundreds of millions of people globally partake in coastal tourism (Orams, 1999). Lake Erie alone supplies drinking water to 11 million people. Coastal waters, though, are degrading due to global changes in land use and climate. One main cause of coastal water degradation is anthropogenic nutrient enrichment of the terrestrial biosphere (Gruber, 2008; Galloway et al., 2008). Rivers export vast quantities of terrestrially derived nutrients from agriculture and urban centers to the coast, where nutrients reduce water quality, compromise drinking and recreational waters, stress fisheries, decrease biodiversity, and in some cases, lead to the development of harmful algal blooms (HABs).

HABs are vast colonies of phytoplankton, and their prevalence is a global environmental problem affecting marine and freshwater systems (NRC, 2000; Dettmann, 2001; Gilbert et al., 2005; Landsberg, 2002). They thrive under conditions of high nutrient input, warm temperatures, and stagnant waters. HABs deteriorate aquatic

ecosystems by blocking sunlight for other organisms and diminishing available dissolved oxygen when they decay. Some phytoplankton also create toxins that harm fish, wildlife, and humans. Toxins can bioaccumulate and affect secondary and tertiary consumers, including humans who ingest exposed fish (Poste et al., 2011). Aside from ecologic and health consequences, HABs are recreational nuisances as they discolor water, kill fish and produce odors, stressing coastal economies that rely on tourism and fishing industries. Over the past several decades, the global occurrence of coastal algal blooms has been increasing in frequency, with blooms covering greater geographic extents and persisting for longer durations (Anderson, 1989; Gilbert et al., 2005a; Heisler et al., 2008). Though there are multiple contributing factors, increasingly frequent and severe blooms have been associated in many coastal zones with increases in human-derived nitrogen (N) and phosphorus (P) loads. For example, in 2011 and 2015 Lake Erie experienced its two largest algal blooms on record, disrupting drinking water supply and triggering fishing and recreational advisories for several days (Michalak et al., 2013). The decline in fishing due to severe algal blooms in Lake Erie is estimated to account for \$2.25 to \$5.58 million in lost fishing expenditure (Wolf et al., 2017). The northern Gulf of Mexico, which supports over one quarter of the United States fisheries, is susceptible to negative ecological impacts from nutrient loading from the Mississippi and Atchafalaya River Basin (Rabalais et al., 1996).

Inorganic N and P are important macronutrients for primary producers like phytoplankton. Their molecular form, concentration, and ratio in water are critical to the maintenance of ecosystem function and health. The transport and transformation of N and

P along flow paths to the coast vary, along with the community composition of phytoplankton that dictates the amount of N that can be fixed from the atmosphere, leading to differences in N and P availability in marine and terrestrial waters. For example, N is generally limiting at marine coastal waters while P is often the limiting nutrient in freshwater lakes (Edmonson, 1970; Vollenwiedel et al., 1976). In marine coastal waters, slower cycling of organic N compared to organic P and enhanced mobilization of P from sediment relative to N (Thomas, 1966; Boyton et al., 1982; Howarth, 1988; Nixon et al., 1981) leads to smaller N:P ratios in shallow marine waters and frequent N limitation (Jackson et al., 1985). Slow internal N flux relative to water exchange further contributes to N limitation (Smith, 1984). Meanwhile in lakes, N-fixing bacteria make up a greater proportion of phytoplankton biomass than in marine estuaries, driving P limitation (Smith, 1983). Greater N:P ratios in lake nutrient inputs compared to estuaries also contribute to P limitation typically observed in lakes (Howarth, 1988).

Nutrients are transported to the coast through multiple hydrologic pathways, including streams and rivers, direct runoff, and groundwater discharge. Upstream inputs of agricultural runoff, sewage, and wastewater loads increase the supply of N and P to downstream systems, altering nutrient ratios and stimulating growth of macroalgae and phytoplankton in coastal ecosystems. The Mississippi River network, which drains approximately 41% of the continental United States is a prime example. Its outlet in southern Louisiana acts as a large point source of nutrients to the Gulf of Mexico, and during summer months, a 20,000 km<sup>2</sup> dead zone forms off its coast (DeLaune et al., 2005; Rabalais et al., 2002).

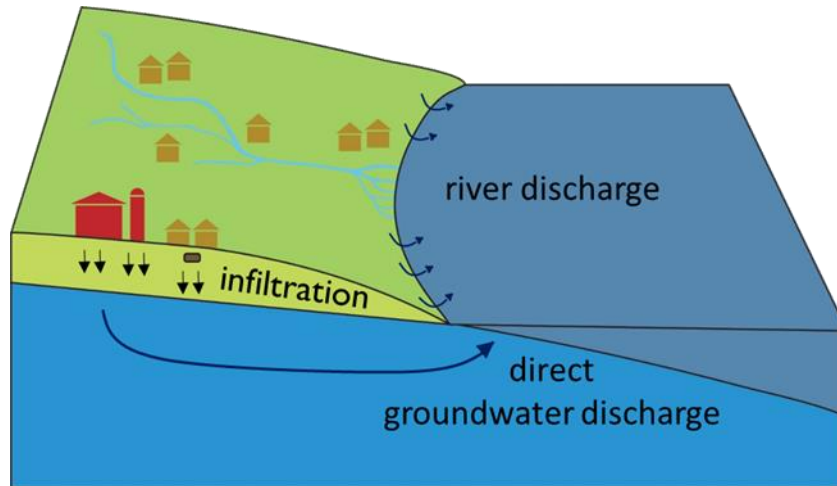


Figure 1.1. Nutrients are transported to the coast in rivers and groundwater.

Fortunately, locations where surface water and groundwater meet can be active areas of nutrient transformation and removal (Duff and Triska, 1990; Hester et al., 2014). For example, where nitrate-rich groundwater flows to bays and creeks, a portion of the nitrate may be removed due to denitrification (Knights and Sawyer et al., 2017). Nitrate is also removed from surface water due to denitrification in biofilms near the sediment-water interface. Although it is evident that nutrient removal occurs near the interface between surface water and groundwater, the processes controlling the transport and removal are not fully understood. This thesis focuses on understanding nutrient transformation near the sediment-water interface in coastal freshwater systems. I specifically focus on two uniquely different, but important, coastal systems in North America plagued by harmful algal blooms: the Great Lakes and the Mississippi Delta region of the Gulf of Mexico.

## 1.2. Thesis Organization

Below is a general description of each chapter and key findings.

In Chapter 2, I examine nutrient contributions from groundwater to the Great Lakes, which hold 20% of the world's surface freshwater (Steel et al., 1990). The Great Lakes have been experiencing annual episodes of algal blooms linked to high nutrient loading from rivers. However, hidden below the lake surface, groundwater discharge provides an additional source of nutrients that is widespread and difficult to measure. I estimate direct groundwater discharge to the Great Lakes coast using geospatial analysis and identify regions prone to nutrient contamination from groundwater sources. Field measurements from one such region show that shallow lakebed sediment is a source of dissolved inorganic N and dissolved P to surface waters.

Chapters 3 and 4 focus on coastal deltas, where terrestrial and marine surface waters meet. Deltaic wetlands are generally thought to buffer nutrient fluxes to marine waters, but they are fragile ecosystems that are drowning due to sea level rise and a reduction in sediment export to the coast (Day et al., 2007; Syvitski et al., 2009). In light of this, recent engineering projects have endeavored to reconstruct delta wetlands by diverting water and sediment from rivers such as the Mississippi to discharge points along the coast, where new delta wetlands can grow. If these reconstructed delta wetlands cannot effectively retain the nutrients they receive, manmade river diversions may exacerbate water quality issues by spreading nutrients across broader coastal areas (Twilley and Rivera-Monroy, 2009).

In Chapter 3 I measure the capacity of Wax Lake delta, a river-dominated delta of the Mississippi River network, to buffer nutrient export to sea. I show that nitrate removal potential is most strongly related to NDVI, a measure of greenness due to vegetation. In Chapter 4, I use a series of synthetic, river-dominated deltas, to expand on findings from Chapter 3. I quantify nitrate removal on simulated deltas in response to morphologic metrics and determine how delta morphology influences nitrate removal.

## **Chapter 2. Direct groundwater discharge and vulnerability to hidden nutrient loads along the Great Lakes coast of the United States**

### 2.1. Introduction

Large algal blooms pose severe problems for lake ecosystems and the coastal communities that surround them (Davis, 1969; Glibert et al., 2005; Backer and McGillicuddy, 2006; Michalak et al., 2013). The sheer biomass of algal blooms can stress ecosystems. Algae deplete oxygen leading to hypoxia and anoxia, and algal mats block sunlight from reaching plants below the surface, reducing stability of plant life in the water column (Anderson et al., 2002; Glibert et al., 2005). Some algae also produce toxins like microcystin and anatoxin that kill fish and harm humans (Landsberg, 2002; Glibert et al., 2005; Backer and McGillicuddy, 2006).

Algal blooms frequently cover large areas of the Great Lakes, which prompted the creation of the Great Lakes Water Quality Agreement between Canada and the United States in the 1960s. The agreement was designed to improve water quality by reducing nutrient loading (Backer and McGillicuddy, 2006; Stow et al., 2015; Dolan, 1993). After an initial reduction in algal blooms and increase in oxygen levels throughout the Great Lakes (Makarewicz, 1993; Makarewicz et al., 1999), conditions began to deteriorate again by the mid-1990s. In 2011, Lake Erie experienced the most extensive algal bloom in recorded history (Burns et al., 2005; Bridgeman et al., 2013; Michalak et al., 2013).

The persistence of algal blooms has been attributed to anthropogenic additions of phosphorous (P) and nitrogen (N) (Glibert et al., 2005). It is important to understand how these nutrients are delivered in order to accurately address water quality issues in the Great Lakes (Matisoff et al., 2016). Nutrients can be transported by rivers or direct groundwater discharge (groundwater that is not intercepted by rivers but rather discharges along the coast). Nutrient loading from rivers can be estimated using measured discharge rates (obtained from river gauging) and nutrient concentrations (Quilbé et al., 2006). However, direct groundwater discharge, i.e. the outflow of terrestrially-derived water across a lakebed, is difficult to quantify. Nutrient concentrations in discharging groundwater are also difficult to ascertain because the sediment-water interface is often a reactive zone that alters concentrations of discharging nutrients (Lewandowski et al., 2015; Robinson, 2015). As a result, accurate measurements of nutrient fluxes to the coast are sparse, and direct groundwater discharge is often overlooked as a source of nutrients that stimulates algal blooms (Kilroy and Coxon, 2005; Lewandowski et al., 2015; Rosenberry et al., 2015).

Direct groundwater discharge occurs wherever hydraulic head in the onshore aquifer is elevated above the lake water table (Grannemann et al., 2000; Robinson, 2015). Most studies of direct groundwater discharge to the Great Lakes have focused on Lake Michigan. Overall, direct groundwater may contribute 1-12% of total water inflow to Lake Michigan (Grannemann et al., 2000; Hoaglund et al., 2002; Robinson, 2015). These rates have generally been estimated using groundwater models or measured hydraulic heads and Darcy's law, which require assumptions about aquifer properties (Grannemann

et al., 2000). Direct measurements of groundwater seepage are sparse. In one study, Cherkauer and Hensel, (1986) used both groundwater models and direct measurements to calculate rates of 153.4 and 87.7 m<sup>3</sup> y<sup>-1</sup> m<sup>-1</sup>, respectively at Mequon, Wisconsin.

Even less is known about nutrient loads associated with direct groundwater discharge to the Great Lakes (Robinson, 2015). Sources of groundwater-borne nutrients to the Great Lakes include agricultural areas, septic systems, leaky infrastructure, and landfills along coastal catchments (Robinson, 2015). In other lakes, water-budget calculations and field observations have been used to quantify nutrient loading (Meinikmann et al., 2013; Meinikmann et al., 2015). Here, I use a water-budget approach to generate new estimates of direct groundwater discharge to the Great Lakes coast of the United States. I then use these estimates to identify areas that may be prone to high nutrient loads from groundwater. Next, I examine a vulnerable location on the Lake Erie coast, where I measured direct groundwater discharge rates and nutrient fluxes. Using insights from field observations, I evaluate strengths and limitations of my vulnerability assessment approach. I show that both large-scale model-based estimates and site-specific field observations are essential for constraining groundwater fluxes and potential nutrient loads to the Great Lakes coast.

## 2.2. Methods

### *Water Budget*

I estimated direct groundwater discharge to the Great Lakes using a water-budget approach that has been previously used to quantify fresh submarine groundwater discharge to oceans (Zektser and Loaiciga, 1993; Destouni et al., 2008; Sawyer et al.,

2016) and is capable of resolving high-resolution continental-scale discharge rates. Briefly, I identified coastal areas of land that fall outside the contributing catchment areas of rivers and streams (Figure 2.1, inset). All runoff in these coastal catchments flows directly and exclusively to the coast. If groundwater divides coincide with topographic boundaries, then groundwater in these catchments also flows exclusively to the coast, and I can consider coastal catchments as recharge zones for direct groundwater discharge to the coast (Figure 2.1). For each coastal recharge zone, I assume that the annual recharge volume equals the annual volume of direct groundwater discharge (Sawyer et al., 2016). Groundwater extraction is considered negligible. Because I include no net groundwater import from upland catchments (Schaller and Fan, 2009a), my assumptions about recharge areas are most appropriate for the shallow unconfined aquifer. The method may neglect a significant component of direct groundwater discharge from confined aquifers that recharge farther inland.

Coastal recharge zones were delineated using high-resolution hydrographic data for the Great Lakes Region of the United States obtained from the National Hydrography Dataset, NHDPlus (McKay et al., 2012). First, coastlines were extracted from the polyline data of rivers, streams, and coasts. A total of 3008 coastal segments were identified with an average length of 2.2 km and a standard deviation of 2.9 km. The coastlines were grouped by reach code, since arbitrarily small coastal segments often share the same reach code, and reach codes tend to divide areas of coastline between rivers and streams. Reach codes are 14-digit integers that combine the 8-digit Hydrologic Unit Code of the U.S. Geological Survey (Seaber et al., 1987) and a unique 6-digit

arbitrary number together forming a unique identifier for each reach of NHDPlus. The association by reach code resulted in 1619 coastal segments with average length of 4.1 km and standard deviation of 6.7 km. Next, the recharge zone for each coastline was extracted using the common NHDPlus integer identifier relating polylines and polygons. The average recharge zone area is 4.3 km<sup>2</sup> and the standard deviation is 11.2 km<sup>2</sup>. None of the coastal recharge zones contain any streams by design. The NHDPlus data is only available for the United States coast (Figure 2.1). Smaller bodies of water within the Great Lakes system, such as St. Clair Lake, are also not included in the dataset. My analysis therefore spans 43% of the Great Lakes coast. Note that while hydrographic datasets exist for the Canadian coastline of the Great Lakes (Lehner et al., 2008), differences in spatial resolution of the underlying topography stand in the way of consistent direct groundwater discharge estimates across scales (Destouni et al., 2008).

Recharge rates were derived from hydroclimatic reconstructions using the second phase of NASA's North American Land Data Assimilation System, NLDAS2 (Xia et al., 2012). Non-infiltrating runoff was excluded since it discharges to the coast as overland flow. For each coastal recharge zone, volumetric recharge (m<sup>3</sup> y<sup>-1</sup>) was calculated by extracting the infiltrating runoff value nearest to the recharge zone centroid and multiplying by area. Direct groundwater discharge per unit length of coast (m<sup>3</sup> y<sup>-1</sup> m<sup>-1</sup>) was obtained by dividing the volumetric recharge rate by shoreline length (m) for each coastal recharge zone.

### *Vulnerability*

I identified coastlines vulnerable to groundwater-borne nutrient inputs using the method of Sawyer et al., (2016) that is based on two criteria: direct groundwater discharge rates and land use within recharge zones. My conceptual model is that groundwater-borne nutrient inputs are greater when a large volume of water discharges to the coast from highly impacted recharge zones. Specifically, I define segments of the coast as vulnerable when two criteria are met: 1) the percentage of agricultural and developed land-cover within the associated recharge zone is above average (37%), and 2) the groundwater flux is above the average value for the United States Great Lakes coast ( $381 \text{ m}^3 \text{ y}^{-1} \text{ m}^{-1}$ ). In each coastal recharge zone, I determined the vulnerable fraction of developed and agricultural land from the National Land Cover Database (NLCD). This includes developed open spaces, developed low, medium, and high intensity areas, pastures, and cultivated crops.

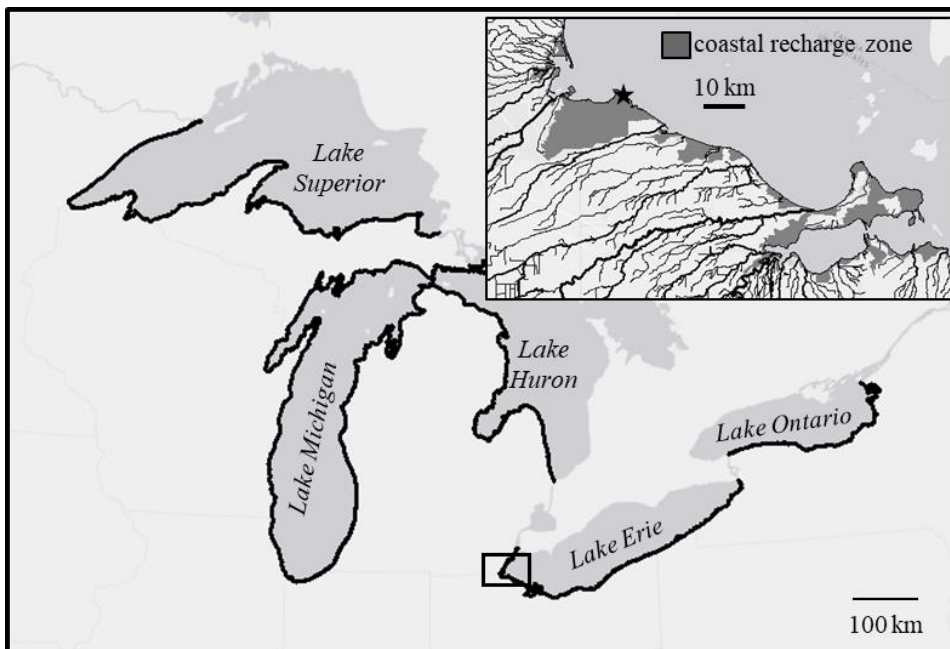


Figure 2.1. Location of the study site (star, inset). Coastal recharge zones contribute water directly to the coast instead of streams. NHDPlus data is only available for the US coastline (bold lines).

My vulnerability analysis does not predict nutrient loads, but instead estimates the likelihood of higher loading rates now and in the future. Biogeochemical transformations can occur along groundwater flow paths and influence nutrient fluxes at the sediment-water interface (Duff and Triska, 1990; Hill, 1996; Kroeger and Charette, 2008). Also, it can take decades for nutrients in recharging water to reach the coast (Meals et al., 2010). The vulnerability analysis is useful for identifying areas that should be considered for measurements or monitoring.

### *Field Site*

I selected a vulnerable beach on Lake Erie for focused measurements of direct groundwater discharge rates and groundwater-borne nutrient fluxes. Due to the heterogeneous nature of the Great Lakes coast, this single field site is not necessarily representative of much of the coast and also provides insufficient data to validate the entire water budget and vulnerability analysis. However, it serves as a platform for considering methodological improvements. The water budget analysis revealed many vulnerable beaches along Lake Erie, but I selected this site for its easy access and logistical advantages. The site (41°41'57.62" N, 83°19'32.95 " W) is located in the lake's western basin at Cedar Point National Wildlife Refuge (Figure 2.1). It lies on a gradually sloping beach, allowing for installation of seepage meters without scuba gear. The beach is part of a spit separating Lake Erie from a highly vegetated marsh to the south. Land use within the recharge zone is mixed. The land immediately adjacent to the beach is marsh and forest, but much of the area is agricultural, and the city of Toledo lies only 18 km southwest. The Maumee River discharges to Lake Erie approximately 12 km west of the

study site. The surficial geology generally consists of recent sand deposits overlying glacial till and lake shale (Fuller, 1996).

### *Seepage Meter Measurements*

Lee-type seepage meters were constructed from the ends of steel drums with an internal diameter of 57 cm (Lee, 1977) and deployed on September 5, 2015. Fifteen seepage meters were arranged along three shore-perpendicular transects: Transect 1, Transect 2, and Transect 3 (Figure 2.1). Seepage meters were spaced approximately 5 m apart, in water depths ranging from 0.6 to 1.5 meters. The distance between each transect was approximately 200 m. In order to resolve shore-parallel variation in seepage rates, additional seepage meters were deployed at even intervals between transects. A nest of four seepage meters, spaced 1 m apart, was also installed to measure small scale-heterogeneity in seepage rates (Figure 2.1).

After installation, seepage meters were allowed to equilibrate for twenty-four hours with open valves prior to taking measurements. Plastic autoclaved collection bags were prefilled with 1.89 liters of lake water and weighed. The bags were attached to seepage meters for approximately two hours, after which they were removed and weighed again. Seepage rates were calculated from the difference between the initial and final water mass per length of sample time. Two rounds of measurements were made on the same day, and the rates were averaged. Weather conditions were generally calm and waves were minimal during both rounds of measurements. Based on the precision of my scale, the precision of my seepage rates was  $\pm 0.24 \text{ cm d}^{-1}$ . This precision was propagated

as a proxy for error when I calculated volumetric fluxes of direct groundwater discharge at the site.

### *Concentrations and Nutrient Fluxes*

To compute nutrient flux to the lake, pore water was sampled next to each seepage meter at a depth of 25 cm below the sediment-water interface. Samples were obtained by suction using a syringe attached to a steel tube (0.5 cm inner diameter and 0.6 cm outer diameter with a screened interval of 3.5 cm). One tubing volume (~24 ml) was discarded before sample collection.

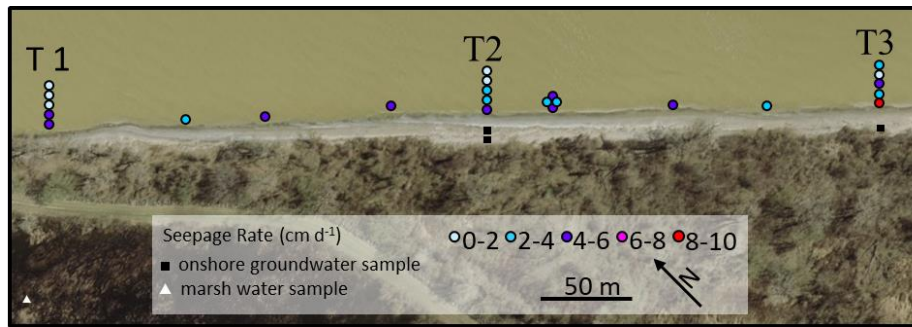


Figure 2.2. Average seepage rates of round 1 and round 2 (circles). Locations of onshore groundwater and marsh water samples are also shown with squares and triangles respectively.

For comparison, water samples were also collected from the lake, nearby marsh, and onshore aquifer. Temporary piezometers were installed to sample onshore groundwater. The piezometers were constructed of 4.5 cm outer-diameter PVC and screened through the water table. The piezometers were fully purged with a peristaltic pump and then sampled. All water samples were filtered (0.45  $\mu\text{m}$ ), immediately placed on ice, and transferred to a freezer within 12 hours of collection.  $\text{NO}_2^- + \text{NO}_3^- - \text{N}$  and  $\text{NH}_4^+ - \text{N}$  were measured using a Skalar flow-injection nutrient analyzer, and their summed concentrations are reported as dissolved inorganic nitrogen (DIN). Major anions,

including phosphate ( $\text{PO}_4^{3-}$ ), were measured using ion chromatography. Detection limits for  $\text{NO}_2^- + \text{NO}_3^- - \text{N}$ ,  $\text{NH}_4^+ - \text{N}$  and  $\text{PO}_4^{3-}$  were 0.014, 0.0026 and 0.019  $\text{mg l}^{-1}$ , respectively.

Nutrient fluxes were calculated as the product of the concentration at each seepage meter and the seepage rate. Where the concentration was below detection, I calculated fluxes using the detection limit.

### 2.3. Great Lakes Analysis

#### *Patterns and Rates of Direct Groundwater Discharge*

The total annual volume of direct groundwater discharge to the Great Lakes (U.S. portion only) is  $2.54 \text{ km}^3 \text{ y}^{-1}$ . The average volumetric flux per unit length of shoreline is  $381 \text{ m}^3 \text{ y}^{-1} \text{ m}^{-1}$ . Lake Erie and Lake Michigan have the highest average fluxes ( $477 \text{ m}^3 \text{ y}^{-1} \text{ m}^{-1}$  and  $410 \text{ m}^3 \text{ y}^{-1} \text{ m}^{-1}$ , respectively). Average flux is lowest to Lake Ontario ( $308 \text{ m}^3 \text{ y}^{-1} \text{ m}^{-1}$ ) (Table 1). Direct groundwater discharge rates vary spatially along the coast of individual lakes (Figure 2.3). Regionally, high discharge rates are concentrated on the south-central and southeastern coasts of Lake Erie, as well as the northeastern and southwestern coasts of Lake Michigan. Other areas of high discharge include the southeastern coast of Lake Superior, northwestern coast of Lake Huron, and eastern coast of Lake Ontario.

Onshore infiltration (percolation of surface water to the subsurface) is a key control on the pattern of direct groundwater discharge that reflects both climate and geology. Infiltration is controlled by precipitation and the capacity of the land surface to accept water. Much of the Great Lakes shoreline is bounded by glacial till and outwash deposits, which can vary widely in permeability. Coastal areas along the Western Lake

Erie Basin (west of Cleveland) generally consist of less permeable silty glacial till. This area corresponds with lower discharge rates on the map (Figure 2.3). East of Cleveland, tills are sandier (Fullerton et al., 1991). Also, bedrock bluffs 15-20 m high make up most of the shoreline east of Cleveland (Morang et al., 2011) and may allow greater head gradients to develop near the coast. The water budget analysis correspondingly shows high discharge rates along the eastern portion of Lake Erie (Figure 2.3). Over small areas, permeable zones such as spits where glacial sands have been reworked may allow for locally elevated infiltration and groundwater discharge rates. My field site is located on one such spit.

The geometry of coastal recharge zones is another key factor influencing patterns of direct groundwater discharge. Although Lake Ontario has the highest infiltration rate among the Great Lakes, its average volumetric flux of groundwater per length of shoreline is lowest. Its recharge zones do not stretch as far inland and therefore contribute less groundwater to the coast. Long, narrow recharge zones convey more groundwater per unit length coastline.

Water extraction is not included in my analysis, and direct groundwater discharge rates are likely overestimated in areas with substantial drawdown. For example, withdrawal due to municipal pumping in Chicago and Milwaukee reduces the amount of groundwater discharge along the southwestern coast of Lake Michigan (Feinstein et al., 2010).

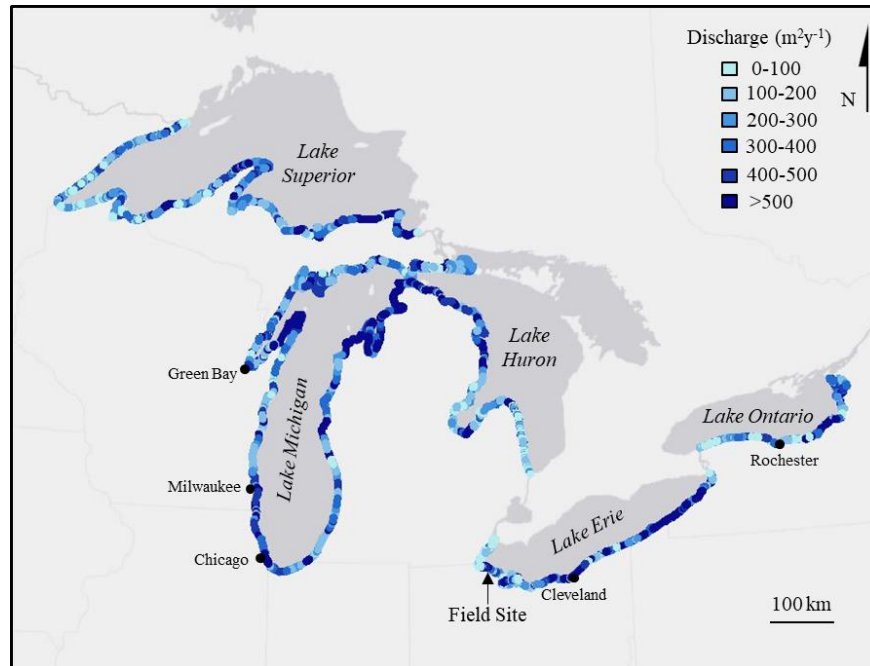


Figure 2.3 Direct groundwater discharge Great Lakes (US). Discharge rates are high ( $>500 \text{ m}^2 \text{ y}^{-1}$ ) along several reaches of coastline; most notably, east and central sections of Lake Erie, northeast Lake Michigan southeast Lake Superior and the southern coast of northwest Lake Huron.

#### *Comparison with other models and methods*

The total volumetric rate of direct groundwater discharge to Lake Michigan ( $0.97 \text{ km}^3 \text{ y}^{-1}$ ) is comparable to results from a groundwater modeling study by Feinstein et al. (2010). They reported a total volumetric discharge rate of only  $0.24 \text{ km}^3 \text{ y}^{-1}$  but suggested that the rate may be up to 3.8 times greater, based on grid sensitivity studies. Both the Lake Michigan model and my water budget analysis predict high discharge rates along the northeast coast of Lake Michigan as well as low discharge rates near Green Bay (compare Figure 3 and Figure 72E in Feinstein et al. (2010)). However, the Lake Michigan model predicts low discharge rates between Milwaukee and Chicago due to municipal groundwater pumping, where my water budget approach incorrectly predicts high rates. Furthermore, a direct comparison of the estimates against the groundwater

model for the entire Lake Michigan coast shows no correlation (Figure 2.4). A comparison of studies for five other specific sites suggests agreement to within an order of magnitude (Figure 2.4). These comparisons underscore the large uncertainties in attempting to estimate direct groundwater discharge rates at any given location.

Lake	Coastline Analyzed (km)	Coastline Analyzed (%)	Infiltration (cm y <sup>-1</sup> )	Volumetric Flow Rate (km <sup>3</sup> y <sup>-1</sup> )	Average Discharge Rate (m <sup>2</sup> y <sup>-1</sup> )	Vulnerable Coastline (%)
Lake Erie	895	65	42	0.42	477	31
Lake Huron	1313	24	31	0.44	337	6
Lake Michigan	2355	88	37	0.97	410	21
Lake Ontario	530	45	45	0.16	308	22
Lake Superior	1576	33	35	0.54	345	0.7
Great Lakes	6669	43	36	2.54	381	15

Table 2.1. Water budget statistics for the Great Lakes.

*Vulnerability to groundwater-borne nutrient inputs*

Of the 6669 km of United States Great Lakes shoreline, 15% is potentially vulnerable to groundwater-borne nutrients (Figure 2.5) based on my criteria (Section 2.2). Lake Erie has the greatest proportion of vulnerable coastline (31%) (Table 2.1). Much of the area near Cleveland is particularly vulnerable, but localized zones occur throughout Lake Erie’s coast. Lake Erie’s high vulnerability is reflective of its high concentration of agricultural and developed land uses, combined with relatively high direct groundwater discharge rates. On average, 76% of Lake Erie’s coastal recharge areas have an above-average fraction of contaminant-prone land use, compared to 28% for the remaining four

Great Lakes combined. The average volumetric discharge rate to the United States Lake Erie coast is  $477 \text{ m}^3 \text{ y}^{-1} \text{ m}^{-1}$ , while the average volumetric discharge for the other four lakes is  $350 \text{ m}^3 \text{ y}^{-1} \text{ m}^{-1}$  (28% lower). Vulnerable areas in the other Great Lakes include the southwestern coast of Lake Michigan from Milwaukee to Chicago and numerous portions of Lake Ontario. Less than 1% of the United States Lake Superior coastline is vulnerable, due to its low rate of direct groundwater discharge, agricultural activity, and development.

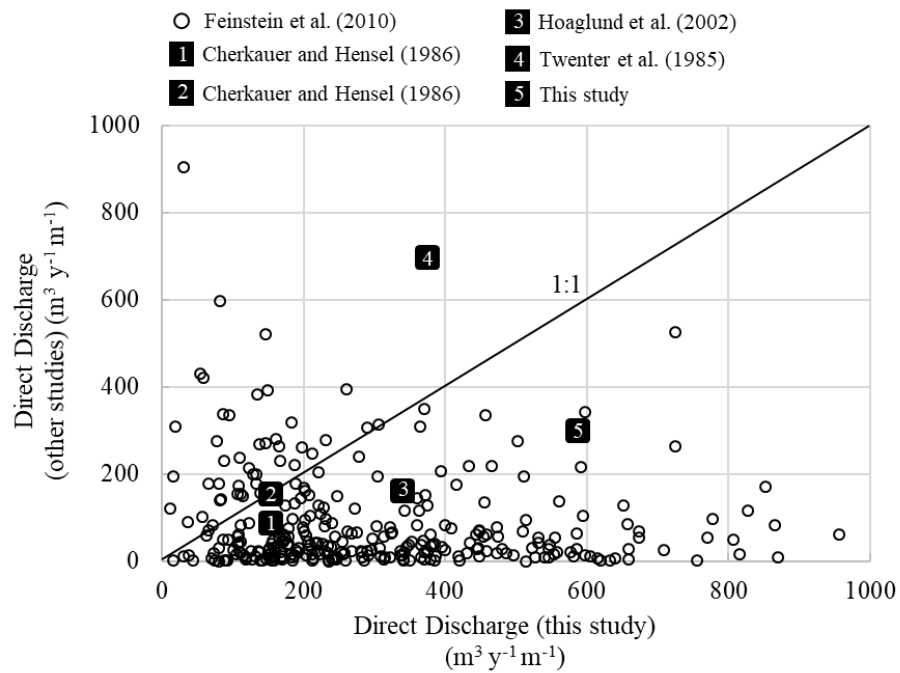


Figure 2.4. Direct groundwater discharge to Great Lakes from water budget analysis in this study compared to results from a groundwater model for the Lake Michigan basin (Feinstein et al., 2010), seepage meter and groundwater model, respectively.

## 2.4. Field Study of a vulnerable beach

### *Direct groundwater discharge*

Seepage meter measurements indicate net discharge across the study site with a mean rate of 3.15 cm d<sup>-1</sup> and range of 0.47 to 10.34 cm d<sup>-1</sup> (Figure 2.2). Net infiltration occurred at only one seepage meter during one round of sampling. Rates were heterogeneous over small spatial scales of meters, although the variation was modest compared to some similar studies (Schneider et al., 2005a; Shaw and Prepas, 1990; Toran et al., 2015). In the nest of four closely-spaced seepage meters, specific discharge rates ranged from 2.9 to 5.1 cm d<sup>-1</sup>. Along transects, seepage meter rates showed similar trends with distance from the shoreline. Nearshore (0-10 m) rates averaged 8.0 cm d<sup>-1</sup> and declined offshore (25-30 m) to approximately 1 cm d<sup>-1</sup>. The offshore trends can be described with an exponential relationship (McBride and Pfannkuch, 1975) (Figure 2.6). The best-fit relationship for the specific discharge rate,  $q$  [m d<sup>-1</sup>], as a function of distance offshore,  $x$  [m], is:

$$q=0.0784e^{-0.081x}. \quad (2.1)$$

Along each 20-meter transect, the integrated groundwater flux (using Riemann sum) was 228, 232, and 320 m<sup>3</sup> y<sup>-1</sup> m<sup>-1</sup>, respectively (average 260±18 m<sup>3</sup> y<sup>-1</sup> m<sup>-1</sup>). However, groundwater discharge should extend beyond these transects (Bokuniewicz, 1980; Burnett et al., 2006; Russoniello et al., 2013). Integrating Equation 1, the total volumetric flux of groundwater per unit length of coast is 354±25 m<sup>3</sup> y<sup>-1</sup> m<sup>-1</sup>. For comparison, the water budget approach yields a greater estimate of 588±181 m<sup>3</sup> y<sup>-1</sup> m<sup>-1</sup>.

The discrepancy between the two methods can be the result of several factors related to the design of my field campaign. First, heterogeneity in seepage rates occurs at a variety of scales, from meters to kilometers. My field site spanned approximately 420 m

of shoreline, or 7.6% of the segment of coastline over which the water budget was calculated. It is plausible that seepage at my study site was locally low compared to the broader area. Additional measurements are needed to understand how local rates at the study site compare with nearby areas within the same coastal recharge zone, but large-scale studies with many seepage meters are rare because they are labor intensive (Burnett et al., 2006). Second, seepage rates vary over annual and seasonal timescales (Michael et al., 2005; Schneider et al., 2005a). Field measurements were taken at the end of summer and would likely be lower than the annual average (Michael et al., 2005). Third, and perhaps most importantly, I only deployed seepage meters at the beach and did not measure seepage in the marsh. Nearshore marshes likely intercept a significant portion of direct groundwater discharge. Some of this discharged groundwater may evaporate, but some may flow to the lake through connecting water bodies and should still be considered direct groundwater discharge. My field-based estimate is likely low because I did not include direct groundwater discharge to the adjacent marsh.

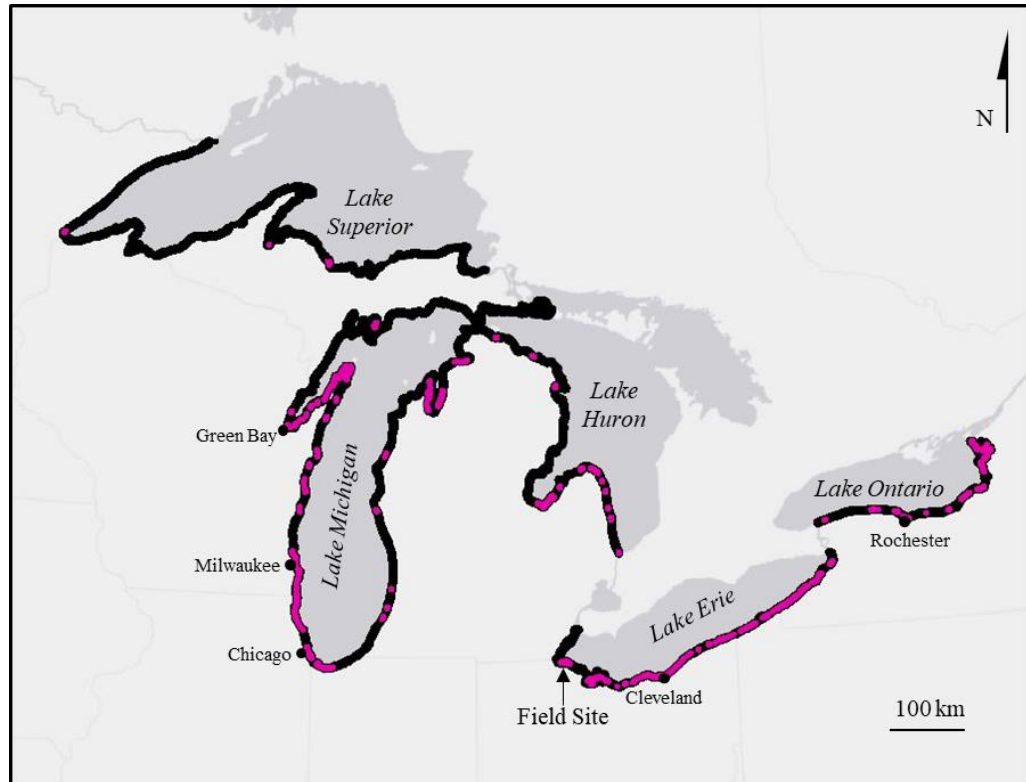


Figure 2.5. Vulnerability of Great Lakes to contaminant from groundwater (pink).

Seepage meter measurements are also prone to errors and uncertainties. Seepage meter measurements may overestimate discharge in high energy environments due to velocity head variations (Libelo and MacIntyre, 1994; Schneider et al., 2005b; Rosenberry, 2008). I did not place my seepage meters in shelters to minimize velocity head effects (Libelo and MacIntyre, 1994; Rosenberry, 2008), but sampling was carried out over relatively calm conditions when currents and waves were minimal. Measured seepage rates can also be reduced by frictional energy losses associated with small diameter plumbing (Rosenberry and Morin, 2004). My seepage meters employed relatively large-diameter plumbing connections (13 cm inner diameter).

Assumptions made in the water budget analysis may as well be a source of uncertainty in the study. For example, groundwater extraction may deduct from direct groundwater discharge or increase recharge due to lowering of the water table (Konikow and Kendy, 2005; Ferguson and Gleeson, 2012). Groundwater extraction is not accounted for in the NLDAS2 dataset, so I do not seek to include it in my water budget for consistency. However, depletion of groundwater due to extraction is minimal for the majority of the Great Lakes' recharge zones, with western Lake Michigan as an exception (Feinstein et al., 2010; Konikow, 2013). Thus, the assumption that extraction is negligible is valid for the majority of my analyzed areas, including my field site. I also assume that groundwater imports from upland catchments are negligible. However, the significance of flow contributions from upland catchments is difficult to measure (Schaller and Fan, 2009b). Regardless, both of these assumptions would tend to cause underestimation of direct groundwater discharge rates, yet my water budget estimate is greater than the rate from seepage meter measurements.

Despite the inherent uncertainties, both field-based and water budget-based methods have advantages. Unlike water budgets, seepage meters can be used to resolve temporal variability and small-scale spatial variability (Bokuniewicz, 1980; Michael et al., 2005; Russoniello et al., 2013). Seepage meters are the only way to directly measure groundwater discharge. Other field-based measurements that use heat tracing or radioactive isotopes rely on indirect measurement of flow (Lee, 1977; Burnett et al., 2006; Russoniello et al., 2013). Meanwhile, water budgets provide a useful tool for examining regional trends in direct groundwater discharge to the Great Lakes system.

Similar techniques have been used to map direct groundwater discharge at high resolution over the Baltic Sea and U.S. seaboards or at low resolution over the global oceans (Zektser and Loaiciga, 1993; Destouni et al., 2008). This approach using the NHDPlus data set allows for high-resolution continental-scale estimates over the United States. Because the resolution of the hydrography dataset influences the estimation of direct groundwater discharge, it is not straightforward to merge analyses across multiple hydrographic datasets from different countries. As the coverage of consistent hydrography datasets expands, the water-budget approach can be used to predict global distributions of direct groundwater discharge (Destouni et al., 2008).

#### *Nutrient Concentrations and Fluxes*

Dissolved phosphorous (DP) concentrations in lakebed pore water were elevated at some locations and averaged  $0.12 \text{ mg l}^{-1}$  (Figure 2.7a, Figure 2.8a). For comparison, DP concentrations in lake water, marsh water, and onshore groundwater were all below detection ( $0.019 \text{ mg l}^{-1}$ ) and reported as the detection limit (Figure 2.7a). There were no discernible spatial trends in the locations of elevated lakebed DP (Figure 2.8a) and no clear relation to ammonium, DIN, or groundwater fluxes. DP fluxes across the lakebed ranged from near zero, where concentrations were below detection, to  $12.94 \text{ mg m}^{-2} \text{ d}^{-1}$ . Integrating along transects, the mass flux of DP per unit length of shoreline was 114.6, 39.7, and  $105.0 \text{ mg m}^{-1} \text{ d}^{-1}$  for Transects 1 through 3, respectively (average of  $86 \pm 6.1 \text{ mg m}^{-1} \text{ d}^{-1}$ ).

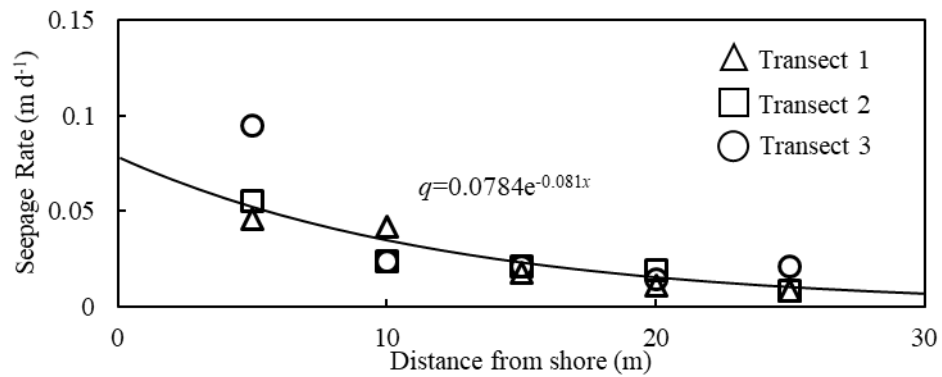


Figure 2.6. Seepage rates decrease exponentially from shore at the study site.

#### *Nutrient transformation near the lakebed interface*

DIN concentrations averaged  $2.57 \text{ mg l}^{-1}$  in lakebed pore water (Figure 2.8b), which mostly consisted of  $\text{NH}_4^+\text{-N}$ . DIN concentrations were low in lake and marsh waters ( $0.021$  and  $0.11 \text{ mg l}^{-1}$ , respectively) (Figure 2.7b). DIN concentrations in onshore groundwater were similar to or greater than lakebed pore water and averaged  $6.0 \text{ mg l}^{-1}$  (Figure 2.7b). However, most of the onshore DIN consisted of  $\text{NO}_3\text{-N}$ . The source of DIN is unclear. Relatively pristine wetlands fringe the beach, but the broader recharge zone includes cultivated crop beyond the immediate vicinity of the study site. High DIN may be anthropogenic in origin if sourced from these distal agricultural areas, or may be produced locally from mineralization of organic matter followed by nitrification, or both. There was no clear relationship between DIN concentrations and groundwater fluxes (Figure 2.8b). DIN fluxes across the lakebed ranged from  $15.5$  to  $323 \text{ mg m}^{-2} \text{ d}^{-1}$ . The mass flux of DIN was  $1340$ ,  $1300$ , and  $3427 \text{ mg m}^{-1} \text{ d}^{-1}$  for Transects 1 through 3, respectively (average of  $2022 \pm 141.3 \text{ mg m}^{-1} \text{ d}^{-1}$ ).

Lakebeds are reactive interfaces that may serve as sources or sinks of nutrients to lake water (Frape and Patterson, 1981; Kroeger and Charette, 2008; LaBaugh et al., 1997). DP can be sourced from sediments (mineralization of organic matter and desorption from autochthonous deposits), excreted by organisms, or derived from mixing with an unknown high DP water source. In contrast, uptake by plants and sorption to metal oxide minerals may reduce DP concentration (Robinson, 2015). At the study site, DP was negligible in onshore groundwater, lake surface water, and marsh samples, but present in most pore water samples, indicating a benthic source (likely organic matter mineralization and/or desorption of legacy P from mineral surfaces). I did not measure total phosphorous (TP) in lake water, but it is known to be elevated (Chaffin et al., 2011) due to inputs from contributing rivers (Baker et al., 2014). The Maumee River delivers a large sediment load from agricultural areas to Lake Erie, and its mouth is located near the study site. Some of the DP in lakebed pore water may be sourced from legacy P in deposits from the Maumee River (Green et al., 1978).

Reactions along shallow flow paths also influence N in groundwater (Duff and Triska, 1990; Hester et al., 2014). Nitrate, often the most common form of N in groundwater, is usually stable in aerobic zones, but is removed via denitrification in anoxic conditions or attenuated by microbial and plant uptake (Hill, 1996; Robinson, 2015). One of the onshore groundwater samples at Cedar Point was particularly high in nitrate (Figure 2.7b), but the lower concentrations in lakebed porewater suggest that much of the nitrate may be removed before discharging to the lake. Dilution of high-nitrate groundwater with low-nitrate lake water or another low nitrate water source could

also cause a decline in nitrate concentrations near the lakebed interface (Altman and Parizek, 1995; Speiran et al., 1998; Spruill, 2000). Unfortunately, chloride concentrations were similar in onshore groundwater and lake water and therefore were not useful for distinguishing dilution and chemical removal (Figure 2.7). Concentrations ranged from 12 to 63 mg l<sup>-1</sup> in lakebed pore water, which is similar to chloride concentrations in pore water from another Lake Erie location (Haack et al., 2005). If removal does occur along subsurface flow paths, near shore sediments along Lake Erie may provide an important ecological service by reducing nitrate prior to discharge.

My water chemistry data highlight the importance of calculating nutrient fluxes with concentrations measured near the sediment-water interface. Using onshore groundwater end members to calculate nutrient fluxes is common practice but not an accurate reflection of potential fluxes at the sediment-water interface (Schuster et al., 2003). Nutrient chemistry can vary over short distances in the subsurface, particularly near contrasting sediment types or converging flow paths with different limiting reactants (Hill et al., 2000). For example, Gu et al. (2007) showed that a sharp oxidation-reduction gradient within the top 15 cm of sediment at Cobb Mill Creek, Virginia, may be responsible for up to 80% loss of nitrate near the sediment-water interface. Rapid changes in chemistry occur at my study site over tens of meters between onshore piezometers and lakebed sampling locations. Using groundwater end member concentrations to calculate nutrient flux at the study site results in average DP and DIN fluxes of 0.68 and 5300 mg m<sup>-1</sup> d<sup>-1</sup> (compared to 86 and 2023 m<sup>-1</sup> d<sup>-1</sup>), underestimating and overestimating DP and DIN fluxes, respectively.

*Significance of direct groundwater discharge as a source of nutrients to Lake Erie*

An important question is whether groundwater is a significant source of nutrients to Lake Erie. I lack distributed chemical data from around Lake Erie to estimate the total flux of groundwater-borne nutrients. However, if I assume nutrient concentrations in groundwater discharge zones around Lake Erie are similar to those at the field site (average DP and DIN concentrations of 0.12 and 2.57 mg l<sup>-1</sup>, respectively), based on the average direct groundwater discharge rate (477 m<sup>2</sup> y<sup>-1</sup>; Table 2.1), and a total coastline length of 1400 km, the total DP and DIN fluxes are 2.5 and 54.3 g s<sup>-1</sup>, respectively. For comparison, these fluxes represent 13% of the DP load and 4% of the DIN load to Lake Erie by the Maumee River, which is a major source of nutrients to Lake Erie (Baker et al., 2014; Stow et al., 2015). I note that rivers also carry a large particulate P load, while most particulate P is likely filtered from discharging groundwater. The DP load is especially important because it is more bioavailable than particulate P (Sonzogni et al., 1982). In summary, groundwater is potentially a small but non-negligible source of nutrients to Lake Erie. Unlike discharge from a river, direct groundwater discharge is diffuse and exhibits high spatial heterogeneity. The complexity in quantifying direct groundwater discharge as a nonpoint source of contamination makes management difficult compared to point source loading.

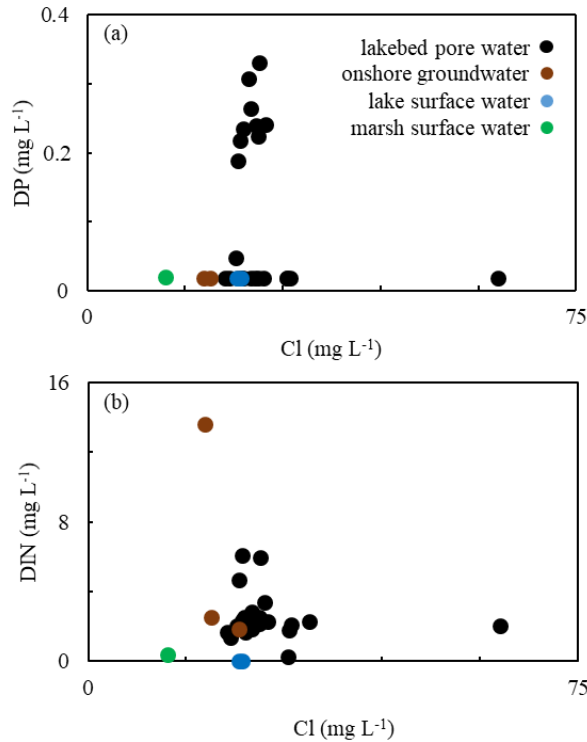


Figure 2.7 .Nutrient concentrations in water with respect to chloride samples from the Cedar Point field study. Lakebed pore water (black dots) is elevated in DP and low in DIN compared to lake surface water.

Though small in magnitude, nutrient fluxes from groundwater can influence primary production because N:P ratios are often significantly greater than in river water (Howarth, 1988; Slomp and Van Cappellen, 2004). The Redfield ratio of 16:1 represents an optimal condition for primary production and phytoplankton development (Howarth, 1988). Higher N:P ratios may favor P limitation, and vice versa (Lapointe, 1997; Weiskel and Howes, 1992). Groundwater at my field site delivers a DIN:DP ratio of 147:1, far exceeding the Redfield ratio and contributing to P limitation. In comparison, a N:P ratio of 21:1 was reported in lake water within the western basin of Lake Erie near Maumee Bay during the 2008 algal bloom (Chaffin et al., 2011). Assuming field measurements are

representative of average P and N concentrations, discharging groundwater is high in N and has the potential to exacerbate P limitation.

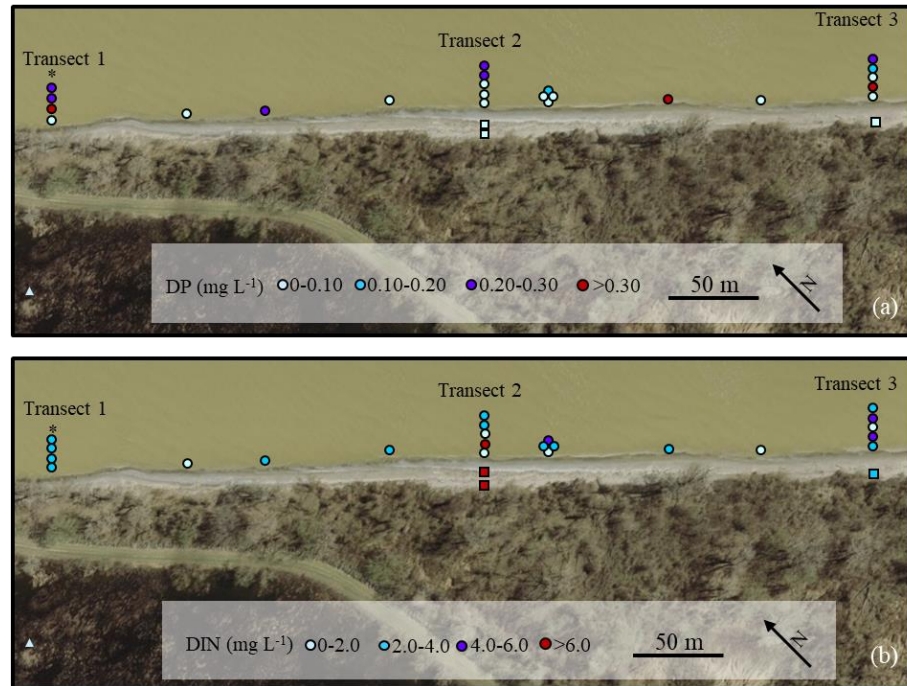


Figure 2.8. DP and DIN concentration at each seepage meter. Squares represent onshore wells and the triangle the marsh sample. Seepage meter #1 (asterisk) was not sampled.

## 2.5. Considerations for assessing vulnerability

My coastal vulnerability map is a useful tool for revealing reaches of shoreline that are susceptible to inconspicuous nutrient loads from direct groundwater discharge. High resolution patterns in vulnerability can be resolved over scales of kilometers. An added benefit is that vulnerability thresholds could be modified to fit different applications. For example, with data on mining activities, thresholds could be selected to map vulnerability to mining-derived contaminants.

My method does not identify locations susceptible to mobilization of legacy P from lakebed sediments. Phosphorus-laden sediments in groundwater discharge zones may be an important source of DP to pore water and ultimately lake water, especially in areas like my field site near the mouth of the Maumee River. Furthermore, biogeochemical turnover of internal P in lakebed sediment may also contribute to P loads in the lake (Lewandowski et al., 2015). DP contributions from onshore groundwater may be negligible. DP is often relatively immobile in groundwater because it tends to react with cations to form a wide range of metal-complex formations, adsorb to sediment and be taken up by plants (Holman et al., 2008; Robinson, 2015). However, growing evidence suggests that the mobility of DP in groundwater has been underappreciated (Crowe et al., 2004; Robertson et al., 2005; Holman et al., 2008; Simonds et al., 2008; Robinson, 2015), and groundwater may sometimes transport consequential amounts of P. My approach for identifying vulnerable coastlines only considers nutrients from onshore groundwater. A more robust vulnerability assessment would consider both potential DP sources from onshore activities in the recharge zone and DP release from sediments in the discharge zone. Including this second source would require an improved understanding of: 1) distributions of legacy P and potential desorption rates, and 2) distributions of organic matter and potential mineralization rates along the Great Lakes coast.

My method also has weaknesses in predicting susceptibility to nitrate loading. Zones with high agricultural and developed land uses may not necessitate high N loads. For example, high N in groundwater samples at Cedar Point were expected based on my vulnerability map. However, it appeared that N was attenuated near the lakebed discharge

zone. N loading may not be high in vulnerable areas if the shallow aquifer provides an attenuation service.

Spatial heterogeneity and temporal variations also complicate vulnerability assessments. Nutrient leaching from the soil to the water table varies across fine scales that depend on soil type, fertilizer input, climatic conditions, vegetation type, and depth to root zones (Coulibaly and Burn, 2004; Lewandowski et al., 2015). Also, land use is heterogeneous and variable at resolutions finer than the average recharge zone. By design, all areas within a given recharge zone are assumed to have a uniform recharge rate and the entire coastline has a uniform discharge rate. It is likely that areas of high and low vulnerability occur within a given recharge zone due to heterogeneity in fluxes or point sources of nutrients such as leaky septic tanks. Nevertheless, this approach provides a good platform for planning more detailed measurements of nutrient loading via groundwater. Vulnerability maps cannot replace direct field measurements.

## 2.6. Conclusion

Water budgets are a simple but powerful tool for revealing patterns of direct groundwater discharge to the coast, which can be used to identify areas of risk for nutrient contamination from groundwater. Of the Great Lakes, Lake Erie has the highest flux of groundwater per unit length of shoreline ( $477 \text{ m}^3 \text{ y}^{-1} \text{ m}^{-1}$ ) along with the highest percentage of vulnerable shoreline (31%). Lake Superior is the least vulnerable to groundwater-borne contamination with only 1% of its coastline marked as vulnerable. In regions where drawdown due to pumping reduces groundwater flow to the coast, the water budget approach may overestimate direct groundwater discharge. However, this

method may also underestimate discharge where regional confined aquifers convey groundwater to the coast. Currently, my approach for mapping vulnerability to groundwater-borne nutrient loads does not consider P sources from the mineralization of organic matter or desorption of legacy P in discharge zones. Vulnerability predictions could be improved with better estimates of P content and potential mobilization rates from lakebed sediments.

The Great Lakes provide drinking water for millions of people in the United States and Canada and serve important economical and recreational purposes. Maps of estimated coastal vulnerability for the Great Lakes are essential for effective management of this fresh water resource. However, there remains limited direct field measurements to validate my approach, and vulnerability maps cannot replace direct field observations of nutrient fluxes from groundwater. A clear need exists for new measurements of groundwater-borne nutrient fluxes to the Great Lakes and other recreational water bodies across a variety of coastal land use types and geologies.

## **Chapter 3. Nutrient Removal across Ecogeomorphic Zones in Wax Lake Delta Louisiana, (USA)**

### 3.1. Introduction

Over the past century, humans have increased global nitrogen availability primarily through fertilizer use and energy production (Galloway et al., 2008). Excess nitrogen leaches from the landscape into shallow groundwater and surface waters, reducing water quality and stimulating the development of algal blooms that can reduce biodiversity and compromise fisheries. As a prime example, the Mississippi River delivers up to 1.6 million tons of nitrogen to the Gulf of Mexico annually, leading to the development of one of the world's largest hypoxic zones (Goolsby et al., 1999; Rabalais et al., 2002; Alexander et al., 2008).

Coastal wetlands act as sinks for nitrate (Odum, 1988; Reddy and Gale 1994, Seitzinger et al., 2006) and deltaic wetlands are ideally positioned to help buffer nutrient loads from rivers (Sawyer et al., 2015). Since deltas form at 40% of all coastal river mouths (Caldwell et al., 2019), they are important final filters of continental water before it is discharged into the ocean. Moreover, deltas are under threat from rising relative sea levels, climate change, and sediment starvation due to the construction of dams and reservoirs (Syvitski et al., 2009). In threatened deltas, river diversion projects are a proposed mechanism to reclaim coastal wetlands by building new land (Day et al., 2007, Twilley and Rivera-Monroy, 2009, Paola et al., 2011, Fofoula-Georgiou et al., 2013).

River diversion projects can benefit from an improved understanding of nitrate retention in deltas and the biophysical factors that control it.

Nitrate may be removed through several mechanisms in deltaic wetlands, including denitrification, biological uptake, and dissimilatory nitrate reduction to ammonium (DNRA) (Saeed and Sun, 2012). Denitrification is a form of anaerobic respiration typically occurring in low oxygen environments and at anoxic microsites (Seitzinger et al., 2006). In the presence of sufficient organic matter, facultative bacteria reduce nitrate to gaseous nitrogen, permanently removing nitrogen from the ecosystem. Plants and microbes take up ammonium and nitrate (biological uptake), converting the inorganic nitrogen to organic forms for use as building blocks for cells and tissues (Vymazal, 1995). However, plants eventually release much of this accumulated nitrogen back into the environment as detrital organic matter (Vymazal, 2007). DNRA involves the reduction of nitrite and nitrate to ammonium, but ammonium is converted back to nitrate by chemolithotrophs through nitrification in the presence of oxygen (Reddy and Patrick, 1984, Burgin and Hamilton, 2007). Thus, both biological uptake and DNRA only temporarily remove nitrate from the aquatic ecosystem, while denitrification is a permanent sink (Saunders and Kalff, 2001; Burgin and Hamilton, 2007).

The efficiency of nitrate removal in wetlands generally depends on the residence time of flowing water and reaction rates (Baker and Vervier, 2004; Hernandez and Mitsch, 2007; Kjellin et al., 2007). For example, riparian wetlands can be highly efficient sinks of nitrate under low discharge rates (Forshay et al., 2005; DeLaune et al., 2005). However, the efficiency of nitrate removal within deltaic wetlands, which can have a

wide range of residence times and reaction rates, remains unclear. Within Wax Lake Delta, 23 - 54% of water that enters the channel network moves through the mostly inundated interiors of islands via overtopping of levees and flow through secondary channels and embayments (Hiatt and Passalacqua, 2018). Travel times through the islands are at least three times greater than those through the channels (Hiatt and Passalacqua 2015), and residence times within islands further increase with hydraulic roughness associated with vegetation (Hiatt et al., 2018). Reaction rates also appear to be heterogeneous, as older islands with more mature soils have higher potential denitrification rates compared to younger islands (Henry and Twilley, 2014). Removal rates may further depend on biophysical parameters such as water depth – a control on sediment-water interactions (Alexander et al., 2000) – and vegetation density – a control on biotic uptake (Hill, 1986).

Given the dependence of nitrate removal on residence times and reaction rates and thus biophysical parameters such as water depth and vegetation density, nitrate removal should vary across ecogeomorphic zones with distinct hydrologic and biogeochemical characteristics such as delta levees, channels, and embayments (defined by Shaw et al. (2013) as the centers of islands that are continually flooded and open to the bay). To understand how nitrate removal varies across ecogeomorphic zones, I measured rates of nitrate removal with benthic chambers in an island of Wax Lake Delta, Louisiana, USA. I relate chamber measurements to environmental parameters associated with ecogeomorphic zones, such as water depth and vegetation cover, in order to upscale nitrate removal estimates to the whole delta. The first upscaling approach estimates

spatially explicit potential nitrate removal rates across the submerged delta area but does not consider transport processes; while the second approach treats the delta as a network of channels and considers the integrated effect of transport and reactions along flow paths through the channel network but only implicitly includes removal in off-channel storage zones like levees and embayments. Despite the simplicity of these disparate upscaling approaches, both calculations suggest that removal represents a small portion of the total incoming nutrient load to Wax Lake Delta under typical summer conditions.

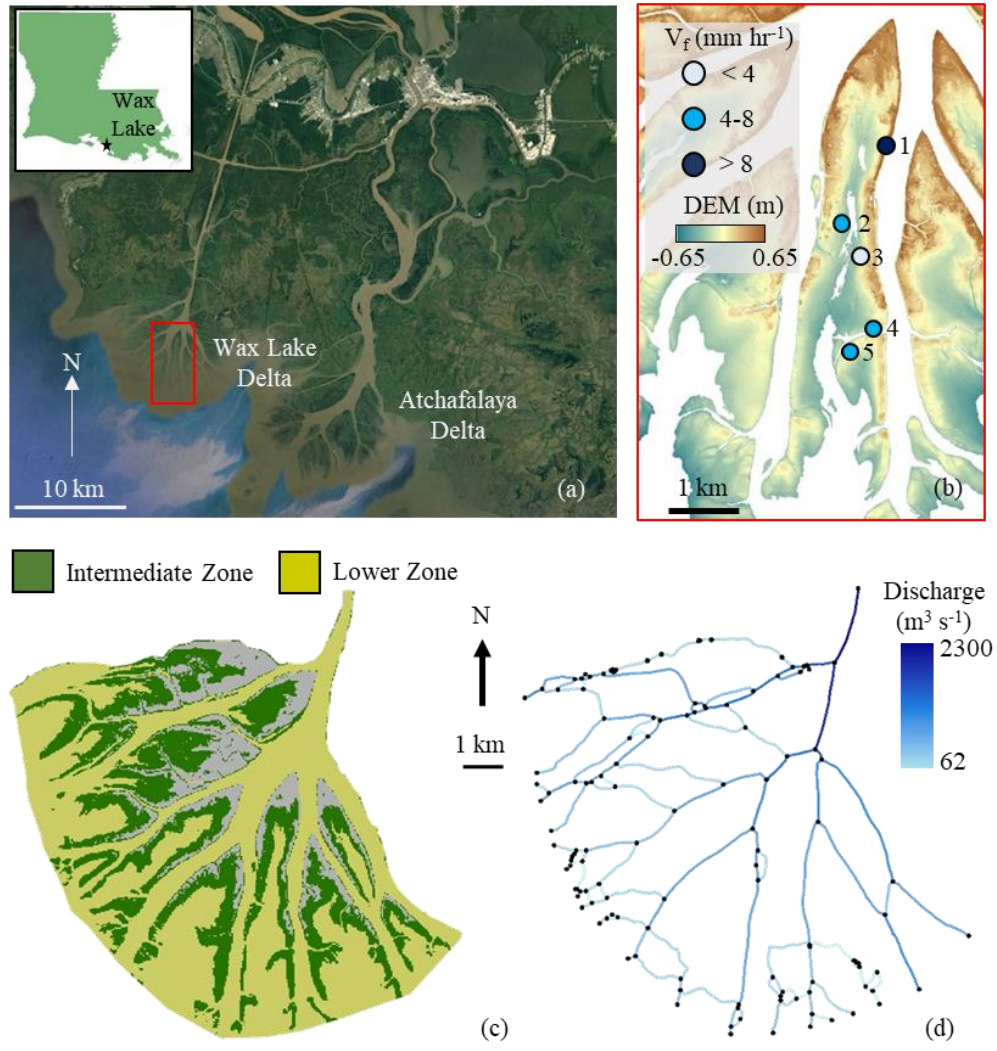


Figure 3.1 (a) Wax Lake Delta, located just west of the Atchafalaya delta. (b) Sampling was done within five daily sites (1-5) spanning a range of elevations on Mike island. Within each main location, up to six benthic chambers were deployed and a mass removal rate ( $V_f$ ) calculated for each chamber. The colors of dots indicate average mass removal rate of nitrate for each of the five sample clusters. (c) Two ecogeomorphic zones were defined based on elevation. Subaerial sections (grey) are not included in the analysis. (d) The channel network was represented as a series of links and nodes and is color-coded by median discharge from Wax Lake Outlet at Calumet, LA (USGS Gage #07381590) at the time of sampling (June 23-27, 2018).

3.2. Methods  
*Study Site*

Wax Lake Delta is an actively-prograding river-dominated delta located in Atchafalaya Bay (Louisiana) and is characterized by a number of arrowhead-shaped islands surrounded by distributary channels (Figure 3.1a-c). The delta developed after the dredging of an artificial channel in 1941 by the US Army Corps of Engineers (Fisk, 1952) and became emergent in 1973 after record flooding (Wellner et al., 2005). Elevation ranges from below 0 to ~0.75 m, referenced to the NAVD88 datum (Wagner et al., 2017). Given that mean sea level across the delta is 0.116 m and tidal range is 0.35 m (NAVD88) (Rosen and Xu, 2013), most of the delta is submerged. The median monthly discharge for 2018 was  $3500 \text{ m}^3 \text{ s}^{-1}$  as measured at USGS Calumet, LA (Gage #07381590). Large river inputs result in low salinity conditions ( $<0.5$  ppt) throughout the delta (Shaw et al., 2013; O'Connor and Moffett, 2014).

Wax Lake Delta can be divided into ecogeomorphic zones based on land surface elevation and vegetation species (Johnson et al., 1985; Olliver and Edmonds, 2017). The highest elevations (above 0.25 m and approximately 13% of the delta) include north-pointing island apexes and are dominated by colonies of *Salix nigra* (Black Willow) (Johnson, et al., 1985; Paola et al., 2011; Carle et al., 2014). For this study, I exclude this upper ecogeomorphic zone because it was generally subaerial throughout my field measurements, and nutrient removal rates in unsaturated soils cannot be estimated from my methods. Intermediate elevations (between -0.12 and 0.25 m, referenced to the NAVD88 datum) include submerged or intertidal levees along channel edges. The intermediate ecogeomorphic zone hosts *Colocasia esculenta* (elephant ear) interspersed with other herbaceous vegetation, such as *Polygonum punctatum* (dotted smartweed).

These herbaceous species can also organize in large monotypic stands near the lower centers of islands (Carle, 2013; Olliver and Edmonds, 2017). The lower ecogeomorphic zone ( $< -0.12$  m) encompasses channels and embayments, or the central and distal (southern) parts of islands. These areas are continuously flooded and characterized by open water or dominated by floating-leafed vegetation such as *Nelumbo lutea* (American lotus) (Johnson et al., 1985; Carle, 2013; Olliver and Edmonds, 2017).

All field measurements were made on Mike Island, located near the center of Wax Lake Delta (Figure 3.1b) with an elevation range from approximately 0.5 m at the apex (north end) to -0.4 m at the distal, southern end.

#### *Field Measurements*

Benthic chambers were used to measure nitrate removal rates on Mike Island at 28 total locations clustered within 5 submerged sites, numbered in a basinward direction from north to south (Figure 3.1b; Appendix A). Specifically, a group of 5 to 6 chambers was deployed at a single site each day during the five-day field campaign between June 23 and June 27, 2018 (only one site was visited each day due to accessibility factors). The deployed group of 5-6 chambers was removed from the site at the end of each field day and redeployed at a new site at the beginning of the next field day. The coordinates of the daily sites were randomly selected from a 30-m resolution grid overlain on the eastern half of the island, which was targeted to exploit the bilateral symmetry of the island (Johnson et al., 1985). I ensured coverage across intermediate and lower elevation platforms by dividing the eastern grid into a northern and southern quadrant and sampling from both. If the selected site for a given day was deemed inaccessible by airboat or

unsafe due to water depth, a new location was randomly chosen. All chambers at a given site were spaced within approximately 30 m of the selected site's coordinates. Site 1 was located on a densely vegetated levee and was the northernmost, upstream site. Site 2 and Site 3 were centrally located within the island's embayment and were heavily and sparsely vegetated, respectively. Site 4 and Site 5 were the two southernmost, downstream sites and were located within the embayment. Site 5 was more densely vegetated than Site 4.

The chambers were constructed from translucent polyethylene barrels (88 cm tall, inner diameter of 51.4 cm) with the top and bottom barrel faces removed. The large volume of the chambers and openness to the atmosphere were chosen to minimize incubation or "bottle effects" (Figure 3.2). Closed or small benthic chambers can allow solutes and gases to accumulate or become depleted, leading to shifts away from natural water chemistry (e.g. O'Brien et al., 2012). Chambers were inserted ~12 cm below the sediment-water interface. The depth of water measured manually in the field within all chambers ranged between 0.31 and 0.53 m. Approximately 30 g of sodium chloride was added to each chamber as a conservative tracer to monitor potential evaporative losses or dilution due to water exchange across the bottom of the chamber. Salinity of all samples remained below 500 ppm. To ensure that changes in nitrate concentration would be detectable within one sampling day, nitrate concentrations were elevated above background by the addition of potassium nitrate (1.5 to 3 g of  $\text{KNO}_3^-$ ). Resulting nitrate concentrations within the chambers were approximately 1.4 to 4.8 mg N l<sup>-1</sup> greater at the start of the experiments compared to water outside the chambers (average concentration

of  $0.81 \text{ mg N l}^{-1}$ ). In order to test the effect of varying concentration on removal rate, two clusters consisting of three benthic chambers each (6 of 28 chambers) were installed less than 0.5 m apart at Site 3. Within each group, one chamber was selected as the control where nitrate concentration remained at the background value ( $0.089 \text{ mg N l}^{-1}$ ). In the other two chambers, concentrations were elevated approximately 5 and 10 times above background.

Basic water quality parameters were monitored with a Yellow Springs Instrument (YSI) ProPlus multiparameter probe to verify that temperature, dissolved oxygen concentrations, and pH remained similar between the benthic chambers and surface water throughout my measuring period (Figure 3.2). Measurements in each chamber and outside the chambers were taken at the time of sample collection (Knights, 2020). In addition to measuring basic water quality parameters, samples were collected from inside and outside the chambers for laboratory analysis of nitrogen constituents and dissolved organic carbon (DOC). During sampling, chambers were gently stirred, and approximately 60 mL was withdrawn from the middle of the water column by syringe. The samples were filtered through  $0.45 \text{ }\mu\text{m}$  Fisherbrand nylon syringe filter into an HDPE pre-rinsed bottle and immediately placed on ice. The sample volume represented, on average,  $\sim 0.72\%$  of total water in the chamber and had a negligible effect on water levels or chemical mass budgets. Samples and YSI measurements were taken before the addition of  $\text{NaCl}$  and  $\text{KNO}_3$ , immediately after, and at selected time intervals (30-90 minutes) throughout the experiment.

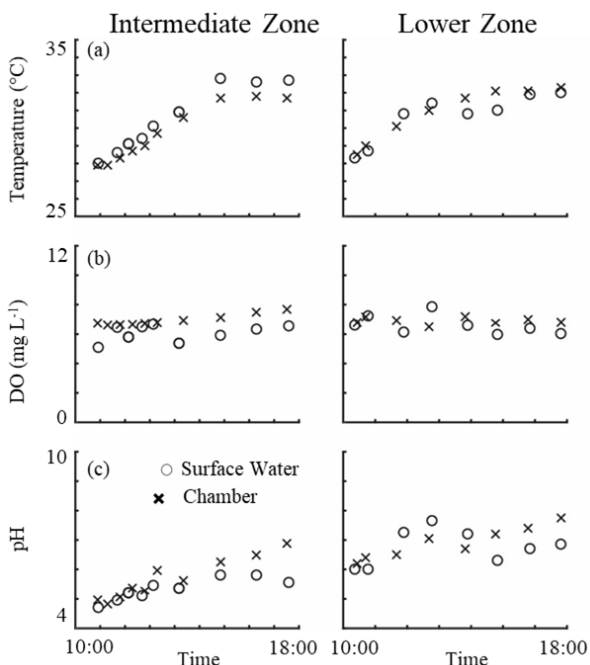


Figure 3.2. Examples of (a) temperature, (b) DO and (c) pH for 2 chambers (x) and surrounding surface water (o) from a submerged levee in the intermediate geomorphic zone (left) and embayment in the lower geomorphic zone (right). Water quality in chambers remained similar to surface water, indicating negligible incubation effects.

At the end of each field day (within 12 hours of sample collection), all samples collected that day were subsampled and filtered through 0.2  $\mu\text{m}$  Fisherbrand nylon syringe filters into combusted glass amber vials for dissolved organic carbon analysis and optical analysis of dissolved organic matter (DOM) pools. The subsample for DOC was immediately refrigerated, and the remaining sample was frozen in the original HDPE bottle for analysis of nitrate, chloride and ammonium.

Nitrate and chloride were measured using ion chromatography (ICS-2100, Dionex), with detection limits of 0.065  $\text{mg N l}^{-1}$  and 0.27  $\text{mg l}^{-1}$ , respectively (Knights, 2020). Ammonium was measured using a Skalar flow-injection nutrient analyzer with a detection limit of 0.027  $\text{mg N l}^{-1}$ . DOC was analyzed using high-temperature combustion

with an OI Aurora 1030W Analytical Total Organic Carbon Analyzer (detection limit: 0.08 mg l<sup>-1</sup>). Three-dimensional (3-D) fluorescence of optically active dissolved organic matter pools was analyzed using a Horiba Scientific Aqualog instrument. The fluorescence index (FI) of organic material was calculated using the slope of an emission curve at an excitation wavelength of 370 nm (Cory et al., 2010).

Sediment cores were collected from the benthic chambers upon the conclusion of sampling each day using a 3.6 cm diameter polyvinyl chloride (PVC) corer (depth of 5 cm). The percent of sediment lost on ignition was determined by combustion at 440°C for 4 hours and used as a measure of organic matter content (Knights, 2020). Sand, silt and clay ratios were determined by hydrometer analysis (Haverland and Hendricks, 1984).

#### *Chamber Removal Rates*

A first-order uptake rate constant ( $k$ ) was calculated for each benthic chamber from the slope of nitrate concentration (natural log) as a function of time (Figure 3.3) (Knights, 2020). All nitrate concentrations within each chamber were corrected for mixing with outside water based on changes in chloride concentration.

Mass transfer velocity ( $V_f$ ) and areal uptake rate ( $U$ ) were calculated from  $k$  (Stream Solute Workshop, 1990):

$$V_f = h \times k \quad (3.1)$$

$$U = V_f \times C \quad (3.2)$$

where  $h$  is water depth in the chamber and  $C$  is normalized concentration.  $V_f$  [L T<sup>-1</sup>] is often used as a measure of removal efficiency relative to availability (Mulholland et al., 2008) and can be considered an average downward velocity for nitrate in the water

column if removal is idealized to occur in the benthic layer.  $U$  [ $M L^{-2} T^{-1}$ ] represents the mass of nitrate removed within the water column per bed surface area per time. Because  $U$  depends linearly on concentration (Eq. 2, Stream Solute Workshop, 1990; Ensign and Doyle, 2006), and the concentration in the chambers was artificially increased, I use  $V_f$  as the dependent variable in my regression analysis, similar to others (Ensign and Doyle, 2006; Wollheim et al., 2006; Wollheim et al., 2008). Some benthic chamber results (5 out of 28 installed) were excluded from further analysis due to complications during field sampling related to impending thunderstorms (4 chambers) and a poor bottom seal connection resulting in substantial mixing of chamber water with surface water (1 chamber).

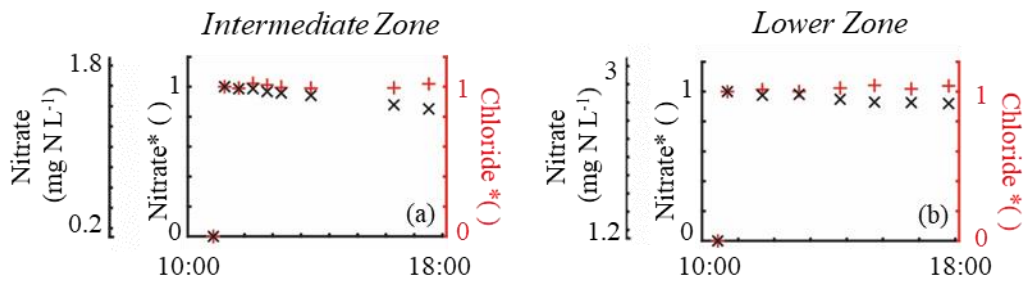


Figure 3.3. Example of individual chamber results normalized to spiked concentrations in (a) one of six submerged levee chambers, (b) one of seventeen embayment chambers. Chloride concentrations (precision: 2%) tended to remain stable while nitrate (precision: 0.8%) concentrations steadily decreased.

### Regression Analysis

Regression models were used to explore environmental controls on potential nitrate removal rates in order to upscale chamber measurements to the entire delta under observed summer conditions. The response variable ( $V_f$ ) was normalized to meet the requirements of statistical tests by applying a Box-Cox transformation (Box and Cox, 1964). Seven independent variables were considered in model development: bed

elevation, water depth, daily change in water depth, ambient nitrate concentration, percent of sediment mass lost on ignition (LOI), sediment grain size, and normalized difference vegetation index (NDVI). Water temperature, DOC concentrations, and FI did not vary between sites and therefore were not included in the regression analysis. Elevation was obtained from a 3 m DEM of Wax Lake Delta (NOAA, 2015) while water depth was measured in the field. Water surface elevation on the delta fluctuates with river discharge, tides and wind (Hiatt and Passalacqua, 2015; Sendrowski and Passalacqua, 2017) and is independent of bed elevation on daily time scales, thus, water depth and bed elevation were included as two independent variables. NDVI was obtained from preprocessed Landsat surface reflectance data via USGS Earth Resources Observation and Science on-demand interface. NDVI measures the greenness in a pixel and is used as a proxy for biomass and vegetation health (Box et al., 1989; Gamon et al., 1995; Serrano et al., 2000). It is calculated as the surface reflectance ratio of near-infrared and red bands and ranges from -1.0 to 1.0. Water absorbs near-infrared light and produces a negative NDVI while bare sediment reflects both near-infrared and red light resulting in a positive NDVI close to 0. On Wax Lake Delta, bare earth or minimally vegetated shallow water tends to result in NDVI between 0 and 0.2 (Olliver and Edmonds, 2017). Landsat imagery for NDVI calculations was acquired on June 30, 2018 (two days after the final day of benthic chamber sampling). Regression models were ranked by Akaike information criteria (AIC) (Akaike, 1974) and variables were selected using backwards stepwise algorithms in R.

### *Upscaling Calculations*

To explore spatial patterns of reactivity across the delta, two independent but complementary approaches were used to upscale benthic chamber measurements of nitrate removal during summer conditions. The first method treats the delta like a static lake, i.e. transport is not considered, and yields spatially distributed potential removal rates based on reaction potentials over all submerged regions of the delta. The second method treats the delta like a network of distributary channels, considers transport, and yields removal rates along each channel segment within the network.

For the method examining reaction potential based on static environmental conditions, I used a regression model to estimate  $V_f$  on a 30-meter by 30-meter resolution grid over the submerged portions of the delta. Subaerial regions were considered those with elevations above 0.25 m. This approach is coarse, as water levels vary over the delta due to wind. Total potential nitrate removal over the submerged delta ( $R$  [ $M T^{-1}$ ]) was estimated by summing the potential removal in each grid cell, assuming the median measured surface water nitrate concentration ( $C$  [ $M L^3$ ]) of  $0.95 \text{ mg N l}^{-1}$  in each cell:

$$R = AC \sum_{i=1}^n V_{fi} \quad (3.3)$$

where  $A$  [ $L^2$ ] is cell area ( $900 \text{ m}^2$ ), and  $V_{fi}$  is the cell-specific mass transfer velocity from the regression model. It is important to note that  $C$  likely varies over the delta due to removal processes, but samples from this study and monitoring stations are too sparse to characterize the variability, so I used the mean from my surface water samples as a best estimate.

I used stream spiraling theory as a second approach to estimate nitrate loss along the network of channels in the delta (Newbold et al., 1981; Mulholland et al., 1985;

Wollheim et al., 2006; Ensign and Doyle 2006; Tank et al., 2006; Wollheim et al., 2008; Ye et al., 2017). Briefly, stream spiraling theory considers the integrated effect of water velocity and biochemical demand, typically envisioned to occur in the bed, on downstream nutrient transport and removal. Nitrate flux exported from each link,  $i$ , in the channel network was determined as:

$$Q_{down}^i C_{down}^i = Q^i C^i \times \exp\left(\frac{-v_f}{H_L^i}\right) \quad (3.4)$$

where  $Q_{down}^i$  [ $L^3 T^{-1}$ ] and  $C_{down}^i$  [ $M L^{-3}$ ] are the discharge and solute concentration of the adjoining link(s) immediately downstream of link  $i$ , and  $Q^i$  and  $C^i$  are the discharge and concentration of the current link. The exponential term is the transfer efficiency or fraction of nitrate that remains in the water column after transport through link  $i$ .  $H_L$  represents the hydraulic load, defined as:

$$H_L^i = \frac{Q^i}{w^i L^i} \quad (3.5)$$

where  $w^i$  and  $L^i$  are the width and length of the current link respectively (Wollheim et al., 2006). At the inlet of Wax Lake Delta, I assumed an incoming nitrate concentration of  $0.95 \text{ mg N l}^{-1}$  and discharge of  $2300 \text{ m}^3 \text{ s}^{-1}$  (median at USGS Gage 07381590 during the time of fieldwork). Unlike the flooded-delta upscaling approach, the channel network analysis does not require a specification of  $V_f$  in off-channel storage zones, which are considered to contribute implicitly to removal along channels in stream spiraling theory. Because it is unclear how to attribute  $V_f$  in channels and their adjacent off-channel storage zones to one link-scale value of  $V_f$ , I assumed all benthic chamber measurements were equally plausible representations of  $V_f$  along links and assigned a single mean  $V_f$

across all links. Though simplistic, this approach is similar to approaches by Wolheim et al. (2006) and Ensign and Doyle (2006). To quantify uncertainty, I repeated the calculation with minimum and maximum  $V_f$  values from my observations.

$H_L^i$  of each channel link was determined based on remotely-sensed surface water observations and a simple flux partitioning scheme, after Tejedor et al. (2015). RivGraph, a Python package (Schwenk et al., 2018; Schwenk et al., 2020), was used to vectorize the channel network from a georeferenced binary image obtained from a 3-m DEM (2012) of Wax Lake Delta (NOAA, 2015) delineating channels from land, resulting in a set of connected links and nodes. RivGraph uses the user-prescribed locations of inlet and outlet nodes, as well as morphologic features obtained from the masks (e.g., link orientation relative to neighboring links and the general downstream direction) to assign flow directions and compute widths of each link. A fractional discharge was computed for each link by assuming a unit discharge at the delta's apex and partitioning this discharge proportionally to the downstream channel widths at each bifurcation or trifurcation (e.g. Tejedor et al., 2017). Local discharge within each channel link was obtained by multiplying the fractional discharge by the observed mean daily discharge over the field sampling period at the delta apex ( $2300 \text{ m}^3 \text{ s}^{-1}$  USGS Gage 07381590, Wax Lake Outlet at Calumet, LA).

### 3.3. Results

#### *Surface Water Chemistry*

Surface water nitrate concentrations varied between 0.07 and 1.2 mg N l<sup>-1</sup> across all chamber locations on Mike Island (mean and median of 0.81 and 0.95 mg N l<sup>-1</sup>,

respectively). The concentration was lowest ( $< 0.1 \text{ mg N l}^{-1}$ ) on the densely vegetated submerged levee of Site 1 (located most upstream). Concentration was greatest ( $>1.0 \text{ mg N l}^{-1}$ ) within the centrally located embayment of Sites 2 and 4. Surface water chloride concentrations did not vary as widely as nitrate across the island (mean of  $20 \text{ mg l}^{-1}$  range of  $18\text{-}22 \text{ mg l}^{-1}$ ). Thus, nitrate to chloride ratios were smallest ( $0.019$ ) at Site 1 and greatest ( $0.26$ ) at Site 4, suggesting substantial nitrate removal occurred at Site 1 (Figure 3.4).

DOC concentration in surface water averaged  $5.1 \text{ mg l}^{-1}$  (range of  $1.1 \text{ mg l}^{-1}$ ) across all sites. Fluorescence index ranged from  $1.58$  to  $1.63$ , indicating a relatively consistent mixture of organic matter sources. For comparison, values  $>1.8$  indicate microbial sources, while values  $<1.4$  indicate terrestrial sources (McKnight et al., 2001).

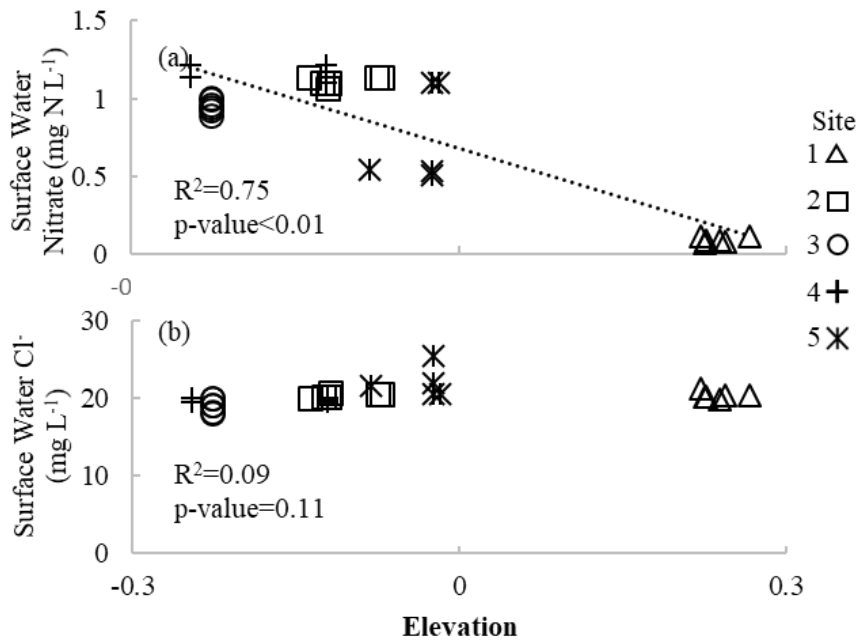


Figure 3.4. Surface water nitrate (a, precision:0.8%) decreases with elevation compared to chloride (b, precision:2%) indicating preferential nitrate processing at higher elevation (levees) on Mike Island.

### *Vegetation*

NDVI across benthic chamber locations ranged from 0.39 at Site 5 (located most downstream within the lower ecogeomorphic zone) to 0.82 at Site 1 (most upstream site, in the intermediate ecogeomorphic zone). Greater NDVI along submerged levees of the intermediate ecogeomorphic zone corresponded to observed dense stands of healthy vegetation. *Colocasia esculenta* (elephant ear) and algal mats were exclusively found in the intermediate ecogeomorphic zone (Site 1). Submerged vegetation such as *Heteranthera dubia* (water star grass) and emergent vegetation like *Sagittaria platyphylla* was found at all sites except Site 3 (in an open, less vegetated region of the lower ecogeomorphic zone). Floating-leafed vegetation, primarily *Nelumbo lutea* (American lotus), was found at all sites.

### *Sediment Properties*

Percent of mass lost on ignition (LOI) averaged  $2.1\% \pm 2.7\%$  across sites. Sediments were silt- and sand-rich with silt content (grain size between 4 and 62.5 microns) ranging from 33 to 79% and sand content (grain size greater than 62.5 microns) ranging from 2% to 60%. Clay content ranged from 0 to 25%. Site 5 (the most downstream) had the greatest sand content (60%) and lowest average LOI (0.74%), while Site 1 (a more proximal and densely vegetated site) had the greatest average LOI (4.8%).

### *Nitrate Removal*

Nitrate removal rates, reported as a mass transfer velocity ( $V_f$ ), ranged from 1.1 to  $19 \text{ mm hr}^{-1}$  within individual chambers (Figure 3.1). The average  $V_f$  across chambers at each site was smallest within the unvegetated lower ecogeographic zone of Site 3 (2.8

mm hr<sup>-1</sup>) and greatest within the densely vegetated intermediate ecogeomorphic zone of Site 1 (13 mm hr<sup>-1</sup>). The high removal kinetics at Site 1 were not only reflected in greater  $V_f$  (2.8 times greater than the other sites) but also the lowest surface water nitrate concentration (average of 0.089 mg N l<sup>-1</sup> compared to 0.99 mg N l<sup>-1</sup> at all other sites).

Within the two clusters of closely spaced benthic chambers,  $U$  increased almost linearly with initial nitrate concentration (Figure 3.5).  $V_f$  appears to follow an exponential relationship with nitrate concentration as reported elsewhere (Covino et al., 2010), however, this relationship is not definitive with only three points (Figure 3.5).  $V_f$  was greatest (5.7 and 4.3 mm hr<sup>-1</sup>) in the unspiked chambers (initial concentration ~1 mg l<sup>-1</sup>).

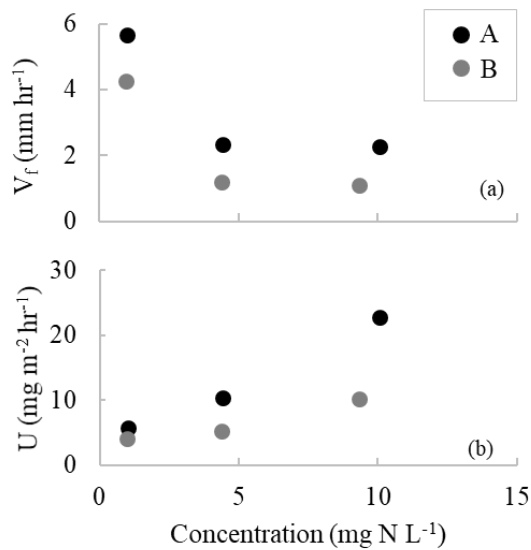


Figure 3.5. The effects of increasing concentration on mass transfer rate ( $V_f$ ) and aerial uptake ( $U$ ) on Mike Island. Two clusters (A and B) of three closely spaced chambers were spiked with various amounts of nitrate. Each cluster had 3 chambers with starting concentrations of ~1x, 5x, and 10x natural surface water. The centers of the two clusters were located approximately 3 m apart from one another at Site 1, and I assume chambers within each cluster had similar reactivities such that only the initial nitrate concentrations differed. The cause of variability between cluster A and B is uncertain, but could be due to heterogeneity in bed surface organic matter that may control for nitrate removal.

### *Regression and Areal Upscaling*

Based on the stepwise algorithm, the regression model (Figure 3.6) included measures of vegetation and nitrate concentration:

$$V_f = \exp (0.035 + 3.37NDVI - 0.17NO_3) \quad (3.6)$$

where  $NDVI$  is normalized difference vegetation index [unitless] and  $NO_3$  is nitrate concentration (in this case, spiked concentration inside chambers) [ $\text{mg N l}^{-1}$ ]. This model explains 72% of the variability in nitrate uptake measured during the experiments.

Solving Equation (6) under mean observed conditions at the chamber locations ( $NDVI$  of 0.65 and  $NO_3$  of  $0.81 \text{ mg N l}^{-1}$ ) results in an expected  $V_f$  of  $8.1 \text{ mm hr}^{-1}$ . Note, this calculation uses the mean observed surface water nitrate concentration to estimate  $V_f$  under natural conditions, as can be expected to occur outside the chambers, rather than manipulated conditions inside the chambers. Holding nitrate concentration constant, as  $NDVI$  increases from the minimum (0.39) to the maximum (0.82) observed across chamber locations (~110% increase), the calculated  $V_f$  responds by ~326% (3.4 to  $14 \text{ mm hr}^{-1}$ ). In contrast, an approximate 17-fold increase in surface water nitrate concentration ( $0.07$  to  $1.2 \text{ mg N l}^{-1}$ ) results in a relatively small 18% decrease in nitrate removal efficiency (i.e. calculated  $V_f$  from  $9.2$  to  $7.5 \text{ mm hr}^{-1}$ ).

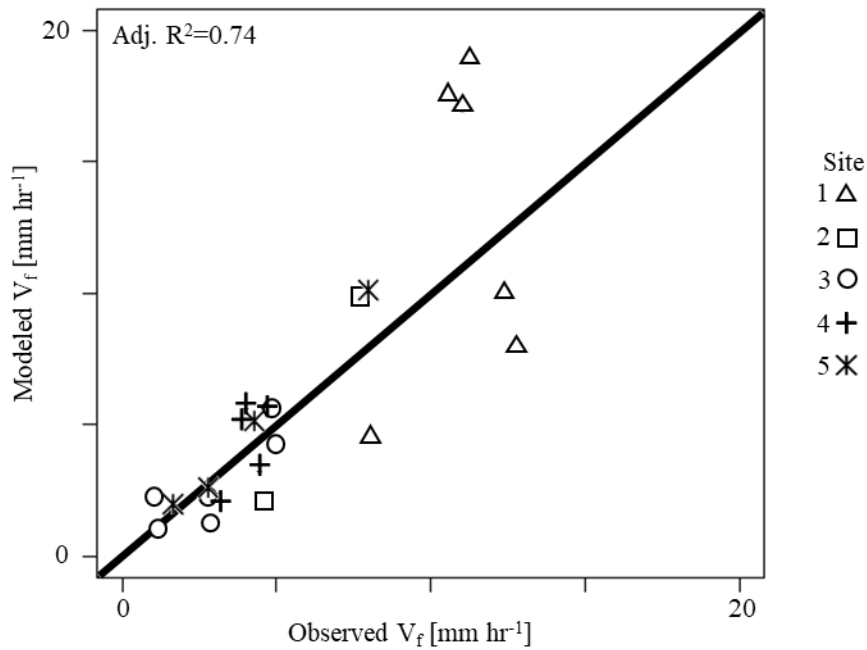


Figure 3.6. Scatter plots of predicted and observed  $V_f$ . Bold line indicates 1:1 relationship.

Using the regression model and the median surface water nitrate concentration of  $0.95 \text{ mg N l}^{-1}$ , I estimate  $V_f$  to vary from 0.25 to 18 across all submerged regions (intermediate and lower zones) (Figure 3.7a). Integrated across the submerged delta, the potential nitrate removal rate is  $230 \text{ kg hr}^{-1}$  and ranges from 16-383  $\text{kg hr}^{-1}$  under scenarios of low ( $0.05 \text{ mg N l}^{-1}$ ) and high ( $1.5 \text{ mg N l}^{-1}$ ) nitrate concentrations typically observed in the lower Atchafalaya River (Lane et al., 2002; BryantMason et al., 2013; Joung et al., 2019) and spanning the range of surface water nitrate concentration observed in the field. Assuming a discharge of  $2300 \text{ m}^3 \text{ s}^{-1}$ , this represents a removal of 3.4% of the incoming nitrate load (range of 4.0 to 3.1% under low to high concentration scenarios). The greatest potential removal rates are generally located in areas with the greatest

amounts of vegetation, on higher northern islands of the western half of the delta and the levees of lower islands (Figure 3.7a). The intermediate elevation ecogeomorphic zone is responsible for 70% of the estimated potential nitrate removal though it only represents 33% of the analyzed inundated area (Table 1). This suggests that inundated delta islands, particularly those with dense vegetation, act as hotspots for biogeochemical processing.

#### *Channel Network Analysis*

Channel network calculations based on the median observed  $V_f$  ( $5.1 \text{ mm hr}^{-1}$ ) in the field (Eq. 3.4) show that each channel link removes only a small percentage ( $<0.1\%$ ) of the total nitrate entering the delta (Figure 3.7c). The maximum removal efficiency in an individual link is 1.9% with most links removing  $< 1\%$  of the nitrate they receive (Figure 3.7b). The estimated removal rate for the collective network is  $79 \text{ kg hr}^{-1}$  and ranges from 18 to  $275 \text{ kg hr}^{-1}$  under scenarios of minimum to maximum  $V_f$  observed in chambers. This represents 1.0% of the incoming nitrate load (range of 0.2% to 3.5% for minimum to maximum  $V_f$ ), which agrees well with the aerial method of upscaling potential removal across the submerged delta. Channel network analysis further indicates that secondary channels and more distal portions of the delta are generally more efficient at processing nitrate (Figure 3.7b); however, these secondary channels and distal bifurcations individually receive small portions of the nitrate load (Figure 3.1d). Because the eastern half of Wax Lake Delta receives a greater portion of the discharge and nutrient load than the western portion, it contributes more to total removal (Figure 3.7c).

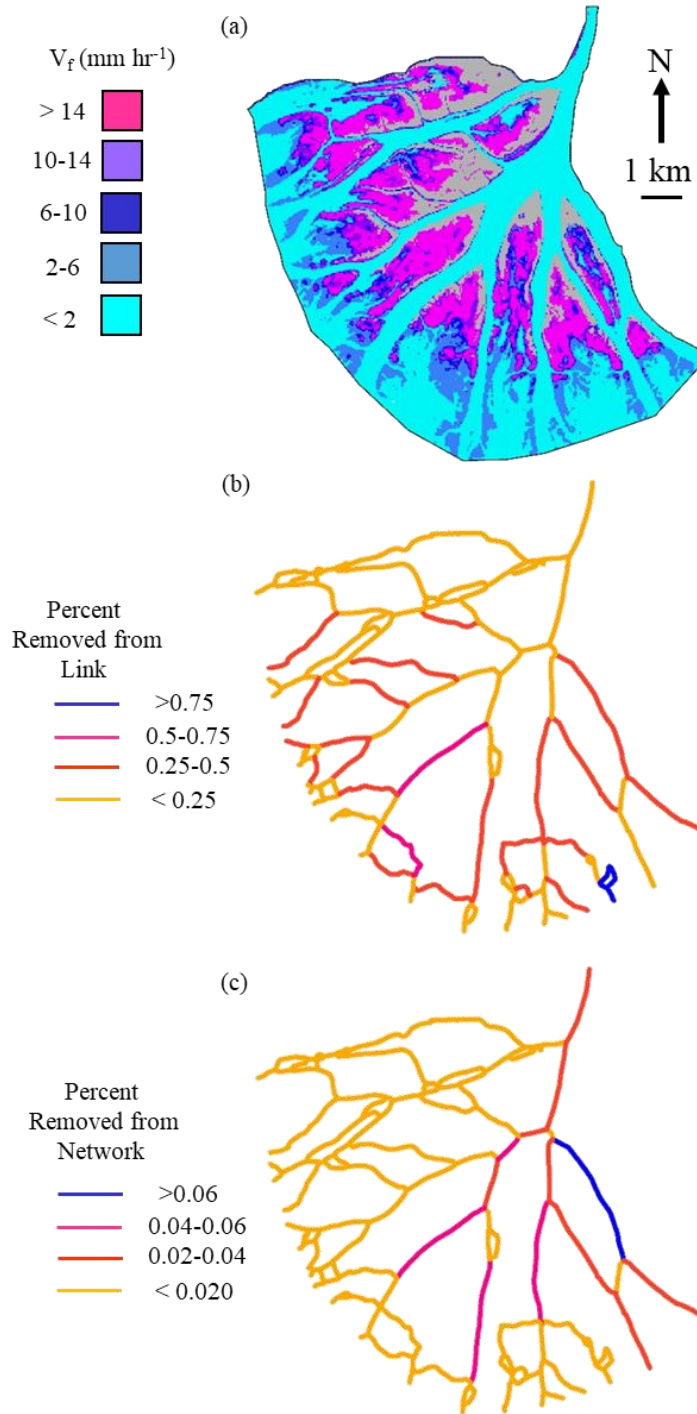


Figure 3.7. (a) Removal rate calculated using submerged-delta approach and using nutrient spiraling approaches. (b-c) Removal rate calculated using nutrient spiraling approach as a percentage of (b) amount of nitrate entering each link and (c) amount of nitrate entering the delta at the apex.

### 3.4. Discussion

#### *Environmental Controls on Nitrate Removal*

In this deltaic wetland, I show that uptake velocity ( $V_f$ ) is most sensitive to the presence and density of vegetation, as measured by NDVI (Equation 6). Nitrate retention and removal increased four-fold between zones of high and low NDVI. Therefore, nitrate removal via plant uptake is likely an important pathway on the delta. Assimilation into plant and algae biomass has previously been demonstrated to be an important nutrient removal pathway in wetlands (Vymazel, 2011; Saed and Sun, 2012). Nitrate removal by plant uptake can range from minimal to up to about 60% of total removal (Kadlec, 1997; Matheson et al., 2002; Day et al., 2004), with plant uptake removing between 4-11% of nitrogen in constructed wetlands (Matheson et al. 2012; Lin et al. 2001). In lake and estuarine sediments, up to 60% of nitrate removal is associated with plant uptake (Rysegaard et al., 1993). If plant assimilation is responsible for similarly high rates here, most of the nitrate removed could be released via mineralization during winter senescence, limiting the long-term impact of removal from the delta.

Locations with high NDVI not only reflect increased chances for plant uptake but may also reflect indirect effects of dense vegetation on other nitrate removal pathways. Detrital material in areas of high NDVI likely contributes to the organic carbon stock in soils (Weisner et al., 1994; Vymazal et al., 1999), which supplies organic carbon for denitrification, a permanent nitrate removal process. The positive relationship between NDVI and LOI (p-value =0.0021) suggests that regions of the delta with greater NDVI are more effective at trapping organic matter (Inwood et al., 2007; Baker and Vervier,

2004). Areas of the delta with greater NDVI may also have older, more developed soils due to the strongly coupled processes of sedimentation and vegetation succession in a prograding delta (Ma et al., 2018), and potential denitrification rates have been shown to increase in older soils (Henry and Twilley, 2014). Topography is yet another variable that coevolves with vegetation (Ma et al., 2018; Johnson et al., 1985) and influences soil saturation, oxidation-reduction potential, and denitrification potential. I do see a positive relationship between NDVI and elevation ( $R^2=0.61$ ,  $p\text{-value}=1.2\times 10^{-5}$ ) but cannot separate the many potential mechanisms that link these variables with net nitrate removal here. Nitrate processing depends on many biogeochemical processes that cannot be measured directly from remote sensing products, and disentangling these processes is an important area for continued research in delta wetlands.

By examining only one island, I acknowledge that my measurements come from a limited window of soil ages, organic matter contents, and soil reduction potential. NDVI across the submerged delta ranges from -0.39 to 0.92, and NDVI from my sites covers only 33% of that range (0.39 to 0.82). By applying a regression model across the entire delta, I am extrapolating my measurements to a wider range of NDVI. I also note that my regression model is not well constrained in the channels, which are areas of low NDVI, where water was too deep for safe benthic chamber deployment. However, my measured range of  $V_f$  (1.1 to 19  $\text{mm hr}^{-1}$ ) is comparable to nitrate removal in other wetlands from similar climates (Table 3.2).

The observed relationship linking greenness with nitrate removal is most representative of summertime conditions. The regression model may also perform well in

other seasons, though year-round field studies would be needed to test this. In winter months, browning vegetation results in lower NDVI values across the entire delta. This would coincide with reduced nitrate removal via plant assimilation. Denitrification also decreases with colder temperatures (Bremner and Shaw 1958; Bachand and Horne, 1999), and lower NDVI during winter months would coincide with decreasing temperatures and denitrification. Although I expect less removal during winter months, my observations are not capable of testing this.

The concentration dependence of nitrate removal rates, both in terms of uptake rate ( $U$ ) and efficiency ( $V_f$ ) (Figure 3.5), suggests that removal mechanisms are not saturated with respect to nitrate. Other studies examining nutrient removal in river networks have also reported a negative correlation between  $V_f$  and nitrate concentration but a positive relationship between aerial uptake rate ( $U$ ) and concentration (Dodds et al., 2002; O'Brien et al., 2007; Mulholland et al., 2008). The inclusion of nitrate concentration as a significant variable in the regression model makes it challenging to apply over distributed areas, as spatially explicit nitrate concentration data are not available. I compensate for this by calculating removal under conditions of high and low nitrate inflow typically observed on the delta (Lane et al., 2002; BryantMason et al., 2013; Joung et al., 2019). It is important to note that removal rate is far less sensitive to nitrate concentration as compared to greenness.

I observe a negligible effect of water depth on the removal rate. The lack of a strong relationship may be due to the relatively small range in water depths captured by my chambers (0.31 to 0.53 m). Studies in rivers have shown that as water depth

increases, the fraction of surface water interacting with a unit area of bed and its reactive biofilms decreases, leading to an inverse relationship between water depth and  $V_f$  (Ensign and Doyle, 2006; Wollheim et al., 2006; Bohlke et al., 2009). For example, relationships between  $V_f$  and depth of inland rivers were demonstrated over ranges from 0.1 to >10 m (Alexander et al., 2000; Bohlke et al., 2009). It is also possible that aquatic vegetation provides critical surfaces for biofilms (Arango et al., 2007) rendering sediment-water interactions less important in controlling the overall denitrification rate in deltas than in rivers.

I also observed no relationship between change in water depth over the sampling day and removal rate, though changes in water depth could correspond with hydrologic connectivity, solute supply, or changes in soil oxic or anoxic conditions. Furthermore, chambers that were deployed during the rising tide could have received an influx of oxygen in surrounding pore waters that might have inhibited denitrification, and vice versa during falling tide (Ensign et al., 2008). However, sampling roughly occurred over the same time period every day, which overlapped with falling tides. Furthermore, the change in water depth across each site was similar, as expected in this microtidal system. Thus, change in water depth held little explanatory power on removal rate.

#### *Delta-Scale Removal*

My calculations suggest the delta has a limited capacity to remove nitrate under typical summertime flow conditions (removal corresponds to 3.1 to 4.0% of the load based on the submerged-delta analysis and 0.2 to 3.5% based on channel network analysis). Estimates from the disparate upscaling approaches agree well with each other,

lending confidence to the result. My estimates reflect summertime removal conditions when primary production is greatest. Although removal rates are less clear in other seasons, the delta is unlikely to process nitrate at a higher rate during winter months when nitrate input into the delta and primary productivity are low. I expect that my estimated removal of up to ~4% therefore reflects upper annual limits.

My two methods of upscaling reveal unique aspects of heterogeneity in nitrate removal across the delta. The submerged-delta results suggest that islands are more biogeochemically reactive than channels, and the regions with greatest potential nitrate removal rates are the intermediate elevation ecogeomorphic zones that are ubiquitous on the northwestern islands but also common on the northern halves and subaqueous levees of southern islands (Figure 3.7a, Table 3.1). Because this method does not consider solute flow paths or nitrate supply, actual removal rates could be lower in regions that are hydrologically disconnected from channels and thus receive a low nitrate flux. This interpretation is consistent with Hiatt et al. (2018), who used particle tracking models to show that islands (both intermediate and lower ecogeomorphic zones) contribute to roughly half of all nitrate removal and that hydrologic exchange between islands and channels is an important control on nitrate fate. In comparison, the nutrient spiraling calculation shows that the eastern branches of the delta tend to be more effective at contributing to overall removal in the network (Figure 3.7c). If I integrate this result with the submerged delta patterns, the implication is that biogeochemical hotspots are likely to be the submerged but vegetated portions of the intermediate geomorphic platform along the eastern, more active channels of the delta because these zones have both high

biogeochemical demand (potential reactivity) and are likely to receive a greater supply of nutrients from the most active channels. The western portion of the delta that is more inactive consists of smaller islands at greater elevation, and while these islands may be more biogeochemically reactive (Figure 3.7a), they receive a lower nutrient load through a network of short channels with low contact times (Figure 3.7b) and therefore can contribute less to overall removal (Figure 3.7c). This implies that, if other deltas behave similarly to Wax Lake Delta, older but hydrologically disconnected portions of deltas may play a relatively small role in nutrient removal, even if those areas have high potential removal rates. Greater resolution and understanding of the interactions between reaction kinetics and transport will require the use of reactive transport models of increasing complexity.

Method	Region	Area of Delta (%)	Discharge In ( $\text{m}^3 \text{ s}^{-1}$ )	Conc. In ( $\text{mg N L}^{-1}$ )	Removal ( $\text{mm hr}^{-1}$ )	Removed (%)
Submerged-Delta	Intermediate Zone	33.3	2300	0.05-1.5	0-19*	2.1-2.7
Submerged-Delta	Lower Zone	66.7	2300	0.05-1.5	0-18*	1-1.3
Network	Channels and Immobile Storage Zones	-	2300	0.95	1.1-19	0.2-3.5

Table 3.1. Summary of input parameters and results for two methods of estimating nitrate removal in Wax Lake Delta. No channel area is used in the network calculation. Asterisks (\*) indicate potential removal rates, where transport is not considered.

### *Response to Environmental Changes*

The future nitrate buffering capacity of the delta will depend on climatic and anthropogenic changes. For instance, if nitrate load increases due to upstream land use or climatic changes, the delta will remove a smaller portion of the load, based on the

observed negative relationship between nitrate concentration and mass transfer velocity (Figure 3.5a). Conversely, if the nitrate load decreases due to improvements in management and policy, the delta will become even more effective at reducing the incoming load. However, these trends are based on field observations from a single summertime season and flow condition. Temperature is also known to influence the mass transfer velocity in rivers (Seitzinger et al., 1988; Donner et al., 2002) and will increase with a changing climate. Furthermore, climate change will bring more extreme storm and flood events (IPCC, 2013; Herring et al., 2014) that will erode portions of the delta and drive changes in vegetation (Carle et al., 2015), one of the strongest predictors of mass transfer velocity in my models. Storms may have a long-term negative impact on the buffering capacity of the delta by eroding wetlands. However, the subaerial regions of delta islands would be most resilient as they are stabilized by more established vegetation communities (Braskerud et al., 2001; Day et al., 2011; Rosen et al., 2013; Nardin and Edmonds, 2014), and these are some of the most effective sites of nutrient removal. If the intermediate elevation embayments remain protected by levees (Figure 3.7a), their removal function may remain intact too. Flooding may further increase nitrate removal on the delta as accretion associated with floods may expand wetland area available for nutrient buffering (Allen et al., 2012; Wagner et al., 2017).

During flood events, partially enclosed embayments could function as activated control points, as an increase in hydrologic connectivity could deliver more nitrate to areas of greater biogeochemical processing (Bernhardt et al., 2017). However, even if the removal rate temporarily increases across inundated areas during a flood, the removal

efficiency may decrease if the nitrate load drastically increases. In other words, embayments may never receive enough water to disproportionately affect overall nutrient fluxes through the delta and therefore may never fit the definition of “control points” conceptualized by Bernhardt et al. (2017). In order to quantify changes in nitrate retention over rising and falling water levels, transient reactive transport models are needed.

Source	Environment	Method	$V_f$ (mm hr <sup>-1</sup> )	U (mg m <sup>-2</sup> hr <sup>-1</sup> )
This Study	Wax Lake Delta	open chamber <sup>1</sup>	1.1-19	7.2-450
Henry & Twilley (2014)	Wax Lake Delta	sediment core incubation <sup>2</sup>	0-1.01	0-3.9
Scott et al. (2008)	Freshwater Wetland	sediment core incubation <sup>2</sup>	21.8-45	3.3-17
Rysgaard et al. (1996)	Coastal Lagoon	sediment core incubation <sup>2</sup>	0-150	0-3.8
Yu et al. (2006)	Coastal Louisiana	benthic chamber <sup>1</sup>	0-4.9	0-56
Childs et al. (2002)	Coastal Louisiana	Acetylene Inhibition <sup>2</sup>	0.40-1.1	2.5-6.7
DeLaune et al. (2005)	Coastal Louisiana	Acetylene Inhibition <sup>2</sup>	4.5-15	2.8-9.2
Lindau et al. (2008)	Coastal Louisiana	Acetylene Inhibition <sup>2</sup>	0.002-2.9	0.01-18

Table 3.2. Removal rate in this study is comparable to other coastal wetlands.

<sup>1</sup> Net Removal

<sup>2</sup> Denitrification

### 3.5. Conclusion

Nitrate removal rates vary across ecogeomorphic zones on Wax Lake Delta, and the best predictor of the potential summertime rate is NDVI, a proxy for vegetation photosynthetic activity and greenness that is widely available. My upscaling calculations suggest that potential hotspots of nitrate removal are located in intermediate-elevation ecogeomorphic zones where NDVI tends to be highest during the summer. Thus, older islands in the northwest region of Wax Lake Delta and the northern perimeters of

younger southeastern islands, where NDVI values are greatest, have the potential to contribute the most to nitrate removal. However, an alternative nutrient spiraling calculation shows that the supply of nitrate across the channel network limits actual removal rates. Because the eastern portion of the channel network receives more water and nutrients, densely vegetated levees on the eastern half of the delta may contribute more to nitrate removal, as they are more hydrologically connected and have the potential to be biogeochemically “hot.” Estimates of nutrient removal and flow to coastal waters are essential for management practices and policy guidance. Importantly, estimates from this study using two different approaches both show that the capacity of Wax Lake Delta to remove nitrate from its receiving waters is limited to less than 4%. This research helps understand the biophysical factors that control heterogeneity in nutrient removal rates in deltas. Future work incorporating numerical simulations of variable flow (riverine, tidal and wind-driven) coupled with spatially heterogeneous removal kinetics will improve estimates of nitrate fate in dynamic delta systems.

## **Chapter 4. The Relationship between Delta Form and Nitrate Removal Function: Computer Modeling Experiments**

### 4.1. Introduction

Deltas receive vast quantities of inorganic nitrogen from land-based human activities in river basins. Excess inorganic nitrogen accelerates the growth of algae and reduces water quality along the coastal ocean (Rabalais et al., 2002; Diaz and Rosenberg, 2008; Rabalais et al., 2017). Harmful algal blooms outcompete aquatic organisms and consume oxygen upon decay (Diaz and Rosenberg, 2008), which stresses animal populations, increases mortality, and disrupts marine and aquatic food webs (Diaz, 2001; Vaquer-Sunyer and Duarte, 2008). For example, an estimated 60 million tons of benthic life perished in vast dead zones in the Black Sea between 1970 and 1980 due to rising phosphorus and nitrogen loading (Mee, 2006).

With more than 40% of global freshwater passing through deltas before discharging to the coast, it is important to understand how deltas influence nutrient chemistry (Syvitski and Saito, 2007). Nutrients that flow through deltas can be altered by physical and biochemical processes within distributary channels and islands (Lane et al., 2003; Friedrich et al., 2003, DeLaune et al., 2005; Hiatt et al., 2018, Knights et al, in revision). Denitrification, an anaerobic, microbially mediated process that converts nitrate in water to elemental nitrogen, is the dominant pathway of nitrate loss in many coastal settings (Whitney et al., 1981; Lane et al., 2003). Other common removal pathways

include assimilation into organic matter by plants (Matheson et al., 2002; Kreililng et al., 2011), dissimilatory reduction of nitrate to ammonium (Tiedje, 1988; Burgin and Hamilton, 2007), and anaerobic ammonium oxidation (Jetten et al., 1998; Rysgaard et al., 2004).

Evidence suggests that most nitrate removal in deltas occurs in wetlands associated with delta islands as opposed to channels (Leopold, 1970; McClain et al., 2003; Lane et al., 2003; DeLaune et al., 2005). For example, Hiatt et al., (2018) examined the potential for nitrate removal in Wax Lake Delta as a function of exposure time and estimated that, depending on island-channel connectivity, inundated islands could remove up to 73% of nitrate they receive from surface water. Similarly, a statistical model suggested that potential nitrate removal rates generally increase with NDVI, a remote measure of greenness due to vegetation that is typically greatest near island heads (Knights et al., in revision). Henry and Twilley (2014) observed positive correlations between delta island age and nitrate removal. These studies demonstrate the potential for deltaic wetlands to remove nitrate, given adequate connection between zones of rapid transport and high reactivity (Powers et al., 2012). However, the connectivity of biogeochemically “hot” wetlands to upstream nutrient sources is not well constrained in many deltas (DeLaune et al., 2005; Hiatt et al., 2018) and likely varies substantially with delta morphology. To gain insight into the potential retention of nitrate in deltas, it is necessary to understand how flow interacts with biogeochemically reactive wetland areas.

In general, transport patterns and rates within deltas depend on morphologic characteristics such as topset gradient, river junction geometry, channel geometry, and the number of distributary channels (Bolla Pittaluga et al., 2003; Edmonds and Slingerland., 2008; Carlson et al., 2018), though flow also varies with vegetation, tides, and wind (Kroger et al., 2009; Nepf, 2012; Buschman et al., 2010; Salles et al., 2015). The morphology of deltas has been studied for several decades (Galloway 1975), but recent advances in both remote sensing and data analysis have led to new morphometrics for characterizing delta shape and growth that may hold insights into the potential for deltas to retain nutrients. Shoreline characteristics such as delta front length and shoreline rugosity are important descriptors of deltaic complexity that are influenced partly by grain size distribution (Wolinksky et al., 2010; Yu et al., 2014; Caldwell and Edmonds, 2014). Other shoreline metrics such as discontinuity associated with channel presence and shoreline sinuosity have been proposed to distinguish tidal, wave and river-dominated deltas (Geleynse et al., 2012). In addition to shoreline metrics, deltaic channel networks and subnetworks have been quantitatively described in terms of the number of channels and channel width distribution (Syvitski and Saito, 2007; Nardin and Fagherazzi, 2012; Piliouras and Rowland, 2020). Metrics quantifying island morphology such as island size distribution and nearest edge distance (proximity of points on islands to the nearest channel) are also commonly used (Edmonds et al., 2011; Piliouras and Rowland; 2020) and may hold predictive power for a delta's nutrient removal efficiency. Recently, graph-theoretic frameworks have been used to quantify delta morphological complexity resulting from varying grain sizes in terms of entropy rates, number of

alternatives pathways, and channel leakage indices (Tejedor et al., 2016; Tejedor et al., 2017; Tejedor et al., 2019).

In this study, I consider how unique delta morphologies, resulting from various grain size distributions, control nitrate removal processes in river-dominated deltas. I hypothesize that nitrate removal efficiency increases with increasing delta topset slope, an indicator of the portion of the delta that sits above sea level where biogeochemically active wetlands form. I further hypothesize that nitrate removal efficiency increases with topologic complexity as measured by non-local entropy, number of alternative pathways for discharging water at channel mouths, and leakage indices between channel subnetworks. Finally, I hypothesize that the mass of nitrate removed increases with delta top area as more surface area provides more opportunity for benthic processing.

I tested these hypotheses with a numerical experiment consisting of 6 synthetically generated deltas with distinct networks and morphology. To lend confidence in the numerical approach, I begin by validating a two-dimensional reactive nitrate transport model for Wax Lake Delta (Louisiana, USA) using measured nitrate concentrations from samples collected on one island over a single week in June of 2018. The goal was not to reproduce all details of the observed nitrate concentrations but the general trends and magnitudes of removal. I then present a sensitivity study in which I analyze nitrate removal on the 6 synthetic deltas (Caldwell and Edmonds, 2014). These findings are useful for inferring potential nutrient removal rates in the world's temperate deltas based on easily quantifiable morphometrics and guiding delta management and restoration decisions for water quality outcomes.

## 4.2. Methods

Model development was performed using Delft3D, a morphodynamic modeling suite with fluid flow, sediment transport, and water quality modules (Deltares 2014, Deltares 2016). Delft3D has been widely used to simulate flow and sediment transport in coastal rivers, estuaries and deltas (Lesser et al., 2004; Van Maren, 2007; Edmonds and Slingerland 2007; Caldwell and Edmonds 2014; Sawyer et al., 2015; Olliver et al., 2020). The fluid flow component solves the depth-averaged, shallow-water equations from the Reynolds-averaged Navier-Stokes equations for incompressible free-surface flow. Thus, it is appropriate for predicting flow in deltas where vertical momentum is relatively small and negligible (Lesser et al., 2004).

Reactive transport was solved using the two-dimensional advection-dispersion reaction equation:

$$\frac{\partial C}{\partial t} = -v_x \frac{\partial C}{\partial x} + D_x \frac{\partial^2 C}{\partial x^2} - v_y \frac{\partial C}{\partial y} + D_y \frac{\partial^2 C}{\partial y^2} - kC \quad (4.1)$$

where  $C$  is nitrate concentration in water [ $\text{M L}^{-3}$ ],  $t$  is time, and  $v_x$  and  $v_y$  are flow velocities in the  $x$  and  $y$  directions, respectively [ $\text{L T}^{-1}$ ].  $D_x$  and  $D_y$  are the hydrodynamic dispersion coefficients in the  $x$  and  $y$  directions, respectively [ $\text{L}^2 \text{T}^{-1}$ ].  $k$  [ $\text{T}^{-1}$ ] is the first-order nitrate removal rate, equivalent to  $V_f/h$ , where  $V_f$  is the nitrate mass transfer velocity [ $\text{L T}^{-1}$ ], and  $h$  is water depth. Equation 4.1 assumes that nitrate removal proceeds as a lumped first-order reaction due to the combined effects of reactions that remove nitrate from the water column (i.e. denitrification, assimilation, and DNRA) and processes that produce it (i.e. nitrification).

Removal kinetics have been shown to vary spatially across deltas (Henry and Twilley, 2014; Knights et al., in revision). Knights et al. (in revision) showed that summertime nitrate removal rates on Wax Lake Delta have a high, positive correlation with NDVI. Other environmental parameters with explanatory power included nitrate concentration and bed elevation. Because vegetation distribution and topography are interrelated in deltaic environments (Cahoon et al., 2011; Ma et al., 2018), and NDVI is not available for synthetic deltas, I use the following equation for nitrate removal kinetics, which depends on elevation instead of NDVI and has been shown to hold statistically high explanatory power for nitrate removal (Knights et al., in revision):

$$V_f = ae^{bz} \quad (4.2)$$

where  $a$  is  $8.41 \text{ m s}^{-1}$ ,  $b$  is  $2.01 \text{ m}^{-1}$ , and  $z$  is bed elevation in meters referenced to mean lower low sea level (MLLW). The coefficient of determination ( $R^2$ ) is 0.62. For a detailed discussion on the parameterization of  $V_f$ , see Knights et al. (in revision).

Equation 4.1 was solved for nitrate removal using the process library configuration in the water quality module of Delft3D (Delft3D-WAQ) with boundary conditions and other model specifications described below.

#### *Wax Lake Delta Test Case*

To test the approach for simulating typical nitrate transport behavior in a temperate, river-dominated delta, I coupled reactive transport with a fully calibrated hydrodynamic model of Wax Lake Delta (Olliver et al., 2020) and compared predicted nitrate concentration with observed values (Figure 4.1). Observations were made on Mike Island using grab samples between June 23 and June 27, 2018. One site was visited each

day, and samples were collected at approximately hourly rates throughout the day. Details on sample collection and analysis are available in Chapter 3. In brief, approximately 60 mL were collected from the water column, filtered to 0.45  $\mu\text{m}$ , immediately placed on ice, and then frozen until analysis for nitrate concentration using ion chromatography (ICS-2100, Dionex) with detection limits of 0.27  $\text{mg l}^{-1}$  (Appendix A).

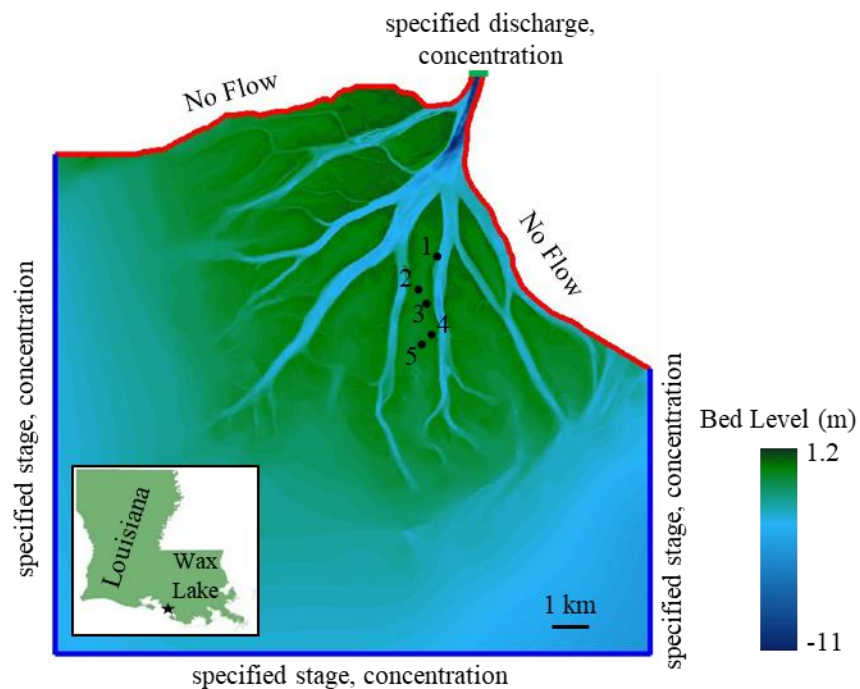


Figure 4.1. Model domain and boundary conditions for Wax Lake Delta in southern Louisiana, USA (inset). No flow boundaries are in red. Constant nitrate concentration and time varying discharge were specified at the upstream boundary (green). Constant concentration and time varying stage were specified at the downstream boundaries (blue). Five sites on Mike Island were used to validate the model.

The model timeframe spanned June 20-27, 2018 in order to encompass three days of spin-up and the subsequent period of field observations. Preliminary testing showed that three days was enough to reach dynamic equilibrium in solute transport. The

hydrodynamic component of the model has been calibrated previously using field-measured water depths in the shallow embayments of Mike Island and is described in detail by Olliver et al. (2020). Briefly, the model bathymetry was created from a 20 m resolution seamless DEM constructed using lidar data over subaerial regions, single-beam bathymetric surveys of the delta front, and multi-beam bathymetric surveys of the distributary channels (NOAA, 2015, Shaw et al., 2016). As in the calibration study, I forced the hydrodynamic model with upstream water discharge from USGS Calumet Gauge, #07381600 and downstream tidal stage levels from NOAA Amerada Pass Gauge, #8764227. The hydrodynamic model time step was 15 seconds.

Reactive transport simulations were run using output water depths and velocities from the hydrodynamic model (Figure 4.1). The river inlet boundary was assigned a linearly increasing nitrate concentration from 1.28 to 1.58 mg N l<sup>-1</sup> over the eight-day simulation period based on observations from USGS gauge 07381590 on the Lower Atchafalaya at Morgan City. Downstream (basinward) boundaries were treated as open concentration boundaries (Figure 4.1) with a Thatcher-Harleman time lag that governs the transition from an advective flux outlet when flow exits the boundary to a specified concentration inlet when flow reverses. The concentration of inflowing water was set to the average concentration of water that exited the domain over the preceding 16 hours (longer than half the tidal period). This long averaging period (chosen based on sensitivity testing) helped maintain an approximately stable nitrate concentration in the distal basin that depended largely on nitrate export from the delta. No Thatcher-Harleman transition was needed at the river inlet boundary, as all flow was consistently directed

into the domain. The initial nitrate concentration was set at  $1.28 \text{ mg N l}^{-1}$  across the delta. The time step for the water quality model was 15 minutes.

### Sensitivity Study

I modeled steady nitrate transport and removal in 6 synthetic river-dominated deltas created in Delft3D. The simulated deltas were built using lognormal distributions of incoming sediment size with median grain diameters ( $D_{50}$ ) varying from 0.01 to 1 mm, resulting in deltas with unique morphologies (Figure 4.2). Details of the delta creation are discussed in Caldwell and Edmonds (2014). In brief, delta evolution was simulated in response to river and sediment discharge into a static body of water that was 7.5 km by 5.625 km (model grid resolution was 25 m). The basin initially consisted of a floor with a slope of 0.000375 to the north. The initial conduit at the southern boundary conveying water and sediment into the model domain was 250 m wide, 2.5 m deep and 500 m long with specified incoming water discharge of  $1000 \text{ m}^3 \text{ s}^{-1}$ . The west, north, and east boundaries of the domain were designated as open with constant water elevation. Incoming sediment discharge was  $0.0377 \text{ m}^3 \text{ s}^{-1}$ . Different delta morphotypes evolved based only on the median grain size of incoming sediment (Caldwell and Edmonds, 2014). Erosion of cohesive sediment was set to occur when the shear stress exceeded a critical shear stress of erosion ( $\tau_{ce}$ ) of  $1 \text{ N m}^{-2}$ . Continuous deposition of mud was achieved by setting the critical shear stress of deposition ( $\tau_{cd}$ ) as  $1000 \text{ N m}^{-2}$ . Each simulation ran for ~290 simulated years.

Delta topset slope was analyzed as an indicator of how the distribution of elevation in the delta top wetland affects nitrate removal (Caldwell and Edmonds, 2014).

Non-Local Entropy Rates ( $nER$ ) were used to calculate how flux diversity in bifurcating channels affected removal (Tejedor et al., 2015). The number of alternative pathways ( $N_{ap}$ ), and leakage index, ( $LI$ ), were used to measure how dynamic and topologic channel complexity influenced removal (Tejedor et al., 2017). The topset area was also calculated to quantify the effect of the area available for sediment-water interactions.

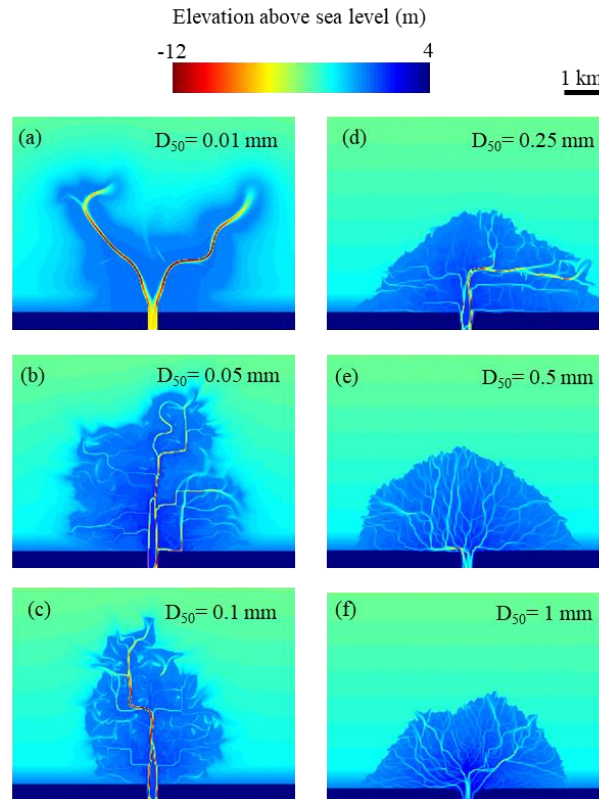


Figure 4.2. Six synthetic deltas with unique geomorphologies were created following Caldwell and Edmonds (2014) by varying the median grain size ( $D_{50}$ ) in incoming sediment.

The synthetic delta DEMs, steady flow fields, and water depths were used as inputs to a steady reactive transport model. Mass transfer velocities were again specified according to elevation (Equation 4.2). This calculation assumes that similar biogeochemical and ecological processes underpin the kinetics of nitrate removal in all

deltas (for example, all deltas have similar temperatures, pH, elevation-dependent plant and microbial communities, and other factors that influence nitrate removal kinetics). The river inlet boundary was assigned a specified concentration of 1 mg N l<sup>-1</sup>. The distal boundaries were treated as open boundaries (or advective flux boundaries, in practice, as the flow was always directed outward in steady models).

The efficiency of nitrate removal in each delta was calculated as the percent difference between the mass flux of nitrate entering the model domain through the river inlet and the mass flux of nitrate leaving through the distal boundaries. Nitrate removal efficiencies were compared with topset slope,  $nER$ ,  $N_{ap}$ , and (Caldwell and Edmonds, 2014; Tejedor et al., 2016; Tejedor et al., 2017). Uptake length ( $S_w$  [L]), or the distance a nitrate molecule travels in the water column before being processed (Newbold et al., 1981), was calculated across the delta grid as:

$$S_w = \frac{|v| \times h}{V_f} . \quad (3)$$

Here,  $h$  is water depth at a time point of interest. Uptake length is a measure of nitrate retention that has been widely used across aquatic environments and reflects the balance between downstream transport and biogeochemical demand in the benthos (Mulholland et al., 1985; Ensign and Doyle, 2006; Ye et al., 2017).

The synthetic deltas were divided into different ecogeomorphic zones based on elevation referenced to mean sea level and associated soil ages and biomass (Olliver and Edmonds, 2017). The upper zone (>0.13 m) consists of island levees and is characterized by dense vegetation, a high percentage of subaerial land, and older soils. The intermediate zone (>-0.24 and <0.13) consists of embayments ranging from densely to

sparsely vegetated areas and younger soils. The lower zone (<0.13) consists of channels and is characterized by sparse vegetation.

### 4.3. Results

#### *Wax Lake Delta Model*

Model velocities and water levels fluctuated daily in response to tidal forcing, but the net flow of nitrate was generally basinward (Figure 4.3a,c; Figure 4.4a). Nitrate concentrations across the delta were generally unattenuated (concentrations were greater than 1 mg N l<sup>-1</sup>) (Figure 4.3b,d). Average downstream concentration measured at the boundaries was 1.09 mg N l<sup>-1</sup>. Some locations in the distal basin experienced brief flow reversals during rising tide, but concentrations remained near 1 mg l<sup>-1</sup> across the basin (Figure 4.3c). Nitrate removal was low within channels, and concentrations remained high. Removal was substantially greater on delta islands near apexes, leading to a few regions where nitrate concentrations approached 0 mg N l<sup>-1</sup>. For example, Site 1, the northernmost site located on a submerged levee at relatively high elevation, had observed concentrations of <0.1 mg N l<sup>-1</sup>, and modeled concentrations varied over tidal timescales from 0.0083 mg N l<sup>-1</sup> to 1.04 mg N l<sup>-1</sup> (Figure 4.4). Modeled concentrations at Sites 2 and 3, located near the center of the islands, also fluctuated between 0.8 mg N l<sup>-1</sup> during low tide to >1 mg N l<sup>-1</sup> during high tide. Observed values at Site 3 reflected this tidal variation. Sampling at Site 2 ceased before low tide due to dangerous thunderstorm activity. Sites 4 and 5, the southernmost locations, were both near the same secondary channel, and both models and observations showed constant, relatively unattenuated nitrate concentrations over the tidal cycle (Figure 4.4).

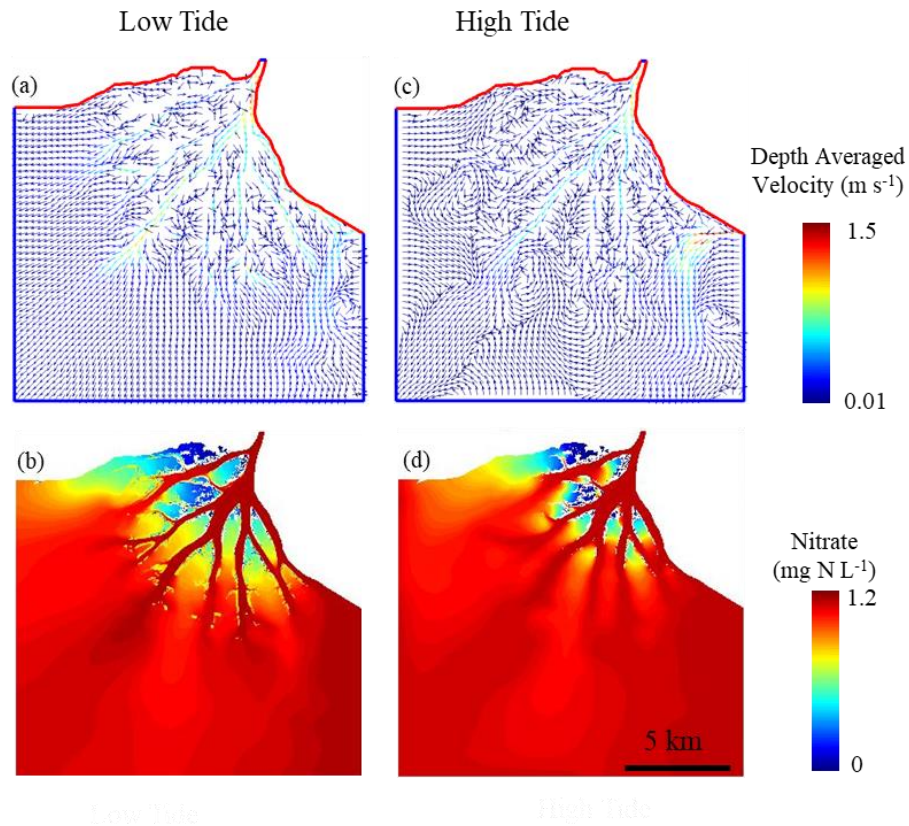


Figure 4.3. Nitrate concentration remains high throughout the channel network but is removed within the islands. During low tide, flow on islands is slow and directed offshore (a), and nitrate concentrations decline (b). At high tide, islands are flooded with water from channels (c), and nitrate concentrations rise (d).

Overall, the model captured both daily average nitrate concentrations and tidal concentration ranges on Mike Island during the sampling week. The modeled inundation of Site 1 with nitrate-rich water was not observed in the field (concentrations were low even at high tide), but this may be due to the effects of sub-grid scale microtopography on flow and reactive transport. Specifically, Site 1 appeared to function as a small, isolated wetland based on qualitative observations of flow conditions, vegetation, and microtopography on the sampling day. It is possible that the site was in a microtopographic depression not captured by the model DEM, leading to less solute

flushing at high tide in the field than in the model. The choice of dispersion coefficient does not appear to improve the fit between model results and observations, based on tests with dispersion coefficients ranging from 1 to 200  $m^2 s^{-1}$  and typical of coastal wetlands and streams (Lautz and Siegel, 2007; Martinez and Wise, 2004; Tayfur and Singh 2005). Beyond Mike Island, the model qualitatively captured observed patterns in nitrate concentration, which have been shown to be greater on younger southern islands and downstream embayments and lower on northern islands and upstream embayments (Henry and Twilley, 2014; Hiatt et al., 2018).

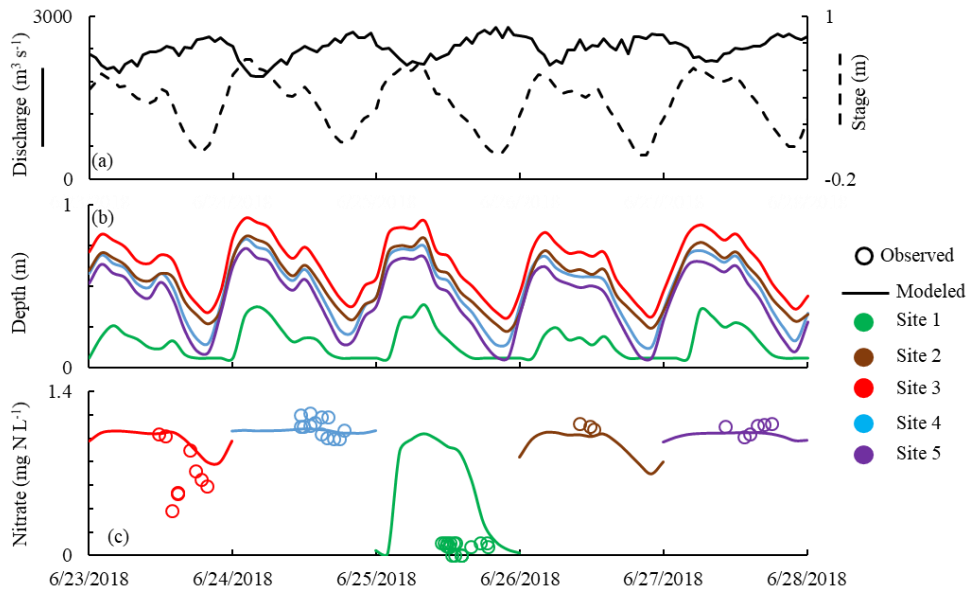


Figure 4.4. (a) Discharge and water level at inlet during field sampling. (b) Modeled water depth at each site. (c) Modeled and measured nitrate concentrations at each site. To improve visibility, only one day of model results is shown for each site, corresponding to days of measurements.

Areas of high potential nitrate removal, measured as a first-order uptake rate constant ( $k$ ,  $\text{d}^{-1}$ ), were ubiquitous on islands during low tide (Figure 4.5a). These hot spots and hot moments of high potential nitrate removal (high  $k$ ) were reduced in size and magnitude during rising tide (Figure 4.5b) as the biogeochemical demand in the benthos ( $V_f$ ) was forced to act over a larger column of nitrate-rich water that inundated the islands from the channels. In other words, areas of the delta such as levees that are highly retentive at low tide are less retentive at high tide. This can also be seen in the uptake length,  $S_w$ , which was as low as 30 m (approaching the model cell size) in some locations on islands and tended to increase slightly at high tide (Figure 4.5c,d). Over the channel network though, uptake length was consistently greater than 10 km (approximately the length of the delta) indicating that much of the nitrate was transported out to sea before being attenuated.

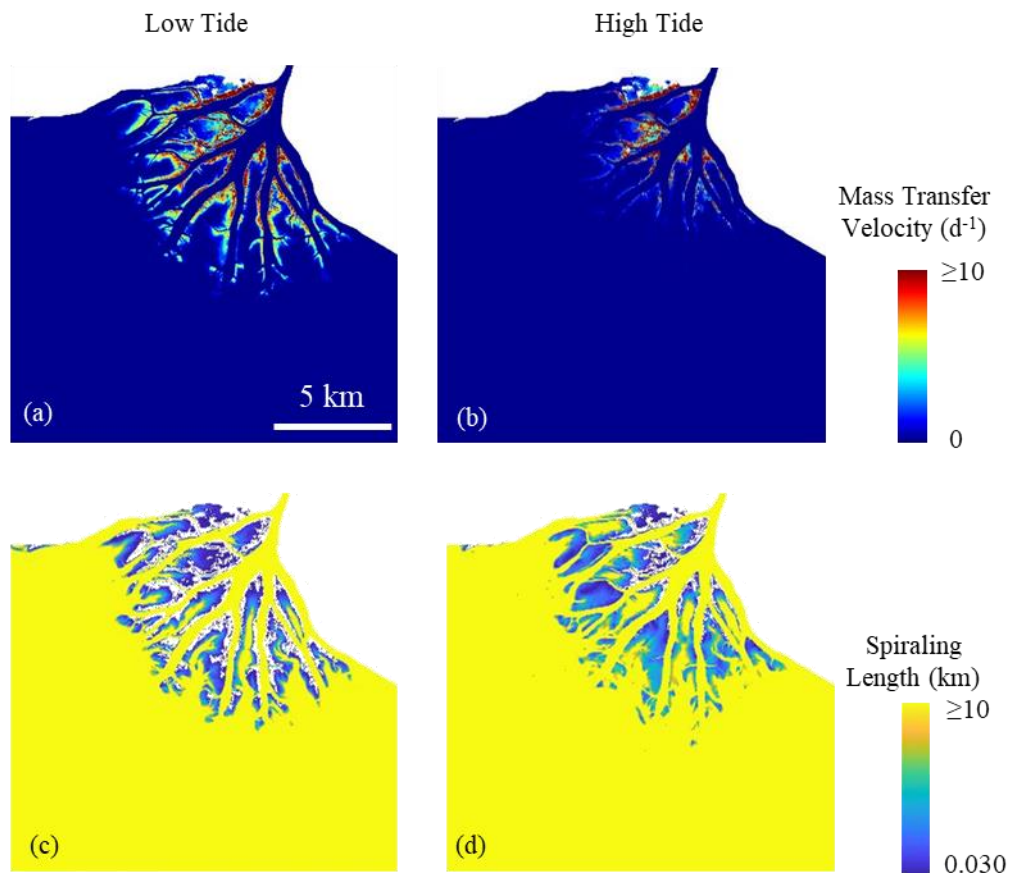


Figure 4.5. (a-b) Nitrate removal potential as a first-order uptake rate constant ( $k$ ) is highest near island apexes and fluctuates between (a) high and (b) low tide. (c-d) Nitrate uptake lengths ( $S_w$ ) across most of the delta are longer than the delta length. Most nitrate will exit the delta without removal.

During the simulated study period (12:00 am June 23 to 12:00 am June 28, 2018) a total of 1170 metric tons of nitrate entered the delta from the river (an average of 234 tons per day). For reference, 1040 tons entered through the downstream boundaries during flow reversals. The total mass of nitrate removed during the study period was 87 tons, representing 7.4% of the terrestrially derived nitrate entering the system from the river. This removal rate is similar to estimates of 0.2 to 4.0% from Knights et al. (in revision). The upper and intermediate ecogeomorphic zones made up 7.5 and 25% of the

delta area and contributed 17 and 41% of removal. The lower zone made up 67.5% of the delta but contributed to 42% of removal.

### *Synthetic Models*

Nitrate levels remained relatively high across all six synthetic deltas, and nitrate was efficiently processed (concentrations approaching  $0 \text{ mg N l}^{-1}$ ) only in areas adjacent to subaerial portions of islands (Figure 4.6). Nitrate concentrations on the fully submerged delta (Figure 4.6a) never fell below 50% of incoming levels. Nitrate uptake lengths were generally several times longer than delta lengths, with median uptake lengths greater than 60 km (Figure 4.7). Uptake lengths were less associated with variable reaction rates (Figure 4.7a) and more associated with transport. Uptake rates were greatest within the channels and least within islands near subaerial regions.

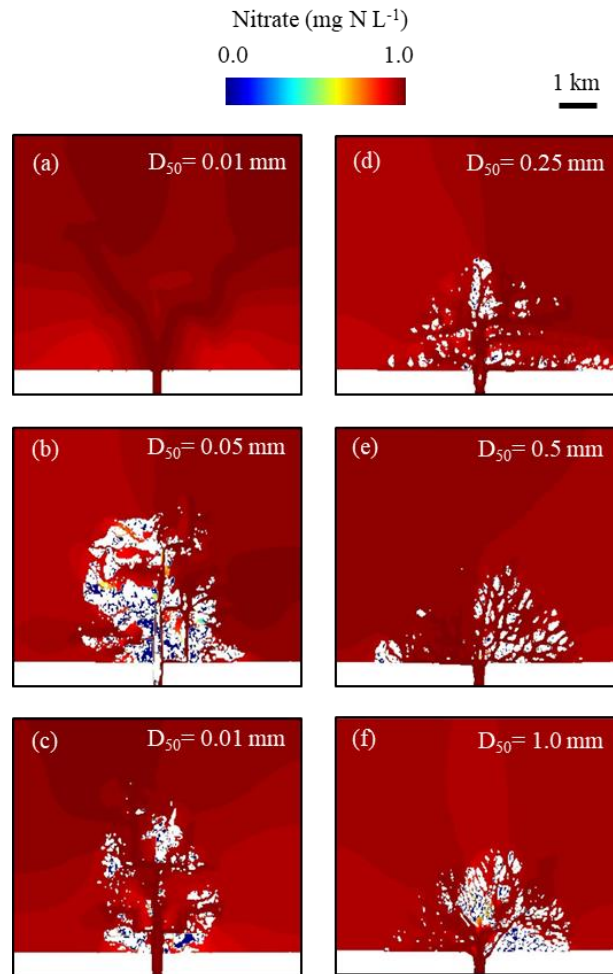


Figure 4.6. Nitrate concentration remained relatively high in all six models. Concentrations were lowest near subaerial portions (white) of islands.

Nitrate removal across all deltas ranged from 2.2 to 5.8 metric tons per day representing only 2.5 to 6.7% of incoming nitrate. On average the upper ecogeomorphic zones covered 36% of the delta yet contributed 65% of removal (Table 4.1). The intermediate and lower zones covered 44 and 20% of the delta and were responsible for 31 and 4% of nitrate removal, respectively. In general, nitrate removal was positively correlated with delta topset slope,  $nER$  and  $N_{ap}$  ( $R^2$  of 0.87, 0.90 and 0.84, respectively) (Figure 4.8). Nitrate removal was negatively correlated with  $LI$  ( $R^2$  of 0.30). Contrary to

my hypothesis, nitrate removal was not positively correlated with delta top area but instead decreased with increasing area ( $R^2$  of 0.61).

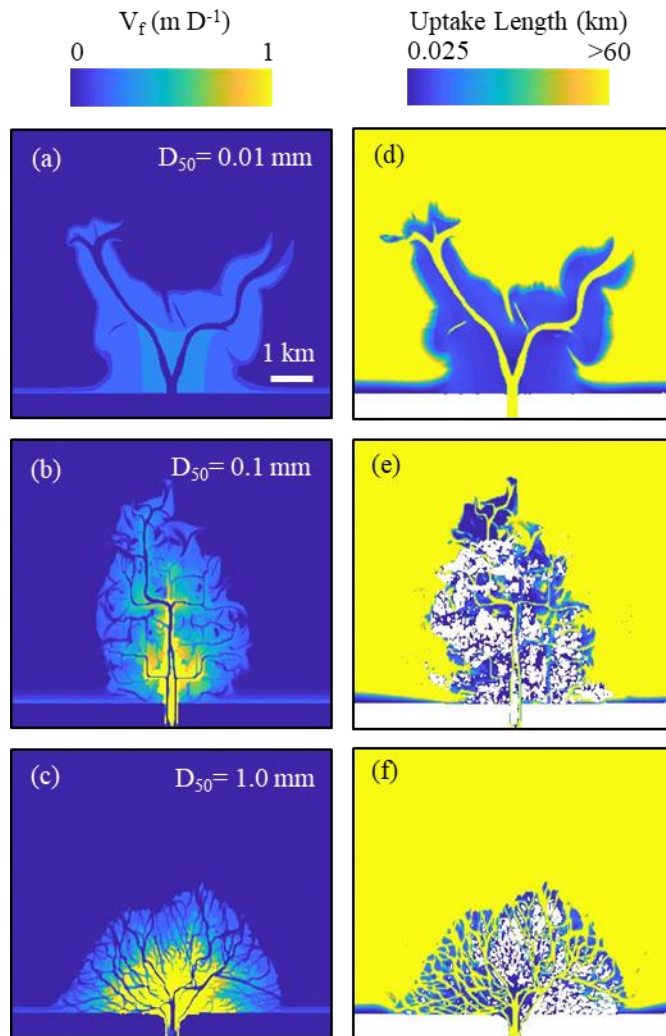


Figure 4.7. (a-c) Mass transfer velocity ( $V_f$ ), (d-f) and corresponding uptake length for deltas formed under fine, intermediate and coarse grain sizes. Despite hot spots of nutrient removal increasing with grain size, uptake length remained high across the deltas.

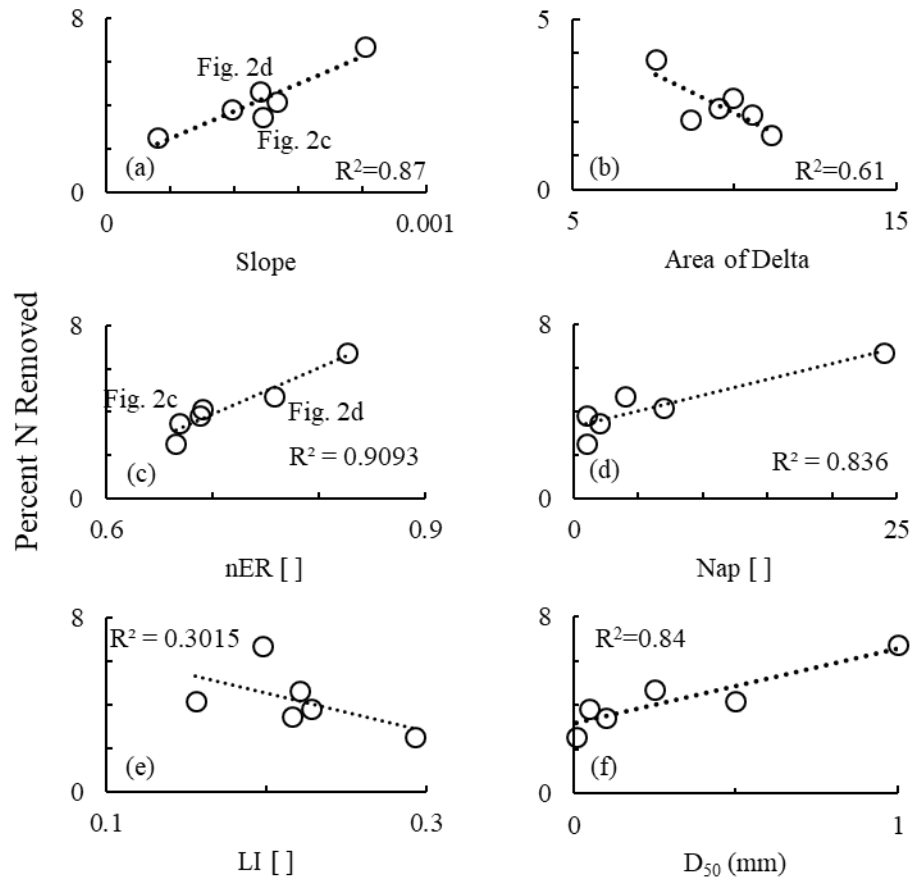


Figure.4.8: (a,c,d) The percent removal is positively correlated to slope,  $nER$ , and  $N_{ap}$  (b) Analysis of the six synthetic deltas suggests a negative relationship between delta area and removal. This implies that delta size may not play an important role in controlling removal efficiency if wetland development and channel complexity are not maximized. (e) There is a weak and negative relationship between  $LI$  and removal rate. (f) The percent of nitrate removed from each delta increases with median grain size.

#### 4.4. Discussion

##### *Controls of Nitrate Removal in Simulated Deltas*

The fast flow of water through river-dominated deltas limits opportunities for nutrient retention, but deltas with more topset area at or above sea level generally have the greatest biogeochemically active areas for nutrient retention (Figure 4.9). Elevation (referenced to sea level) is a master biogeochemical variable (Johnson et al., 1985; Carle et al., 2015; Ma et al., 2018; Knights et al., in revision). For example, elevation is

positively correlated with vegetation density (Carle et al., 2015; Ma et al., 2018), and nitrate assimilation into plant biomass can account for a significant portion of removal from estuarine sediment (Vymazal, 2011). Also, greater denitrification rates, associated with older, more reduced sediment, are found at higher elevations on prograding deltas (Henry and Twilley, 2014).

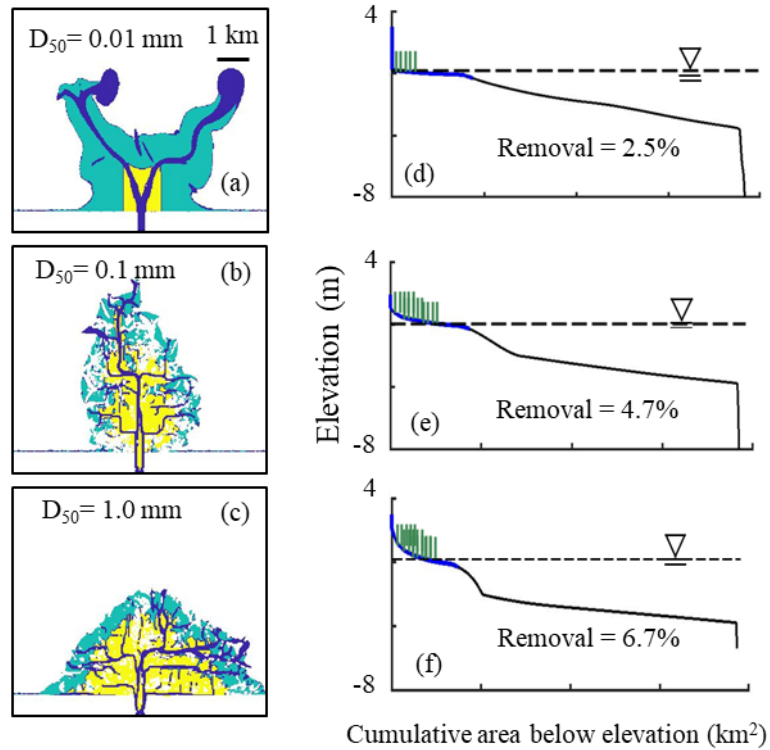


Figure 4.9. Three deltas representing geomorphologic endmembers and showing upper zones (yellow) intermediate (cyan) and lower zones (blue). On average, the upper ecogeomorphic zone makes up ~36% of the delta but contributes 65% of removal. (d-f) Corresponding cumulative area curves of the delta-top (blue) and basin (black). The horizontal line represents mean sea level. The percent of nitrate removed increases with delta top slope and median elevation above mean sea level.

The strong positive relationship between delta top slope and removal exists because steeply sloping prograding deltas deposit more sediment closer to and above mean sea level. Soils near and marginally above mean sea level provide ideal locations

for highly active wetlands to develop (Ma et al., 2018). In contrast, vegetation and organic matter in fully submerged soils are relatively limited. In the synthetic deltas, the least efficient delta (only removing 2.5% of the nitrate load; Figure 6 a and Figure 8) is fully submerged and has the smallest percentage of area within the upper ecogeomorphic zone (7.8%) (Table 4.1). By comparison, the most efficient delta has 41% associated with the upper ecogeomorphic zone.

Delta top slope explains 87% of the variability between removal rates (Figure 4.8a), however, two deltas with similar slopes had noticeably different removal rates of 3.45 and 4.67% (Figure 4.2d,c). These differences might be explained by the distribution of flow within these deltas. Nonlocal entropy quantifies the uncertainty of flow partitioning at a channel junction (Tejedor et al., 2016), and deltas with high *nER* have channel junctions with large degrees of asymmetric flux partitioning, meaning that the diversity of fluxes delivered to the shoreline is maximized. As *nER* increases, nitrate supply to highly reactive areas may increase, leading to gains in removal efficiency (Powers et al., 2012). Indeed, of the two deltas with similar slopes, the delta with greater *nER* (median grain size of 0.25 mm, Figure 4.2d) was more efficient at removing nitrate than the delta with a lower *nER* (median grain size of 0.1 mm, Figure 4.2c, Table 4.2).

I expected nitrate removal to increase with increasing delta size, however, contrary to my hypothesis, removal decreases with delta top area (Figure 4.8b). In order to examine the relationship between delta area and nitrate removal independently from the confounding effects of elevation-dependent removal kinetics I repeated the simulations using uniform removal kinetics across each delta ( $6.39 \text{ mm hr}^{-1}$ ,

representative of the average  $V_f$  measured in Wax Lake delta) (Knights et al., in revision). Reactions were inhibited outside the delta top area (blue lines Figure 9 as delineated based on the 0 m elevation contour referenced to MLLW (Olliver et al., 2020)). For these simulations, nitrate removal does increase with delta area as expected—the larger the delta top wetland, the more nitrate it can remove. This trend is overwhelmed by the strong positive relationship between nitrate removal kinetics and elevation and the tradeoff between delta top area and delta top elevation. This finding has important implications for management practices aimed at creating new delta land (Paola et al., 2011). If all delta land is similarly active, the creation of larger deltas would help buffer coastal nitrate loading and might appear to be a feasible endeavor. However, field observations suggest that not all delta land is similarly active (Knights et al., in revision), and it may be more efficient to construct smaller deltas with greater proportions of high-standing area than larger low-lying deltas.

#### *Coastal Water Quality Implications*

Nitrate retention rates ranging from 2.5 to 6.7% of the incoming load (under the long-term steady discharge conditions that created these deltas) indicate a modest capacity of similar river-dominated deltas to buffer nitrate fluxes to the coast (Table 4.1). These findings compare well with previously calculated estimates for Wax Lake Delta (Chapter 3). Low retention rates can be attributed to the fact that these temperate river-dominated deltas are mostly transport-dominated and reaction limited. The few areas such as island levees with very short uptake lengths (on the order of tens of meters) cannot contribute much to removal as they are not well connected hydrologically to

focused zones of discharge through channels (Powers et al., 2012). As a proof of concept, I created another model scenario ( $D_{50}=1$ , Figure 4.2,f) where nitrate removal kinetics in delta top wetlands were increased to 25 times the mean observed values in Wax Lake Delta ( $V_f = 150 \text{ mm hr}^{-1}$  in locations above mean sea level,  $V_f = 0$  in channels and elsewhere below mean sea level). This simulation was not designed to replicate realistic removal rates but to give insight into the percentage of flow that moves from the channels onto delta islands and embayments, as any nitrate that escapes the channels will be removed under the extreme biogeochemical demand prescribed outside the channels. Nitrate removal increased from 6.7 to 22.3%, suggesting that at most, only a quarter of flow from channels interacts with delta islands. This finding aligns well with previous estimates that 23-54% of channel flux enters delta islands (Hiatt and Passalacqua, 2015). Even if removal kinetics in island retention zones were much greater than in Equation 4.2, less than 25% of nitrate would be removed unless hydrologic connectivity were greater. In these river-dominated deltas, the natural distribution of flow through channel and island networks may impose fundamental limits on hydrologic connectivity and thus nitrate retention.

The greatest removal rates are achieved for coarse-grained deltas (Figure 4.8d) because they grow with steeper topset gradients (Caldwell and Edmonds, 2014) that support denser vegetation (Ma et al., 2018) and more bioreactive soils (Henry and Twilley, 2014) at greater elevations. The relationship between grain size and topset elevation occurs because a higher bed shear stress (and thus greater topset gradient) is required for transporting larger grain sizes (Parker et al., 1998; Whipple et al., 1998).

Although finer-grained sediment is more cohesive, fine sediments form shallowly sloping deltas. The low settling rate of fine-grained sediment results in greater sediment bypass and more distal deposition (Caldwell and Edmonds, 2014). From a managerial standpoint, it is important to consider median grain size when creating river diversions for delta development (Paola et al., 2011) in order to promote the formation of steeply sloping deltas with more emergent wetlands, which may maximize removal.

Another implication is that deltas draining active coastal margins with high relief catchments and presumably coarser sediments may have greater nitrate removal potential, all other factors held constant (temperature, plant communities, river discharge, and incoming nitrate concentrations). The Sacramento-San Joaquin River delta and the Skagit delta may fall into this category. Fine-grained, gently sloping deltas in passive margins such as Orinoco River Delta may have comparatively reduced nutrient removal capacity. There is a need for more studies to assess nitrate removal in natural deltas around the world and understand how their removal efficiencies relate to delta topset slope and grain size, among other morphologic factors.

The synthetic delta simulations here are simplistic versions of natural deltas, as they do not consider fluctuating discharge. I also chose an incoming nitrate concentration representative of mixed land use. Nitrate uptake in streams and wetlands is inversely proportional to background concentrations (Tank et al., 2008; Mulholland et al., 2009; Hall et al., 2009), and removal efficiency would likely improve if incoming nitrate concentration were reduced. However, nitrate removal in these pristine systems may be less consequential to ecosystem health.

The models are most representative of temperate river-dominated deltas during summer flow conditions, and removal efficiencies may differ over seasons, in tidal- or wave-dominated deltas, or in high-latitude deltas. Over seasons, it is unlikely that removal efficiency would increase in winter because colder temperatures lead to slower denitrification kinetics (Bremner and Shaw 1958; Bachand and Horne, 1999), and winter senescence results in limited assimilation into biomass. At higher latitudes, removal efficiency could be lower due to both colder temperatures and permafrost, which can restrict liquid water interactions with organic-rich soil (Keuper et al., 2007). Further analyses of other types of deltas under different hydrodynamics are necessary to understand nutrient fate and inform managerial practices.

The Wax Lake model in this study and others (Hiatt, et al., 2018) showed that removal on islands depends on flow conditions, suggesting that removal could vary strongly over seasons as discharge changes, and over different wind and tidal conditions. For example, Hiatt et al. (2018) showed that fractional nitrate removal across the islands of Wax Lake Delta fluctuated with spring and neap tides. During spring tides, nitrate removal was limited to the northern extremities of only a few islands. During neap tides, a much larger percentage of island areas experienced removal. Nitrate removal patterns were similarly responsive to diurnal tidal fluctuations in this validation model. However, the steady simulations of synthetic deltas cannot be used to understand temporal changes in nitrate removal due to flow conditions or biological factors such as plant growth or

decomposition.

<b>D<sub>50</sub></b> <b>(mm)</b>	<b>Removed</b> <b>(tons N d<sup>-1</sup>)</b>	<b>Removal</b> <b>(%)</b>	<b>Upper</b> <b>(%)</b>	<b>Int.</b> <b>(%)</b>	<b>Lower</b> <b>(%)</b>	<b>Upper</b> <b>Area (%)</b>	<b>Int. Area</b> <b>(%)</b>	<b>Low Area</b> <b>(%)</b>
0.01	2.2	2.5	14	80	6	41	27	32
0.05	3.3	3.8	70	27	3	37	16	47
0.1	3.0	3.5	70	27	3	45	17	38
0.25	4.0	4.7	76	21	3	39	17	44
0.5	3.6	4.2	72	24	4	45	24	31
1	5.8	6.7	87.5	10	2.5	7.8	23	69.8

Table 1. Nitrate removal and ecogeomorphic area for synthetic deltas.

<b>D50</b>	<b>Slope</b>	<b>Area (km<sup>2</sup>)</b>	<b>nER</b>	<b>Nap</b>	<b>LI</b>
1	0.000808567	7.5625	0.826082634	24	0.1973
0.5	0.000531788	9.5125	0.691078078	7	0.1554
0.25	0.000480946	9.958125	0.758059481	4	0.2205
0.1	0.000488906	8.6375	0.669197959	2	0.2156
0.05	0.000394405	10.55875	0.688306238	1	0.2278
0.01	0.000161823	11.15	0.665844679	1	0.2923

Table 2. Geometrics of synthetic deltas. All simulations were run at steady state an incoming discharge of 1000 m<sup>3</sup> day<sup>-1</sup> and nitrate flux of 86.4 tons day<sup>-1</sup>.

#### 4.5. Conclusion

Nitrate retention in river-dominated temperate deltas is likely limited to a small percentage (perhaps <25%) of the incoming load due to the limited exchange between channels and islands. Average nitrate uptake lengths are larger than the delta length scale, indicating that most nitrate is transported to sea before being processed. Nitrate retention increases with delta topset gradient because steeper topsets produce greater wetland areas with high biogeochemical demand. In land reclamation projects, this steeper gradient can be achieved by diverting sediments with a coarser grain size distribution. Future research

considering a wider range of temporal effects (seasons, floods, and tides) on both reactivity and transport can improve estimations of nitrate fate in deltas.

## Chapter 5. Summary

### 5.1. Synthesis

In recent history, rivers have become enriched in nutrients, leading to a global deterioration of coastal waters (Galloway et al., 2008). Hydrodynamic and biogeochemical processes occurring at the coast, particularly at microbially active sediment-water interfaces, modify the chemistry of discharging waters. Thus, nutrients exported through coastal subsurface environments (beach faces and lake beds) and surface environments (delta wetlands) are not identical, and transformations along coastal interfaces are often difficult to measure. This thesis examined the controls on nutrient transport and processing at the coast by focusing on two coastal freshwater systems, namely coastal aquifers of the Great Lakes and temperate, river-dominated deltas.

### 5.2. Key Findings and Future Work

The primary question asked in this thesis is how nutrients in groundwater and surface water are modified by biogeochemical processes at the coastal interface, particularly in areas of nutrient enrichment that are prone to harmful algal blooms. Two approaches targeting different coastal systems were adopted. The first coastal system was the surface water-groundwater interface of the United States Great Lakes coast. I used water budgets, the National Hydrography Dataset, and the North American Land Data Assimilation System to estimate groundwater discharge to the Great Lakes. I showed that water budgets are a simple but powerful tool for revealing patterns of direct groundwater discharge to the coast and areas of risk for nutrient contamination from groundwater. Of the Great Lakes, estimates show that Lake Erie has the highest flux of groundwater per

unit length of shoreline ( $477 \text{ m}^3 \text{ y}^{-1} \text{ m}^{-1}$ ) along with the highest percentage of vulnerable shoreline (31%). Field analysis of a vulnerable beach in Lake Erie showed that onshore groundwater was high in nitrate and low in phosphate while offshore discharging groundwater was low in nitrate and high in phosphate. This suggests that the shallow near shore aquifer of Lake Erie is removing nitrate while phosphate is being mobilized from lakebed sediment.

River-dominated marine deltas are the second type of coastal system examined in this thesis. First, Wax Lake delta was used as an analog for a temperate delta to identify ecogeomorphic controls on nitrate removal kinetics across delta wetlands. I showed that nitrate removal rates vary across ecogeomorphic zones on Wax Lake delta, and the best predictor of the potential summertime nitrate removal rate is NDVI, a widely available proxy for vegetation photosynthetic activity and greenness. Upscaling these calculations suggests that potential hotspots of nitrate removal are located in intermediate-elevation ecogeomorphic zones. Thus, older islands in the northwest region of Wax Lake delta and the northern perimeters of younger southeastern islands are most reactive and have the potential to contribute the most to nitrate removal.

An alternative nutrient spiraling calculation shows that the supply of nitrate across the channel network limits actual removal rates. Levees and other intermediate-elevation ecogeomorphic zones along primary channels, especially those located on the eastern half of the delta, are likely to be both biogeochemically “hottest” and receive more nitrate flux than levees and embayments in the western and distal regions of the delta.

Analysis using simulated river-dominated deltas indicates that the average distance a molecule of nitrate travels downstream before being processed is generally larger than the delta length scales, resulting in a limited capacity of river-dominated delta to remove nitrate. Removal is likely limited to a small portion of the incoming load in most river-dominated deltas but increases as the proportion of high-sitting (relative to mean sea level), reactive wetlands increases. Estimates of nutrient removal and flow to coastal waters are essential for management practices and policy guidance. This research provides an important step in understanding the biophysical factors that control heterogeneity in nutrient removal rates in deltas. Models indicate that the removal capacity of constructed river-dominated deltas can be maximized if coarser sediments (which build more steeply sloping deltas) are used in sediment diversion projects aimed at creating new delta land.

This thesis demonstrates the importance of coastal aquatic systems in regulating the export of nutrients to lakes and the oceans. The study areas chosen here were all located in temperate regions with long summer seasons that support biological activity. However, a large percentage of the global coastline lies in high latitudes (defined above or below 67 degrees N or S, respectively). These coastal systems are expected to have drastically different microbiological and ecohydrologic processes. Moreover, surface water-groundwater interactions there are strongly influenced by permafrost. Therefore, nutrient fate in high-latitude coastal systems is poorly understood and an important area for future research.

Arctic deltas, in particular, deliver nutrients needed for biological productivity to a warming Arctic Ocean. The six largest Arctic rivers are responsible for transporting two-thirds of the pan-Arctic discharge to the Arctic Ocean, and the majority of riverine flow to the Arctic Ocean passes through deltas before discharging to the ocean (Holmes et al., 2018). Arctic deltas remain frozen for significant parts of the year and therefore have different flow conditions and wetland biology than temperate deltas. Permafrost thawing and erosion leads to development of thousands of Arctic lakes representing an estimated area of up to 380,000 km<sup>2</sup> (Goldman et al, 2012). Lakes in Arctic deltas are permanently connected to the channel network, permanently disconnected, or temporarily connected depending on flow conditions (Emmerton et al., 2007). Also, seasonal episodes of freezing and thawing result in annual pulses of high discharge corresponding with ice break-up in the spring. In some rivers, up to half of annual discharge is associated with the spring freshet (Holmes et al, 2012). Future work will aim to develop models that explore how permafrost thaw alters nutrient flux through Arctic deltas. I plan to upscale a series of one-dimensional models using bifurcation geometries of Arctic deltas extracted from remote sensing to elucidate nutrient flux to the Arctic Ocean. In order to inform models, field campaigns will be conducted where nitrogen isotopes and benthic chambers will be used to understand nitrogen processing in Arctic deltas.

## Reference

- Akaike, H. (1974). A new look at the statistical model identification. *IEEE transactions on automatic control*, 19(6), 716-723.
- Alexander, R. B., Smith, R. A., & Schwarz, G. E. (2000). Effect of stream channel size on the delivery of nitrogen to the Gulf of Mexico. *Nature*, 403(6771), 758-761.
- Alexander, R. B., Smith, R. A., Schwarz, G. E., Boyer, E. W., Nolan, J. V., & Brakebill, J. W. (2008). Differences in phosphorus and nitrogen delivery to the Gulf of Mexico from the Mississippi River Basin. *Environmental science & technology*, 42(3), 822-830.
- Allen, Y. C., Couvillion, B. R., & Barras, J. A. (2012). Using multitemporal remote sensing imagery and inundation measures to improve land change estimates in coastal wetlands. *Estuaries and Coasts*, 35(1), 190-200.
- Altman, S. J., & Parizek, R. R. (1995). Dilution of nonpoint-source nitrate in groundwater. *Journal of Environmental Quality*, 24(4), 707-718.
- Anderson, D. M. (1989). Toxic algal blooms and red tides: a global perspective. *Red tides: biology, environmental science and toxicology*, 11-16.
- Anderson, D. M., Glibert, P. M., & Burkholder, J. M. (2002). Harmful algal blooms and eutrophication: nutrient sources, composition, and consequences. *Estuaries*, 25(4), 704-726.

- Arango, C. P., Tank, J. L., Schaller, J. L., Royer, T. V., Bernot, M. J., & David, M. B. (2007). Benthic organic carbon influences denitrification in streams with high nitrate concentration. *Freshwater Biology*, *52*(7), 1210-1222.
- Bachand, P. A., & Horne, A. J. (1999). Denitrification in constructed free-water surface wetlands: II. Effects of vegetation and temperature. *Ecological engineering*, *14*(1-2), 17-32.
- Backer, L. C., & McGillicuddy Jr, D. J. (2006). Harmful algal blooms: at the interface between coastal oceanography and human health. *Oceanography (Washington, DC)*, *19*(2), 94.
- Baker, D. B., Confesor, R., Ewing, D. E., Johnson, L. T., Kramer, J. W., & Merryfield, B. J. (2014). Phosphorus loading to Lake Erie from the Maumee, Sandusky and Cuyahoga rivers: The importance of bioavailability. *Journal of Great Lakes Research*, *40*(3), 502-517.
- Baker, M. A., & Vervier, P. (2004). Hydrological variability, organic matter supply and denitrification in the Garonne River ecosystem. *Freshwater Biology*, *49*(2), 181-190.
- Bernhardt, E. S., Blaszczak, J. R., Ficken, C. D., Fork, M. L., Kaiser, K. E., & Seybold, E. C. (2017). Control points in ecosystems: moving beyond the hot spot hot moment concept. *Ecosystems*, *20*(4), 665-682.
- Böhlke, J. K., Antweiler, R. C., Harvey, J. W., Laursen, A. E., Smith, L. K., Smith, R. L., & Voytek, M. A. (2009). Multi-scale measurements and modeling of

- denitrification in streams with varying flow and nitrate concentration in the upper Mississippi River basin, USA. *Biogeochemistry*, 93(1-2), 117-141.
- Bokuniewicz, H. (1980). Groundwater seepage into Great South Bay, New York. *Estuarine and Coastal Marine Science*, 10(4), 437-444.
- Bolla Pittaluga, M., Repetto, R., & Tubino, M. (2003). Channel bifurcation in braided rivers: Equilibrium configurations and stability. *Water Resources Research*, 39(3).
- Box, E. O., Holben, B. N., & Kalb, V. (1989). Accuracy of the AVHRR vegetation index as a predictor of biomass, primary productivity and net CO<sub>2</sub> flux. *Vegetatio*, 80(2), 71-89.
- Box, G. E., & Cox, D. R. (1964). An analysis of transformations. *Journal of the Royal Statistical Society: Series B (Methodological)*, 26(2), 211-243.
- Boynton, W. R., Kemp, W. M., & Keefe, C. W. (1982). A comparative analysis of nutrients and other factors influencing estuarine phytoplankton production. In *Estuarine comparisons* (pp. 69-90). Academic Press.
- Braskerud, B. C. (2001). The influence of vegetation on sedimentation and resuspension of soil particles in small constructed wetlands. *Journal of Environmental Quality*, 30(4), 1447-1457.
- Bremner, J. M., & Shaw, K. (1958). Denitrification in soil. II. Factors affecting denitrification. *The Journal of Agricultural Science*, 51(1), 40-52.

- Bridgeman, T. B., Chaffin, J. D., & Filbrun, J. E. (2013). A novel method for tracking western Lake Erie Microcystis blooms, 2002–2011. *Journal of Great Lakes Research*, 39(1), 83-89.
- BryantMason, A., Jun Xu, Y., & Altabet, M. A. (2013). Limited capacity of river corridor wetlands to remove nitrate: A case study on the Atchafalaya River Basin during the 2011 Mississippi River Flooding. *Water Resources Research*, 49(1), 283-290.
- Burgin, A. J., & Hamilton, S. K. (2007). Have we overemphasized the role of denitrification in aquatic ecosystems? A review of nitrate removal pathways. *Frontiers in Ecology and the Environment*, 5(2), 89-96.
- Burnett, W. C., Aggarwal, P. K., Aureli, A., Bokuniewicz, H., Cable, J. E., Charette, M. A., ... & Moore, W. S. (2006). Quantifying submarine groundwater discharge in the coastal zone via multiple methods. *Science of the total Environment*, 367(2-3), 498-543.
- Burns, N. M., Rockwell, D. C., Bertram, P. E., Dolan, D. M., & Ciborowski, J. J. (2005). Trends in temperature, Secchi depth, and dissolved oxygen depletion rates in the central basin of Lake Erie, 1983–2002. *Journal of Great Lakes Research*, 31, 35-49.
- Buschman, F. A., Hoitink, A. J. F., Van Der Vegt, M., & Hoekstra, P. (2010). Subtidal flow division at a shallow tidal junction. *Water Resources Research*, 46(12).
- Cahoon, D. R., White, D. A., & Lynch, J. C. (2011). Sediment infilling and wetland formation dynamics in an active crevasse splay of the Mississippi River delta. *Geomorphology*, 131(3-4), 57-68.

- Caldwell, R. L., & Edmonds, D. A. (2014). The effects of sediment properties on deltaic processes and morphologies: A numerical modeling study. *Journal of Geophysical Research: Earth Surface*, 119(5), 961-982.
- Caldwell, R. L., Edmonds, D. A., Baumgardner, S., Paola, C., Roy, S., & Nienhuis, J. H. (2019). A global delta dataset and the environmental variables that predict delta formation on marine coastlines. *Earth Surface Dynamics*, 7(3), 773-787.
- Carle, M. (2013). Spatial structure and dynamics of the plant communities in a prograding river delta: Wax Lake Delta, Atchafalaya Bay, Louisiana.
- Carle, M. V., Sasser, C. E., & Roberts, H. H. (2015). Accretion and vegetation community change in the Wax Lake Delta following the historic 2011 Mississippi River flood. *Journal of Coastal Research*, 31(3), 569-587.
- Carle, M. V., Wang, L., & Sasser, C. E. (2014). Mapping freshwater marsh species distributions using WorldView-2 high-resolution multispectral satellite imagery. *International journal of remote sensing*, 35(13), 4698-4716.
- Carlson, B., Piliouras, A., Muto, T., & Kim, W. (2018). Control of basin water depth on channel morphology and autogenic timescales in deltaic systems. *Journal of Sedimentary Research*, 88(9), 1026-1039.
- Chaffin, J. D., Bridgeman, T. B., Heckathorn, S. A., & Mishra, S. (2011). Assessment of *Microcystis* growth rate potential and nutrient status across a trophic gradient in western Lake Erie. *Journal of Great Lakes Research*, 37(1), 92-100.

- Cherkauer, D. S., & Hensel, B. R. (1986). Groundwater flow into lake Michigan from Wisconsin. *Journal of Hydrology*, 84(3-4), 261-271.
- Cory, R. M., Miller, M. P., McKnight, D. M., Guerard, J. J., & Miller, P. L. (2010). Effect of instrument-specific response on the analysis of fulvic acid fluorescence spectra. *Limnology and Oceanography: Methods*, 8(2), 67-78.
- Coulibaly, P., & Burn, D. H. (2004). Wavelet analysis of variability in annual Canadian streamflows. *Water Resources Research*, 40(3).
- Covino, T. P., McGlynn, B. L., & McNamara, R. A. (2010). Tracer Additions for Spiraling Curve Characterization (TASCC): Quantifying stream nutrient uptake kinetics from ambient to saturation. *Limnology and Oceanography: methods*, 8(9), 484-498.
- Crowe, A. S., Shikaze, S. G., & Ptacek, C. J. (2004). Numerical modelling of groundwater flow and contaminant transport to Point Pelee marsh, Ontario, Canada. *Hydrological Processes*, 18(2), 293-314.
- Davis, M. B. (1969). Climatic changes in southern Connecticut recorded by pollen deposition at Rogers Lake. *Ecology*, 50(3), 409-422.
- Day, J. W., Boesch, D. F., Clairain, E. J., Kemp, G. P., Laska, S. B., Mitsch, W. J., ... & Simenstad, C. A. (2007). Restoration of the Mississippi Delta: lessons from hurricanes Katrina and Rita. *science*, 315(5819), 1679-1684.
- Day, J. W., Kemp, G. P., Reed, D. J., Cahoon, D. R., Boumans, R. M., Suhayda, J. M., & Gambrell, R. (2011). Vegetation death and rapid loss of surface elevation in two

- contrasting Mississippi delta salt marshes: The role of sedimentation, autocompaction and sea-level rise. *Ecological Engineering*, 37(2), 229-240.
- DeLaune, R. D., Jugsujinda, A., West, J. L., Johnson, C. B., & Kongchum, M. (2005). A screening of the capacity of Louisiana freshwater wetlands to process nitrate in diverted Mississippi River water. *Ecological Engineering*, 25(4), 315-321.
- Deltares. 2014. Delft3D-FLOW: Simulation of Multi-Dimensional Hydrodynamic Flows and Transport Phenomena, Including Sediments (User Manual). Delft, The Netherlands: Deltares.
- Deltares. Water Quality and Aquatic Ecology [User Manual]; Deltares: Delft, The Netherlands, 2016; 394p
- Destouni, G., Shibuo, Y., & Jarsjö, J. (2008). Freshwater flows to the sea: Spatial variability, statistics and scale dependence along coastlines. *Geophysical Research Letters*, 35(18).
- Dettmann, E. H. (2001), Effect of Water Residence Time on Annual Export and Denitrification of Nitrogen in Estuaries: A Model Analysis, *Estuaries*, 24(4), 481-490.
- Diaz, R. J. (2001). Overview of hypoxia around the world. *Journal of environmental quality*, 30(2), 275-281.
- Diaz, R. J., & Rosenberg, R. (2008). Spreading dead zones and consequences for marine ecosystems. *science*, 321(5891), 926-929.

- Dodds, W. K., López, A. J., Bowden, W. B., Gregory, S., Grimm, N. B., Hamilton, S. K., ... & Morrall, D. (2002). N uptake as a function of concentration in streams. *Journal of the North American Benthological Society*, 21(2), 206-220.
- Dolan, D. M. (1993). Point source loadings of phosphorus to Lake Erie: 1986–1990. *Journal of Great Lakes Research*, 19(2), 212-223.
- Donner, S. D., Coe, M. T., Lenters, J. D., Twine, T. E., & Foley, J. A. (2002). Modeling the impact of hydrological changes on nitrate transport in the Mississippi River Basin from 1955 to 1994. *Global Biogeochemical Cycles*, 16(3), 16-1.
- Duff, J. H., & Triska, F. J. (1990). Denitrifications in Sediments from the Hyporheic Zone Adjacent to a Small Forested Stream. *Canadian Journal of Fisheries and Aquatic Sciences*, 47(6), 1140–1147.
- Edmonds, D. A., & Slingerland, R. L. (2007). Mechanics of river mouth bar formation: Implications for the morphodynamics of delta distributary networks. *Journal of Geophysical Research: Earth Surface*, 112(F2).
- Edmonds, D. A., & Slingerland, R. L. (2008). Stability of delta distributary networks and their bifurcations. *Water Resources Research*, 44(9).
- Edmonds, D. A., Paola, C., Hoyal, D. C., & Sheets, B. A. (2011). Quantitative metrics that describe river deltas and their channel networks. *Journal of Geophysical Research: Earth Surface*, 116(F4).
- Edmondson, W. T. (1970). Phosphorus, nitrogen, and algae in Lake Washington after diversion of sewage. *Science*, 169(3946), 690-691.

- Emmerton, C. A., Lesack, L. F., & Marsh, P. (2007). Lake abundance, potential water storage, and habitat distribution in the Mackenzie River Delta, western Canadian Arctic. *Water Resources Research*, 43(5).
- Ensign, S. H., & Doyle, M. W. (2006). Nutrient spiraling in streams and river networks. *Journal of Geophysical Research: Biogeosciences*, 111(G4).
- Ensign, S. H., Piehler, M. F., & Doyle, M. W. (2008). Riparian zone denitrification affects nitrogen flux through a tidal freshwater river. *Biogeochemistry*, 91(2-3), 133-150.
- Feinstein, D. T., Hunt, R. J., & Reeves, H. W. (2010). *Regional groundwater-flow model of the Lake Michigan Basin in support of Great Lakes Basin water availability and use studies*. U. S. Geological Survey.
- Ferguson, G., & Gleeson, T. (2012). Vulnerability of coastal aquifers to groundwater use and climate change. *Nature Climate Change*, 2(5), 342-345.
- Fisk, H. N. (1952). *Geological investigation of the Atchafalaya Basin and the problem of Mississippi River diversion*. Waterways Experiment Station.
- Forshay, K. J., & Stanley, E. H. (2005). Rapid nitrate loss and denitrification in a temperate river floodplain. *Biogeochemistry*, 75(1), 43-64.
- Foufoula-Georgiou, E., Syvitski, J., Paola, C., Hoanh, C. T., Tuong, P., Vörösmarty, C., ... & Twilley, R. (2011). International year of deltas 2013: a proposal. *Eos, Transactions American Geophysical Union*, 92(40), 340-341.

- Frape, S. K., & Patterson, R. J. (1981). Chemistry of interstitial water and bottom sediments as indicators of seepage patterns in Perch Lake, Chalk River, Ontario 1. *Limnology and Oceanography*, 26(3), 500-517.
- Friedrich, J., Dinkel, C., Grieder, E., Radan, S., Secrieru, D., Steingruber, S., & Wehrli, B. (2003). Nutrient uptake and benthic regeneration in Danube Delta Lakes. *Biogeochemistry*, 64(3), 373-398.
- Fuller, J. A. (1996). *Distribution of surficial sediments in Ohio's nearshore (Lake Erie) as interpreted from sidescan sonar and 3.5 kHz subbottom data*. US Department of the Interior, US Geological Survey.
- Fullerton, D. S., Richmond, G. M., Cowan, W. R., Sevon, W. D., Goldthwait, R. P., Farrand, W. R., ... & Richmond, G. M. (1991). *Quaternary geologic map of the Lake Erie 4 degrees x 6 degrees quadrangle, United States and Canada* (No. 1420 (NK-17)).
- Galloway, W. E. (1975). Process framework for describing the morphologic and stratigraphic evolution of deltaic depositional systems.
- Galloway, J. N., Townsend, A. R., Erisman, J. W., Bekunda, M., Cai, Z., Freney, J. R., ... & Sutton, M. A. (2008). Transformation of the nitrogen cycle: recent trends, questions, and potential solutions. *Science*, 320(5878), 889-892.
- Gamon, J. A., Field, C. B., Goulden, M. L., Griffin, K. L., Hartley, A. E., Joel, G., ... & Valentini, R. (1995). Relationships between NDVI, canopy structure, and photosynthesis in three Californian vegetation types. *Ecological Applications*, 5(1), 28-41.

- Geleynse, N., Voller, V. R., Paola, C., & Ganti, V. (2012). Characterization of river delta shorelines. *Geophysical research letters*, 39(17).
- Glibert, P. M., Anderson, D. M., Gentien, P., Granéli, E., & Sellner, K. G. (2005). The global, complex phenomena of harmful algal blooms.
- Goldman, C. R., Kumagai, M., & Robarts, R. D. (Eds.). (2012). *Climatic change and global warming of inland waters: impacts and mitigation for ecosystems and societies*. John Wiley & Sons.
- Gomez-Velez, J. D., Harvey, J. W., Cardenas, M. B., & Kiel, B. (2015). Denitrification in the Mississippi River network controlled by flow through river bedforms. *Nature Geoscience*, 8(12), 941-945.
- Goolsby, D. A., Battaglin, W. A., Lawrence, G. B., Artz, R. S., Aulenbach, B. T., Hooper, R. P., ... & Stensland, G. J. (1999). Flux and sources of nutrients in the Mississippi-Atchafalaya River Basin: Topic 3 Report for the Integrated Assessment on Hypoxia in the Gulf of Mexico.
- Grannemann, N. G. (2000). *The importance of ground water in the Great Lakes region* (No. 4008). US Department of the Interior, US Geological Survey.
- Green, D. B., Logan, T. J., & Smeck, N. E. (1978). Phosphate Adsorption-Desorption Characteristics of Suspended Sediments in the Maumee River Basin of Ohio. *Journal of Environmental Quality*, 7(2), 208-212.
- Gruber, N., & Galloway, J. N. (2008). An Earth-system perspective of the global nitrogen cycle. *Nature*, 451(7176), 293-296.

- Gu, C., Hornberger, G. M., Mills, A. L., Herman, J. S., & Flewelling, S. A. (2007). Nitrate reduction in streambed sediments: Effects of flow and biogeochemical kinetics. *Water Resources Research*, *43*(12).
- Haack, S. K., Neff, B. P., Rosenberry, D. O., Savino, J. F., & Lundstrom, S. C. (2005). An evaluation of effects of groundwater exchange on nearshore habitats and water quality of western Lake Erie. *Journal of Great Lakes Research*, *31*, 45-63.
- Hall Jr, R. O., Tank, J. L., Sobota, D. J., Mulholland, P. J., O'Brien, J. M., Dodds, W. K., ... & Meyer, J. L. (2009). Nitrate removal in stream ecosystems measured by <sup>15</sup>N addition experiments: total uptake. *Limnology and Oceanography*, *54*(3), 653-665.
- Haverland, R., Hendricks, D., & Knisei, V. (1984). Microtrac particle-size analyzer: An alternative particle. size determination method for sediment and soils , *Science*, *138*(2).
- Heisler, J., Glibert, P. M., Burkholder, J. M., Anderson, D. M., Cochlan, W., Dennison, W. C., ... & Lewitus, A. (2008). Eutrophication and harmful algal blooms: a scientific consensus. *Harmful algae*, *8*(1), 3-13.
- Henry, K. M., & Twilley, R. R. (2014). Nutrient biogeochemistry during the early stages of delta development in the Mississippi River deltaic plain. *Ecosystems*, *17*(2), 327-343.
- Hernandez, M. E., & Mitsch, W. J. (2007). Denitrification in created riverine wetlands: Influence of hydrology and season. *Ecological Engineering*, *30*(1), 78-88.

- Herring, S. C., Hoerling, M. P., Peterson, T. C., & Stott, P. A. (2014). Explaining extreme events of 2013 from a climate perspective. *Bulletin of the American Meteorological Society*, 95(9), S1-S104.
- Hester, E. T., Young, K. I., & Widdowson, M. A. (2014). Controls on mixing-dependent denitrification in hyporheic zones induced by riverbed dunes: A steady state modeling study. *Water Resources Research*, 50(11), 9048-9066.
- Hiatt, M. R. (2013). A network-based analysis of river delta surface hydrology: an example from Wax Lake Delta.
- Hiatt, M., & Passalacqua, P. (2015). Hydrological connectivity in river deltas: The first-order importance of channel-island exchange. *Water Resources Research*, 51(4), 2264-2282.
- Hiatt, M., Castañeda-Moya, E., Twilley, R., Hodges, B. R., & Passalacqua, P. (2018). Channel-island connectivity affects water exposure time distributions in a coastal river delta. *Water Resources Research*, 54(3), 2212-2232.
- Hill, A. R. (1996). Nitrate removal in stream riparian zones. *Journal of environmental quality*, 25(4), 743-755.
- Hill, A. R., Devito, K. J., Campagnolo, S., & Sanmugadas, K. (2000). Subsurface denitrification in a forest riparian zone: interactions between hydrology and supplies of nitrate and organic carbon. *Biogeochemistry*, 51(2), 193-223.
- Hill, B. H. (1986). The role of aquatic macrophytes in nutrient flow regulation in lotic ecosystems. In *Rationale for Sampling and Interpretation of Ecological Data in the Assessment of Freshwater Ecosystems*. ASTM

- Hoaglund III, J. R., Huffman, G. C., & Grannemann, N. G. (2002). Michigan basin regional ground water flow discharge to three Great Lakes. *Groundwater*, 40(4), 390-406.
- Holman, I. P., Whelan, M. J., Howden, N. J., Bellamy, P. H., Willby, N. J., Rivas-Casado, M., & McConvey, P. (2008). Phosphorus in groundwater—an overlooked contributor to eutrophication?. *Hydrological Processes: An International Journal*, 22(26), 5121-5127.
- Holmes, Robert Max, et al. "Seasonal and annual fluxes of nutrients and organic matter from large rivers to the Arctic Ocean and surrounding seas." *Estuaries and Coasts* 35.2 (2012): 369-382.
- Howarth, R. (1988). Nutrient Limitation of Net Primary Production in Marine Ecosystems. *Annual Review of Ecology and Systematics*, 19(1), pp.89-110.
- Howarth, R. W., Marino, R., Lane, J., & Cole, J. J. (1988). Nitrogen fixation in freshwater, estuarine, and marine ecosystems. 1. Rates and importance 1. *Limnology and Oceanography*, 33(4part2), 669-687.
- Inwood, S. E., Tank, J. L., & Bernot, M. J. (2007). Factors controlling sediment denitrification in midwestern streams of varying land use. *Microbial Ecology*, 53(2), 247-258.
- IPCC Climate Change 2013: The Physical Science Basis (eds Stocker, T. F. et al.) (Cambridge Univ. Press, 2013).

- Jackson, G. A., & Williams, P. M. (1985). Importance of dissolved organic nitrogen and phosphorus to biological nutrient cycling. *Deep Sea Research Part A. Oceanographic Research Papers*, 32(2), 223-235.
- Jetten, M. S., Strous, M., Van de Pas-Schoonen, K. T., Schalk, J., van Dongen, U. G., van de Graaf, A. A., ... & Kuenen, J. G. (1998). The anaerobic oxidation of ammonium. *FEMS microbiology reviews*, 22(5), 421-437.
- Johnson, W. B., Sasser, C. E., & Gosselink, J. G. (1985). Succession of vegetation in an evolving river delta, Atchafalaya Bay, Louisiana. *The Journal of Ecology*, 973-986.
- Joung, D., Guo, L., & Shiller, A. M. (2019). Role of the Atchafalaya River Basin in regulating export fluxes of dissolved organic carbon, nutrients, and trace elements to the Louisiana Shelf. *Journal of Hydrology X*, 2, 100018.
- Kadlec, R. H. (1997). An autotrophic wetland phosphorus model. *Ecological Engineering*, 8(2), 145-172.
- Keuper, F., van Bodegom, P. M., Dorrepaal, E., Weedon, J. T., van Hal, J., van Logtestijn, R. S., & Aerts, R. (2012). A frozen feast: Thawing permafrost increases plant-available nitrogen in subarctic peatlands. *Global Change Biology*, 18(6), 1998-2007.
- Kilroy, G., & Coxon, C. (2005). Temporal variability of phosphorus fractions in Irish karst springs. *Environmental Geology*, 47(3), 421-430.

- Kjellin, J., Hallin, S., & Wörman, A. (2007). Spatial variations in denitrification activity in wetland sediments explained by hydrology and denitrifying community structure. *Water Research*, *41*(20), 4710-4720.
- Knights, D., Brown, A. M., Sawyer, A. H., Barnes, R. T., Edmonds, D. A., & Olliver, E. A. (2019). Nitrate removal across ecogeomorphic zones in Wax Lake Delta, Louisiana (USA). *AGUFM*, 2019, B41D-01.
- Knights, D., Sawyer, A. H., Barnes, R. T., Musial, C. T., & Bray, S. (2017). Tidal controls on riverbed denitrification along a tidal freshwater zone. *Water Resources Research*, *53*(1), 799-816
- Konikow, L. F. (2013). *Groundwater depletion in the United States (1900-2008)*. Reston, Virginia: US Department of the Interior, US Geological Survey.
- Konikow, L. F., & Kendy, E. (2005). Groundwater depletion: A global problem. *Hydrogeology Journal*, *13*(1), 317-320.
- Kreiling, R. M., Richardson, W. B., Cavanaugh, J. C., & Bartsch, L. A. (2011). Summer nitrate uptake and denitrification in an upper Mississippi River backwater lake: the role of rooted aquatic vegetation. *Biogeochemistry*, *104*(1-3), 309-324.
- Kroeger, K. D., & Charette, M. A. (2008). Nitrogen biogeochemistry of submarine groundwater discharge. *Limnology and Oceanography*, *53*(3), 1025-1039.
- Kröger, R., Moore, M. T., Locke, M. A., Cullum, R. F., Steinriede Jr, R. W., Testa Iii, S., ... & Cooper, C. M. (2009). Evaluating the influence of wetland vegetation on chemical residence time in Mississippi Delta drainage ditches. *Agricultural Water Management*, *96*(7), 1175-1179.

- LaBaugh, J. W., Winter, T. C., Rosenberry, D. O., Schuster, P. F., Reddy, M. M., & Aiken, G. R. (1997). Hydrological and chemical estimates of the water balance of a closed-basin lake in north central Minnesota. *Water Resources Research*, 33(12), 2799-2812.
- Landsberg, J. H. (2002). The effects of harmful algal blooms on aquatic organisms. *Reviews in Fisheries Science*, 10(2), 113-390.
- Lane, R. R., Day, J. W., Marx, B., Reves, E., & Kemp, G. P. (2002). Seasonal and spatial water quality changes in the outflow plume of the Atchafalaya River, Louisiana, USA. *Estuaries*, 25(1), 30-42.
- Lane, R. R., Mashriqui, H. S., Kemp, G. P., Day, J. W., Day, J. N., & Hamilton, A. (2003). Potential nitrate removal from a river diversion into a Mississippi delta forested wetland. *Ecological Engineering*, 20(3), 237-249.
- Lapointe, B. E. (1997). Nutrient thresholds for bottom-up control of macroalgal blooms on coral reefs in Jamaica and southeast Florida. *Limnology and Oceanography*, 42(5part2), 1119-1131.
- Lee, D. R. (1977). A device for measuring seepage flux in lakes and estuaries  
1. *Limnology and Oceanography*, 22(1), 140-147.
- Lehner, B., Verdin, K., & Jarvis, A. (2008). New global hydrography derived from spaceborne elevation data. *Eos, Transactions American Geophysical Union*, 89(10), 93-94.

- Leopold, A. (1970). *A Sand County almanac: With other essays on conservation from Round River*. Outdoor Essays & Reflections.
- Lesser, G. R., Roelvink, J. V., Van Kester, J. A. T. M., & Stelling, G. S. (2004). Development and validation of a three-dimensional morphological model. *Coastal engineering*, 51(8-9), 883-915.
- Lewandowski, J., Meinikmann, K., Nützmann, G., & Rosenberry, D. O. (2015). Groundwater—the disregarded component in lake water and nutrient budgets. Part 2: effects of groundwater on nutrients. *Hydrological processes*, 29(13), 2922-2955.
- Libelo, E. L., & MacIntyre, W. G. (1994). Effects of surface-water movement on seepage-meter measurements of flow through the sediment-water interface. *Applied Hydrogeology*, 2(4), 49-54.
- Liddel, M., & Yenko, M. (2020). *Fisheries of the United States*, 2018.
- Lin, Y. F., Jing, S. R., Wang, T. W., & Lee, D. Y. (2002). Effects of macrophytes and external carbon sources on nitrate removal from groundwater in constructed wetlands. *Environmental pollution*, 119(3), 413-420.
- Ma, H., Larsen, L. G., & Wagner, R. W. (2018). Ecogeomorphic feedbacks that grow deltas. *Journal of Geophysical Research: Earth Surface*, 123(12), 3228-3250.
- Makarewicz, J. C. (1993). Phytoplankton biomass and species composition in Lake Erie, 1970 to 1987. *Journal of Great Lakes Research*, 19(2), 258-274.

- Makarewicz, J. C., Lewis, T. W., & Bertram, P. (1999). Phytoplankton composition and biomass in the offshore waters of Lake Erie: pre-and post-Dreissena introduction (1983–1993). *Journal of Great Lakes Research*, 25(1), 135-148.
- Matheson, F. E., Nguyen, M. L., Cooper, A. B., Burt, T. P., & Bull, D. C. (2002). Fate of <sup>15</sup>N-nitrate in unplanted, planted and harvested riparian wetland soil microcosms. *Ecological Engineering*, 19(4), 249-264.
- Martinez, C. J., & Wise, W. R. (2003). Analysis of constructed treatment wetland hydraulics with the transient storage model OTIS. *Ecological Engineering*, 20(3), 211-222.
- Matisoff, G., Kaltenberg, E. M., Steely, R. L., Hummel, S. K., Seo, J., Gibbons, K. J., ... & Johnson, L. T. (2016). Internal loading of phosphorus in western Lake Erie. *Journal of Great Lakes Research*, 42(4), 775-788.
- McBride, M. S., & Pfannkuch, H. O. (1975). The distribution of seepage within lakebeds. *J. Res. US Geol. Surv*, 3(5), 505-512.
- McClain, M. E., Boyer, E. W., Dent, C. L., Gergel, S. E., Grimm, N. B., Groffman, P. M., ... & McDowell, W. H. (2003). Biogeochemical hot spots and hot moments at the interface of terrestrial and aquatic ecosystems. *Ecosystems*, 301-312.
- McKay, L., Bondelid, T., Dewald, T., Johnston, J., Moore, R., & Rea, A. (2012). NHDPlus Version 2: user guide. *US Environmental Protection Agency*.
- McKnight, D. M., Boyer, E. W., Westerhoff, P. K., Doran, P. T., Kulbe, T., & Andersen, D. T. (2001). Spectrofluorometric characterization of dissolved organic matter for

- indication of precursor organic material and aromaticity. *Limnology and Oceanography*, 46(1), 38-48.
- Meals, D. W., Dressing, S. A., & Davenport, T. E. (2010). Lag time in water quality response to best management practices: A review. *Journal of environmental quality*, 39(1), 85-96.
- Mee, L. (2006). Reviving dead zones. *Scientific American*, 295(5), 78-85.
- Meinikmann, K., Hupfer, M., & Lewandowski, J. (2015). Phosphorus in groundwater discharge—A potential source for lake eutrophication. *Journal of Hydrology*, 524, 214-226.
- Meinikmann, K., Lewandowski, J., & Nützmann, G. (2013). Lacustrine groundwater discharge: Combined determination of volumes and spatial patterns. *Journal of Hydrology*, 502, 202-211.
- Michael, H. A., Mulligan, A. E., & Harvey, C. F. (2005). Seasonal oscillations in water exchange between aquifers and the coastal ocean. *Nature*, 436(7054), 1145-1148.
- Michalak, A. M., Anderson, E. J., Beletsky, D., Boland, S., Bosch, N. S., Bridgeman, T. B., ... & DePinto, J. V. (2013). Record-setting algal bloom in Lake Erie caused by agricultural and meteorological trends consistent with expected future conditions. *Proceedings of the National Academy of Sciences*, 110(16), 6448-6452.
- Morang, A., Mohr, M. C., & Forgette, C. M. (2011). Longshore sediment movement and supply along the US shoreline of Lake Erie. *Journal of Coastal Research*, 27(4), 619-635.

- Mulholland, P. J., Newbold, J. D., Elwood, J. W., & Ferren, L. A. (1985). Phosphorus spiraling in a woodland stream: Seasonal variations. *Ecology*, *66*(3), 1012–1023.
- Mulholland, P. J., Helton, A. M., Poole, G. C., Hall, R. O., Hamilton, S. K., Peterson, B. J., ... & Dodds, W. K. (2008). Stream denitrification across biomes and its response to anthropogenic nitrate loading. *Nature*, *452*(7184), 202.
- Mulholland, P. J., Hall Jr, R. O., Sobota, D. J., Dodds, W. K., Findlay, S. E., Grimm, N. B., ... & Ashkenas, L. R. (2009). Nitrate removal in stream ecosystems measured by <sup>15</sup>N addition experiments: denitrification. *Limnology and Oceanography*, *54*(3), 666-680.
- Nardin, W., & Edmonds, D. A. (2014). Optimum vegetation height and density for inorganic sedimentation in deltaic marshes. *Nature Geoscience*, *7*(10), 722.
- Nardin, W., & Fagherazzi, S. (2012). The effect of wind waves on the development of river mouth bars. *Geophysical Research Letters*, *39*(12).
- National Marine Fisheries Service (2020) Fisheries of the United States, 2018. U.S. Department of Commerce, NOAA Current Fishery Statistics No. 2018 Available at: <https://www.fisheries.noaa.gov/national/commercial-fishing/fisheries-united-states-2018>
- Nepf, H. M. (2012). Flow and transport in regions with aquatic vegetation. *Annual review of fluid mechanics*, *44*, 123-142.
- Newbold, J. D., Elwood, J. W., O'Neill, R. V., & Winkle, W. V. (1981). Measuring nutrient spiralling in streams. *Canadian Journal of Fisheries and Aquatic Sciences*, *38*(7), 860-863.

- Nixon, S. W. (1981). Remineralization and nutrient cycling in coastal marine ecosystems. In *Estuaries and nutrients* (pp. 111-138). Humana Press.
- NOAA, 2015. USGS Atchafalaya 2 LiDAR. NOAA's Ocean Service, Office for Coastal Management (OCM), Charleston, SC.
- NRC (2000), Clean Coastal Waters: Understanding and Reducing the Effects of Nutrient Pollution, 428 pp., National Academies Press.
- O'Brien, J. M., Hamilton, S. K., Podzikowski, L., & Ostrom, N. (2012). The fate of assimilated nitrogen in streams: an in situ benthic chamber study. *Freshwater Biology*, 57(6), 1113-1125.
- O'Connor, M. T., & Moffett, K. B. (2015). Groundwater dynamics and surface water–groundwater interactions in a prograding delta island, Louisiana, USA. *Journal of hydrology*, 524, 15-29.
- Ocampo, C. J., Oldham, C. E., & Sivapalan, M. (2006). Nitrate attenuation in agricultural catchments: Shifting balances between transport and reaction. *Water Resources Research*, 42(1).
- Odum, W. E. (1988). Comparative ecology of tidal freshwater and salt marshes. *Annual review of ecology and systematics*, 19(1), 147-176.
- Oldham, C. E., Farrow, D. E., & Peiffer, S. (2013). A generalized Damköhler number for classifying material processing in hydrological systems. *Hydrology and Earth System Sciences*, 17(3), 1133-1148.

- Olliver, E. A., & Edmonds, D. A. (2017). Defining the ecogeomorphic succession of land building for freshwater, intertidal wetlands in Wax Lake Delta, Louisiana. *Estuarine, Coastal and Shelf Science*, 196, 45-57.
- Olliver, E. A., Edmonds, D. A., & Shaw, J. B. (2020). Influence of floods, tides, and vegetation on sediment retention in Wax Lake Delta, Louisiana, USA. *Journal of Geophysical Research: Earth Surface*, 125(1), e2019JF005316.
- Orams, M. (1999). *Marine tourism: development, impacts and management*. Psychology Press.
- Paerl, H. W., Pinckney, J. L., Fear, J. M., & Peierls, B. L. (1998). Ecosystem responses to internal and watershed organic matter loading: consequences for hypoxia in the eutrophying Neuse River Estuary, North Carolina, USA. *Marine Ecology Progress Series*, 166, 17-25.
- Parker, G., Paola, C., Whipple, K. X., & Mohrig, D. (1998). Alluvial fans formed by channelized fluvial and sheet flow. I: Theory. *Journal of Hydraulic engineering*, 124(10), 985-995.
- Paola, C., Twilley, R. R., Edmonds, D. A., Kim, W., Mohrig, D., Parker, G., ... & Voller, V. R. (2011). Natural processes in delta restoration: Application to the Mississippi Delta. *Annual review of marine science*, 3, 67-91.
- Piliouras, A., & Rowland, J. C. (2020). Arctic river delta morphologic variability and implications for riverine fluxes to the coast. *Journal of Geophysical Research: Earth Surface*, 125(1), e2019JF005250.

- Poste, A. E., Hecky, R. E., & Guildford, S. J. (2011). Evaluating microcystin exposure risk through fish consumption. *Environmental science & technology*, *45*(13), 5806-5811.
- Powers, S. M., Johnson, R. A., & Stanley, E. H. (2012). Nutrient retention and the problem of hydrologic disconnection in streams and wetlands. *Ecosystems*, *15*(3), 435-449.
- Quilbé, R., Rousseau, A. N., Duchemin, M., Poulin, A., Gangbazo, G., & Villeneuve, J. P. (2006). Selecting a calculation method to estimate sediment and nutrient loads in streams: application to the Beaurivage River (Québec, Canada). *Journal of Hydrology*, *326*(1-4), 295-310.
- Rabalais, N. N., Turner, R. E., & Wiseman Jr, W. J. (2002). Gulf of Mexico hypoxia, aka “The dead zone”. *Annual Review of ecology and Systematics*, *33*(1), 235-263.
- Rabalais, N. N., Diaz, R. J., Levin, L. A., Turner, R. E., Gilbert, D., & Zhang, J. (2017). Dynamics and distribution of natural and human-caused hypoxia. *Biogeosciences*
- Rabalais, N. N., Turner, R. E., Justić, D., Dortch, Q., Wiseman, W. J., & Gupta, B. K. S. (1996). Nutrient changes in the Mississippi River and system responses on the adjacent continental shelf. *Estuaries*, *19*(2), 386-407.
- Reddy, K. R., & Gale, P. M. (1994). Wetland processes and water quality: a symposium overview. *Journal of environmental quality*, *23*(5), 875-877.
- Reddy, K. R., Patrick, W. H., & Broadbent, F. E. (1984). Nitrogen transformations and loss in flooded soils and sediments. *Critical Reviews in Environmental Science and Technology*, *13*(4), 273-309.

- Robertson, D. M., Rose, W. J., & Saad, D. A. (2005). *Water quality, hydrology, and phosphorus loading to Little St. Germain Lake, Wisconsin, with special emphasis on the effects of winter aeration and ground-water inputs*. US Department of the Interior, US Geological Survey.
- Robinson, C. (2015). Review on groundwater as a source of nutrients to the Great Lakes and their tributaries. *Journal of Great Lakes Research*, 41(4), 941-950.
- Rosen, T., & Xu, Y. J. (2013). Recent decadal growth of the Atchafalaya River Delta complex: Effects of variable riverine sediment input and vegetation succession. *Geomorphology*, 194, 108-120.
- Rosenberry, D. O. (2008). A seepage meter designed for use in flowing water. *Journal of Hydrology*, 359(1-2), 118-130.
- Rosenberry, D. O., & Morin, R. H. (2004). Use of an electromagnetic seepage meter to investigate temporal variability in lake seepage. *Groundwater*, 42(1), 68-77.
- Rosenberry, D. O., Lewandowski, J., Meinikmann, K., & Nützmann, G. (2015). Groundwater-the disregarded component in lake water and nutrient budgets. Part 1: effects of groundwater on hydrology. *Hydrological processes*, 29(13), 2895-2921.
- Russoniello, C. J., Fernandez, C., Bratton, J. F., Banaszak, J. F., Krantz, D. E., Andres, A. S., ... & Michael, H. A. (2013). Geologic effects on groundwater salinity and discharge into an estuary. *Journal of hydrology*, 498, 1-12.
- Rysgaard, S., Risgaard-Petersen, N., Nielsen, L. P., & Revsbech, N. P. (1993). Nitrification and denitrification in lake and estuarine sediments measured by the

- 15N dilution technique and isotope pairing. *Appl. Environ. Microbiol.*, 59(7), 2093-2098.
- Rysgaard, S., Glud, R. N., Risgaard-Petersen, N., & Dalsgaard, T. (2004). Denitrification and anammox activity in Arctic marine sediments. *Limnology and oceanography*, 49(5), 1493-1502.
- Saeed, T., & Sun, G. (2012). A review on nitrogen and organics removal mechanisms in subsurface flow constructed wetlands: dependency on environmental parameters, operating conditions and supporting media. *Journal of environmental management*, 112, 429-448.
- Salles, P., Valle-Levinson, A., Sottolichio, A., & Senechal, N. (2015). Wind-driven modifications to the residual circulation in an ebb-tidal delta: Arcachon Lagoon, Southwestern France. *Journal of Geophysical Research: Oceans*, 120(2), 728-740.
- Saunders, D. L., & Kalff, J. (2001). Nitrogen retention in wetlands, lakes and rivers. *Hydrobiologia*, 443(1-3), 205-212.
- Sawyer, A. H., David, C. H., & Famiglietti, J. S. (2016). Continental patterns of submarine groundwater discharge reveal coastal vulnerabilities. *Science*, 353(6300), 705-707.
- Sawyer, A. H., Edmonds, D. A., & Knights, D. (2015). Surface water-groundwater connectivity in deltaic distributary channel networks. *Geophysical Research Letters*, 42(23), 10-299.

- Schaller, M. F., & Fan, Y. (2009). River basins as groundwater exporters and importers: Implications for water cycle and climate modeling. *Journal of Geophysical Research: Atmospheres*, 114(D4).
- Schneider, R. L., Negley, T. L., & Wafer, C. (2005). Factors influencing groundwater seepage in a large, mesotrophic lake in New York. *Journal of Hydrology*, 310(1-4), 1-16.
- Schuster, P. F., Reddy, M. M., LaBaugh, J. W., Parkhurst, R. S., Rosenberry, D. O., Winter, T. C., ... & Dean, W. E. (2003). Characterization of lake water and ground water movement in the littoral zone of Williams Lake, a closed-basin lake in north central Minnesota. *Hydrological Processes*, 17(4), 823-838.
- Schwenk, J. P., Piliouras, A., & Rowland, J. C. (2020). Determining flow directions in river channel networks using planform morphology and topology. *Earth Surface Dynamics (Online)*, 8(LA-UR-19-22689).
- Schwenk, J., Tejedor, A., Fofoula-Georgiou, E., & Rowland, J. C. (2018, December). Automatic Extraction of Delta Channel Network Topology. In *AGU Fall Meeting Abstracts*.
- Seaber, P. R., Kapinos, F. P., & Knapp, G. L. (1987). Hydrologic unit maps.
- Seitzinger, S. P. (1988). Denitrification in freshwater and coastal marine ecosystems: ecological and geochemical significance. *Limnology and oceanography*, 33(4part2), 702-724.

- Seitzinger, S., Harrison, J. A., Böhlke, J. K., Bouwman, A. F., Lowrance, R., Peterson, B., ... & Drecht, G. V. (2006). Denitrification across landscapes and waterscapes: a synthesis. *Ecological applications*, *16*(6), 2064-2090.
- Sendrowski, A., & Passalacqua, P. (2017). Process connectivity in a naturally prograding river delta. *Water Resources Research*, *53*(3), 1841-1863.
- Serrano, L., Filella, I., & Penuelas, J. (2000). Remote sensing of biomass and yield of winter wheat under different nitrogen supplies. *Crop science*, *40*(3), 723-731.
- Shaw, J. B., Mohrig, D., & Whitman, S. K. (2013). The morphology and evolution of channels on the Wax Lake Delta, Louisiana, USA. *Journal of Geophysical Research: Earth Surface*, *118*(3), 1562-1584.
- Shaw, R. D., & Prepas, E. E. (1990). Groundwater-lake interactions: I. Accuracy of seepage meter estimates of lake seepage. *Journal of Hydrology*, *119*(1-4), 105-120.
- Shaw, J. B., Ayoub, F., Jones, C. E., Lamb, M. P., Holt, B., Wagner, R. W., ... & Mohrig, D. (2016). Airborne radar imaging of subaqueous channel evolution in Wax Lake Delta, Louisiana, USA. *Geophysical Research Letters*, *43*(10), 5035-5042
- Simonds, F. W., Swarzenski, P. W., Rosenberry, D. O., Reich, C. D., & Paulson, A. J. (2008). Estimates of Nutrient Loading by Ground-Water Discharge into the Lynch Cove Area of Hood Canal, Washington. *Scientific Investigations Report*.
- Slomp, C. P., & Van Cappellen, P. (2004). Nutrient inputs to the coastal ocean through submarine groundwater discharge: controls and potential impact. *Journal of Hydrology*, *295*(1-4), 64-86.

- Smith, S. V. (1984). Phosphorus versus nitrogen limitation in the marine environment  
1. *Limnology and oceanography*, 29(6), 1149-1160.
- Smith, V. H. (1983). Low nitrogen to phosphorus ratios favor dominance by blue-green  
algae in lake phytoplankton. *Science*, 221(4611), 669-671.
- Sonzogni, W. C., Chapra, S. C., Armstrong, D. E., & Logan, T. J. (1982). Bioavailability  
of phosphorus inputs to lakes 1. *Journal of Environmental Quality*, 11(4), 555-  
563.
- Speiran, G. K., Hamilton, P. A., & Woodside, M. D. (1998). *Natural Processes for  
Managing Nitrate in Ground Water Discharged to Chesapeake Bay and other  
surface waters: more than forest buffers*. US Department of the Interior, US  
Geological Survey.
- Spruill, T. B. (2000). Statistical evaluation of effects of riparian buffers on nitrate and  
ground water quality. *Journal of Environmental Quality*, 29(5), 1523-1538.
- Stow, C. A., Cha, Y., Johnson, L. T., Confesor, R., & Richards, R. P. (2015). Long-term  
and seasonal trend decomposition of Maumee River nutrient inputs to western  
Lake Erie. *Environmental science & technology*, 49(6), 3392-3400.
- Syvitski, J. P., & Saito, Y. (2007). Morphodynamics of deltas under the influence of  
humans. *Global and Planetary Change*, 57(3-4), 261-282.
- Syvitski, J. P., Kettner, A. J., Overeem, I., Hutton, E. W., Hannon, M. T., Brakenridge, G.  
R., ... & Nicholls, R. J. (2009). Sinking deltas due to human activities. *Nature  
Geoscience*, 2(10), 681.

- Tank, J. L., Bernot, M. J., & Rosi-Marshall, E. J. (2006). Nitrogen limitation and uptake. In F. R. Hauer & G. A. Lamberti (Eds.), *Methods in stream ecology* (2nd ed., pp. 213–238). San Diego, CA: Academic Press.
- Tank, J. L., Rosi-Marshall, E. J., Baker, M. A., & Hall, R. O. (2008). Are rivers just big streams? A pulse method to quantify nitrogen demand in a large river. *Ecology*, 89(10), 2935-2945.
- Tayfur, G., & Singh, V. P. (2005). Predicting longitudinal dispersion coefficient in natural streams by artificial neural network. *Journal of Hydraulic Engineering*, 131(11), 991-1000.
- Tejedor, A., Longjas, A., Caldwell, R., Edmonds, D. A., Zaliapin, I., & Foufoula-Georgiou, E. (2016). Quantifying the signature of sediment composition on the topologic and dynamic complexity of river delta channel networks and inferences toward delta classification. *Geophysical Research Letters*, 43(7), 3280-3287.
- Tejedor, A., Longjas, A., Edmonds, D. A., Zaliapin, I., Georgiou, T. T., Rinaldo, A., & Foufoula-Georgiou, E. (2017). Entropy and optimality in river deltas. *Proceedings of the National Academy of Sciences*, 114(44), 11651-11656.
- Tejedor, A., Longjas, A., Zaliapin, I., & Foufoula-Georgiou, E. (2015). Delta channel networks: 1. A graph-theoretic approach for studying connectivity and steady state transport on deltaic surfaces. *Water Resources Research*, 51(6), 3998-4018.
- Tejedor, A., Longjas, A., Kantz, H., Foufoula-Georgiou, E., Passalacqua, P., & Moreno, Y. (2019, January). A general framework to study multi-process connectivity: Multilayer Networks. In *Geophysical Research Abstracts* (Vol. 21).

- Tiedje, J. M. (1988). Ecology of denitrification and dissimilatory nitrate reduction to ammonium. *Biology of anaerobic microorganisms*, 717, 179-244.
- Thomas, W. H. (1966). Surface Nitrogenous Nutrients and Phytoplankton in the Northeastern Tropical Pacific Ocean 1. *Limnology and Oceanography*, 11(3), 393-400.
- Toran, L., Nyquist, J., Rosenberry, D., Gagliano, M., Mitchell, N., & Mikochik, J. (2015). Geophysical and hydrologic studies of lake seepage variability. *Groundwater*, 53(6), 841-850.
- Twilley, R. R., & Rivera-Monroy, V. (2009). Sediment and nutrient tradeoffs in restoring Mississippi River delta: restoration vs eutrophication. *Journal of Contemporary Water Research & Education*, 141(1), 39-44.
- Van Maren, D. S., Winterwerp, J. C., Wu, B. S., & Zhou, J. J. (2009). Modelling hyperconcentrated flow in the Yellow River. *Earth Surface Processes and Landforms*, 34(4), 596-612.
- Vaquer-Sunyer, R., & Duarte, C. M. (2008). Thresholds of hypoxia for marine biodiversity. *Proceedings of the National Academy of Sciences*, 105(40), 15452-15457.
- Vollenweider, R. A. (1976). Advances in defining critical loading levels for phosphorus in lake eutrophication. *Memorie dell'Istituto Italiano di Idrobiologia, Dott. Marco de Marchi Verbania Pallanza*.
- Vymazal, J. (1995). *Algae and element cycling in wetlands*. Lewis Publishers Inc.

- Vymazal, J. (2007). Removal of nutrients in various types of constructed wetlands. *Science of the total environment*, 380(1-3), 48-65.
- Vymazal, J. (2011). Plants used in constructed wetlands with horizontal subsurface flow: a review. *Hydrobiologia*, 674(1), 133-156.
- Vymazal, J., Dušek, J., & Květ, J. (1999). Nutrient uptake and storage by plants in constructed wetlands with horizontal sub-surface flow: a comparative study. *Nutrient cycling and retention in natural and constructed wetlands*, 85-100.
- Wagner, W., Lague, D., Mohrig, D., Passalacqua, P., Shaw, J., & Moffett, K. (2017). Elevation change and stability on a prograding delta. *Geophysical Research Letters*, 44(4), 1786-1794.
- Webster, J. R. (1975). *Analysis of potassium and calcium dynamics in stream ecosystems on three southern Appalachian watersheds of contrasting vegetation* (Doctoral dissertation, University of Georgia)
- Wetzel, R.G. 1975. Limnology. W.B. Saunders, Philadelphia, PA, pp. 14-15.
- Weiskel, P. K., & Howes, B. L. (1992). Differential transport of sewage-derived nitrogen and phosphorus through a coastal watershed. *Environmental science & technology*, 26(2), 352-360.
- Weisner, S. E., Eriksson, P. G., Granéli, W., & Leonardson, L. (1994). Influence of macrophytes on nitrate. *Ambio*, 23(6), 363-366.
- Wellner, R., Beaubouef, R., Van Wagoner, J., Roberts, H., & Sun, T. (2005). Jet-plume depositional bodies—the primary building blocks of Wax Lake Delta.

- Whipple, K. X., Parker, G., Paola, C., & Mohrig, D. (1998). Channel dynamics, sediment transport, and the slope of alluvial fans: experimental study. *The Journal of geology*, *106*(6), 677-694.
- Whitney, D. M., Chalmers, A. G., Haines, E. B., Hanson, R. B., Pomeroy, L. R., & Sherr, B. (1981). The cycles of nitrogen and phosphorus. In *The ecology of a salt marsh* (pp. 163-181). Springer, New York, NY.
- Wolinsky, M. A., Edmonds, D. A., Martin, J., & Paola, C. (2010). Delta allometry: Growth laws for river deltas. *Geophysical Research Letters*, *37*(21).
- Wolf, D., Georgic, W., & Klaiber, H. A. (2017). Reeling in the damages: Harmful algal blooms' impact on Lake Erie's recreational fishing industry. *Journal of environmental management*, *199*, 148-157.
- Wollheim, W. M., Vörösmarty, C. J., Bouwman, A. F., Green, P., Harrison, J., Linder, E., ... & Syvitski, J. P. (2008). Global N removal by freshwater aquatic systems using a spatially distributed, within-basin approach. *Global Biogeochemical Cycles*, *22*(2).
- Wollheim, W. M., Vörösmarty, C. J., Peterson, B. J., Seitzinger, S. P., & Hopkinson, C. S. (2006). Relationship between river size and nutrient removal. *Geophysical Research Letters*, *33*(6).
- Workshop, S. S. (1990). Concepts and methods for assessing solute dynamics in stream ecosystems. *Journal of the North American Benthological Society*, *9*(2), 95-119.
- Xia, Y., Mitchell, K., Ek, M., Sheffield, J., Cosgrove, B., Wood, E., ... & Livneh, B. (2012). Continental-scale water and energy flux analysis and validation for the

- North American Land Data Assimilation System project phase 2 (NLDAS-2): 1. Intercomparison and application of model products. *Journal of Geophysical Research: Atmospheres*, 117(D3).
- Ye, S., Reisinger, A. J., Tank, J. L., Baker, M. A., Hall, R. O., Rosi, E. J., & Sivapalan, M. (2017). Scaling dissolved nutrient removal in river networks: A comparative modeling investigation. *Water Resources Research*, 53(11), 9623-9641.
- Yu, J. B., Fu, Y. Q., Li, Y. Z., Han, G. X., Wang, Y. L., Zhou, D., ... & Meixner, F. X. (2011). Effects of water discharge and sediment load on evolution of modern Yellow River Delta, China, over the period from 1976 to 2009.
- Zektser, I. S., & Loaiciga, H. A. (1993). Groundwater fluxes in the global hydrologic cycle: past, present and future. *Journal of Hydrology*, 144(1-4), 405-427.

## Appendix A. Wax Lake Delta Field Supplement



Figure A1. Photo of installed open atmospheric benthic chambers (a) with and (b) without vegetation.

Chamber	Vf		C0			Elevation		NDVI	LOI	Sand	Silt	Clay
	(mm_hr)	Kt_1_hr	cham	C_bac	Cl (initial)	h_av (m)						
6_23 A1	2.2629	0.0049	10.07	0.892	20.06	0.46	-0.227	0.5118	0.85	29.7	57.0	13.36
6_23 A2	2.3362	0.0046	4.43	0.941	19.169	0.51	-0.227	0.5118	0.85	29.7	57.0	13.36
6_23 A3	5.6511	0.0117	1.01	1.006	19.993	0.48	-0.227	0.5118	0.85	29.7	57.0	13.36
6_23 B1	1.1035	0.0023	9.33	0.992	19.149	0.48	-0.227	0.5118	0.85	29.7	57.0	13.36
6_23 B2	1.2053	0.0026	4.37	0.928	18.155	0.47	-0.227	0.5118	0.85	29.7	57.0	13.36
6_23 B3	4.2686	0.0092	0.97	0.966	18.060	0.47	-0.227	0.5118	0.85	29.7	57.0	13.36
6_24 A1	5.1858	0.0115	2.90	1.101	19.890	0.45	-0.121	0.5408	1.92	26.4	61.1	12.52
6_24 A2	5.2614	0.0122	2.75	1.106	19.825	0.43	-0.121	0.5408	2.06	2.4	79.1	18.55
6_24 B1	1.9824	0.0056	5.93	1.140	19.935	0.35	-0.246	0.6269	1.62	37.1	42.1	20.74
6_24 B2	5.6010	0.0150	3.56	1.220	19.462	0.37	-0.245	0.6269	1.81	32.9	50.3	16.76
6_24 B3	3.3994	0.0099	3.83	1.220	19.462	0.34	-0.121	0.6269	1.85	53.9	32.5	13.6
6_25 A1	18.9753	0.0437	1.81	0.068	20.160	0.43	0.225	0.7989	0.85	48.0	38.8	13.27
6_25 B1	4.5083	0.0102	3.73	0.084	20.144	0.44	0.226	0.7989	4.37	44.7	39.3	16.05
6_25 B2	18.7469	0.0486	2.18	0.110	20.389	0.39	0.266	0.7989	2.26	33.6	66.4	0
6_25 C1	11.4147	0.0290	2.28	0.078	20.371	0.39	0.244	0.8165	10.8	13.9	59.4	26.7
6_25 C2	7.9426	0.0168	1.43	0.083	19.754	0.47	0.239	0.8165	6.32	29.2	70.8	0
6_25 D1	9.9795	0.0211	1.58	0.113	21.221	0.47	0.222	0.8165	4.41	18.4	77.1	4.49
6_26 T4	9.9914	0.0190	3.83	1.098	20.221	0.53	-0.125	0.7913	1.36	26.8	73.2	0
6_26 T6	2.1998	0.0046	4.89	1.134	20.432	0.48	-0.071	0.6971	2.87	13.0	60.9	26.1
6_27 L3	1.8355	0.0059	4.67	1.099	20.494	0.31	-0.018	0.3864	0.45	63.0	37.0	0
6_27 N1	2.7286	0.0084	7.29	1.099	20.494	0.33	-0.024	0.6558	0.83	56.1	43.5	0.44
6_27 N2	5.5302	0.0165	4.66	0.509	21.861	0.34	-0.024	0.6558	0.83	56.1	43.5	0.44
6_27 N3	10.8883	0.0306	0.99	0.534	25.386	0.36	-0.024	0.6558	0.83	56.1	43.5	0.44

Table A1. Chemistry Data for Benthic Chambers. C0 cham and C-bac are spiked and unspiked nitrate concentrations in mg N l<sup>-1</sup>. Cl (initial) is initial chloride concentration in mg l<sup>-1</sup> and h\_av is average water depth in m. LOI, sand, silt and clay represent percent lost on ignition and percent sand, silt and clay in sediment.

## Appendix B. Python and R Codes

Below is code for calculating nitrate removal in downstream links for a distributary channel network in Python.

```
#!/usr/bin/env python3
# -*- coding: utf-8 -*-
"""
Created on Mon Jun 24 09:20:36 2019 (D. Knights)
Designed to calculate nitrate removal in distributary river networks using two different
analytical solutions.

@author: deonknights

"""

import geopandas as gpd
import numpy as np
import pandas as pd
import math

#To load shp files
#Update paths for nodes and links before proceeding
linkspath="/Users/deonknights/Desktop/Knights12LANL/RS/Mackenzie/MackenzieUpdated6_24/Mackenzie624Join/Mackenzie624Join2.shp"
nodespath="/Users/deonknights/Desktop/Knights12LANL/RS/Mackenzie/MackenzieUpdated6_24/Mackenzie_nodes_flux.shp"
linkssheet=gpd.read_file(linkspath)
nodessheet=gpd.read_file(nodespath)

#To remove the four extra links and one extra node (super apex?) in linkssheet and
nodessheet
extralinks=[9113,9114,9115,9116]
extranode=[8045]

for e in extralinks:
    linkssheet=linkssheet[linkssheet.id.values != e]
```

```

nodessheet=nodessheet[nodessheet.id.values !=extranode]

#To change the data types from strings to floats
linkssheet['wid_adj']=linkssheet['wid_adj'].astype(float)
linkssheet['len_adj_ol']=linkssheet['len_adj_ol'].astype(float)

#Characteristics of the dataset and model set up.#
dflength=len(linkssheet.index) #Length of dataframe
#Please set your discharge, temperature and concentration

Discharge_main=256518.71 #[m3/min] Decade Winter
#Discharge_main=861555.656 #[m3/min] Decade Summer
#Discharge_main=936000 #For other situations
Discharge=Discharge_main/0.66052 #To adjust percentage of flow from main channel to
whole delta

Temp=0 #[C] Decade Winter Temperature
#Temp=14 #[c] Decade Summer Temperature
Temp_ref=20 #[C]

#TEMPERATURE CORRECTION COEFFICIENTS
#theta=1.047 #[] (A nitrogen model for European catchments: INCA, new model
structure and equations)
Q10=2.71 #[] (Using Ambus 1993. Wollheim 2008 uses 2)

concentration=122000 #[ug N m3] Decade Winter Concentration
#concentration=51000 #[ug N m3] Decade Summer Concentration
#concentration=79792.28 #For other situations

#vf_ref=0.027 #From Blaen (minimum)
#vf_ref=0.003214 #High from Alexander
vf_ref=0.0000654680 # From Wollheim
vf=vf_ref*Q10**((Temp-Temp_ref)/10)

#Setting up columns that will remain constant
Q=[0.000000000001]*dflength
flux2=[0.000000000001]*dflength
HI=[0.000000000001]*dflength
Te=[0.000000000001]*dflength
Te2=[0.000000000001]*dflength
con_in=[0.000000000001]*dflength
con_out=[0.000000000001]*dflength

```

```
con2_in=[0.000000000001]*dflength
con2_out=[0.000000000001]*dflength
k_local=[0.000000000001]*dflength
v_local=[0.000000000001]*dflength
```

```
linkssheet['Q']=Q
linkssheet['flux2']=flux2
linkssheet['HI']=HI
linkssheet['Te']=Te
linkssheet['Te2']=Te2
linkssheet['con_in']=con_in
linkssheet['con_out']=con_out
linkssheet['con2_in']=con2_in
linkssheet['con2_out']=con2_out
linkssheet['k_local']=k_local
linkssheet['v_local']=v_local
```

```
for n in linkssheet.index:
    linkssheet.at[n,'flux2']=10**linkssheet.at[n,'flux']
```

```
for n in linkssheet.index:
    linkssheet.at[n,'Q']=linkssheet.at[n,'flux2']*Discharge
```

```
for n in linkssheet.index:
```

```
linkssheet.at[n,'HI']=linkssheet.at[n,'Q']/linkssheet.at[n,'wid_adj']/linkssheet.at[n,'len_adj_ol'] #[1/min]
```

```
for n in linkssheet.index:
    linkssheet.at[n,'Te']=math.exp((-vf)/linkssheet.at[n,'HI'])
```

```
#Varying k by channel size
```

```
for n in linkssheet.index:
    if linkssheet.at[n,'Q']<1698:
        linkssheet.at[n,'k_local']=0.00032
        linkssheet.at[n,'v_local']=0.00032*0.983
    elif linkssheet.at[n,'Q']>=1698 and linkssheet.at[n,'Q']<16980:
        linkssheet.at[n,'k_local']=0.00008
        linkssheet.at[n,'v_local']=0.00008*1.93
    elif linkssheet.at[n,'Q']>=16980 and linkssheet.at[n,'Q']<51000:
        linkssheet.at[n,'k_local']=0.000035
        linkssheet.at[n,'v_local']=0.000035*3.228
    else:
```

```

linkssheet.at[n,'k_local']=0.0000035
linkssheet.at[n,'v_local']=0.0000035*3.79

```

```

for n in linkssheet.index:

```

```

    linkssheet.at[n,'Te2']=math.exp(-
(linkssheet.at[n,'k_local'])*0.2612*linkssheet.at[n,'wid_adj']*linkssheet.at[
    n,'len_adj_ol']*((linkssheet.at[n,'Q'])**-0.6034)*(Q10**((Temp-Temp_ref)/10)))

```

```

#To calculate concentration in and out for the first link

```

```

linkIDs=[8885,8790,6519,8014]

```

```

fluxin_tot2=[]

```

```

fluxin2_tot2=[]

```

```

for linkID in linkIDs:

```

```

    linkssheet.loc[linkssheet.id==linkID,'con_in']=concentration
    linkssheet.loc[linkssheet.id==linkID,'con_out']=linkssheet.loc[
        linkssheet.id==linkID,'con_in']*linkssheet.loc[linkssheet.id==linkID,'Te']
    linkssheet.loc[linkssheet.id==linkID,'con2_in']=concentration
    linkssheet.loc[linkssheet.id==linkID,'con2_out']=linkssheet.loc[
        linkssheet.id==linkID,'con2_in']*linkssheet.loc[linkssheet.id==linkID,'Te2']

```

```

    fluxin_index=np.where(linkssheet.id.values==linkID)[0]

```

```

    fluxin_tot=(linkssheet.con_in.values[fluxin_index]*linkssheet.Q.values[fluxin_index])

```

```

    fluxin_tot2.append(fluxin_tot)

```

```

fluxin2_tot=(linkssheet.con2_in.values[fluxin_index]*linkssheet.Q.values[fluxin_index])

```

```

    fluxin2_tot2.append(fluxin2_tot)

```

```

fluxin_tot_m=sum(fluxin_tot2)

```

```

fluxin2_tot_m=sum(fluxin2_tot2)

```

```

#Two functions for calculating upstream and downstream links

```

```

def downstreamlinks(linkID,linkssheet,nodessheet):

```

```

    linkIDindex=np.where(linkssheet.id.values==linkID)[0] #index for linkID

```

```

    nodeids=linkssheet.conn.values[linkIDindex]

```

```

    nodeids=nodeids[0].split(',')

```

```

    nodeids=[int(n) for n in nodeids]

```

```

nodeID=nodeids[1] #The downstream node: [1] indicates the second value
(downstream).
nodeIDindex=np.where(nodessheet.id.values==nodeID)[0]

downlinkids=nodessheet.conn.values[nodeIDindex]
downlinkids=downlinkids[0].split(',')
downlinkids=[int(n) for n in downlinkids]
downlinkids.remove(linkID)
#At this point above we have the downstream node and IDs of only the downstream
links.

```

```

downstream=[]

```

```

for lid in downlinkids:
    downlinksrow=np.where(linkssheet.id.values==lid)[0]
    downlinksconn=linkssheet.conn.values[downlinksrow]
    downlinksconn=downlinksconn[0].split(',')
    downlinksconn=[int(n) for n in downlinksconn]

```

```

    if downlinksconn[0]==nodeID: #check
        downstream.append(lid)

```

```

return downstream

```

```

def upstreamlinks(linkID,linksheet,nodessheet):
    linkIDindex=np.where(linksheet.id.values==linkID)[0] #index for linkID

    nodeids=linksheet.conn.values[linkIDindex]
    nodeids=nodeids[0].split(',')
    nodeids=[int(n) for n in nodeids]

    nodeID=nodeids[0] #upstream node [0] indicates the first value (upstream)
    nodeindex=np.where(nodessheet.id.values==nodeID)[0]

    linkids=nodessheet.conn.values[nodeindex]
    linkids=linkids[0].split(',')
    linkids=[int(n) for n in linkids]
    linkids.remove(linkID)

    upstream=[]

    for lid in linkids:

```

```

linksrow=np.where(linkssheet.id.values==lid)[0]
linksconn=linkssheet.conn.values[linksrow]
linksconn=linksconn[0].split(',')
linksconn=[int(n) for n in linksconn]
if linksconn[1]==nodeID:
    upstream.append(lid)

return upstream

todo=[8882,8884,8782,8750,6395,9101]
done={8885,8790,6519,8014} #Why does this not show up in the variable explorer??
end_done=[]

while len(todo)>0:
    currentlink=todo.pop(0)
    us_links=upstreamlinks(currentlink,linkssheet,nodessheet)

    isthisdone=[us in done for us in us_links]

    if False not in isthisdone: # Check if we can do the link
        # solve link
        con_up=[]
        flux_up=[]
        con2_up=[]
        flux2_up=[]
        for upstreamout in us_links:
            con_up.append(linkssheet.con_out.values[linkssheet.id==upstreamout][0])
            flux_up.append(linkssheet.flux2.values[linkssheet.id==upstreamout][0])
            con2_up.append(linkssheet.con2_out.values[linkssheet.id==upstreamout][0])
            flux2_up.append(linkssheet.flux2.values[linkssheet.id==upstreamout][0])

        con_upaverage=sum(np.asarray(con_up)*np.asarray(flux_up))/sum(flux_up)
        con2_upaverage=sum(np.asarray(con2_up)*np.asarray(flux2_up))/sum(flux2_up)
        linkssheet.loc[linkssheet.id==currentlink,'con_in']=con_upaverage
        linkssheet.loc[linkssheet.id==currentlink,'con2_in']=con2_upaverage

        #Calculating the concentration out for the current link
        linkssheet.loc[linkssheet.id==currentlink,'con_out']=linkssheet.loc[

linkssheet.id==currentlink,'con_in']*linkssheet.loc[linkssheet.id==currentlink,'Te']
        done.update([currentlink])

        linkssheet.loc[linkssheet.id==currentlink,'con2_out']=linkssheet.loc[

```

```
linkssheet.id==currentlink,'con2_in']*linkssheet.loc[linkssheet.id==currentlink,'Te2']
```

```
#Since the current link is done finding the downstream links to put into todo  
ds_links=downstreamlinks(currentlink,linkssheet,nodessheet)
```

```
for dsl in ds_links:
```

```
    if dsl not in todo:
```

```
        todo.append(dsl)
```

```
isthisrecorded=[currentlink]
```

```
if ds_links==[] and any(x in end_done for x in isthisrecorded)==False:
```

```
    end_done.append(currentlink)
```

```
else: # What needs to happen if we can't do the link
```

```
    todo.append(currentlink)
```

```
#Post Processing
```

```
end_done2=linkssheet[linkssheet['id'].isin(end_done)]
```

```
fluxout_each_m=(end_done2.con_out.values*end_done2.Q.values)
```

```
fluxout2_each_m=(end_done2.con2_out.values*end_done2.Q.values)
```

```
fluxout_tot_m=sum(fluxout_each_m)
```

```
fluxout2_tot_m=sum(fluxout2_each_m)
```

```
percentremoved_m=(fluxin_tot_m-fluxout_tot_m)/fluxin_tot_m*100
```

```
percentremoved2_m=(fluxin2_tot_m-fluxout2_tot_m)/fluxin2_tot_m*100
```

```
print(percentremoved_m)
```

```
print(percentremoved2_m)
```

```
#TO EXPORT
```

```
linkscolor=pd.DataFrame(linkssheet.drop(columns="geometry"))
```

```
#linkscolor.to_csv('linkscolor.csv')
```

```
#np.savetxt("end_done_m.csv", end_done, delimiter=",", fmt='%f')
```

```
#np.savetxt("end_done2_m.csv", end_done2, delimiter=",", fmt='%f')
```

Below is code for calculating multiple linear regressions in R

```
 #(2/27/19) DKnights R script. Intended for final MLR (7/29/19).
```

```
#Useful commmnads:
```

```
 #(1) Ctrl+Enter to run current line
```

```

#Packages that were installed. Only need to do this once.
#install.packages("readxl")
#install.packages("ggplot2")

#Next import data
library(readxl)
Delta<-read_excel(file.choose())

Delta$LargeScaleGroup<-as.factor(Delta$LargeScaleGroup)
Delta$SmallScaleGroup<-as.factor(Delta$SmallScaleGroup)
Delta$VegIn<-as.factor(Delta$VegIn)
Delta$VegAmb<-as.factor(Delta$VegAmb)
Delta$SpeciesInDom<-as.factor(Delta$SpeciesInDom)
Delta$Samb_emergent<-as.factor(Delta$Samb_emergent)
Delta$Samb_submerged<-as.factor(Delta$Samb_submerged)
Delta$Samb_floating<-as.factor(Delta$Samb_floating)
Delta$DominantAmbient<-as.factor(Delta$DominantAmbient)

##Multiple Linear Regression. Stare here.

Vfm<-
lm(Vfmm~C0_n+h_av+Silt+OrganicMatter+Elevation+NDVI3+HeightChange+Sand+Cl
ay,data=Delta)
#VegIn+NDVI3+Sand+Silt+HeightChange
library(car)
summary(powerTransform(Vfm,family="bcPower"))
# make sure to read the output from the previous line. Take a look at the screenshot.
Delta$bc<-bcPower(Delta$Vfmm,0)

bcm<-
lm(bc~C0_n+h_av+Silt+OrganicMatter+Elevation+NDVI3+HeightChange+Sand+Clay,
data=Delta)
#no: Temp+DOCamb+FIamb+NDVI3
summary(bcm)
shapiro.test(Delta$bc)

## model selection
library(MASS)
stepwise<-stepAIC(bcm,direction = "backward")

## final model #change name and parameters here
bc_final<-lm(bc~C0_n+NDVI3,data=Delta)
#+Elevation+OrganicMatter+h_av+Clay+NDVI3

```

```

summary(bc_final)
confint(bc_final)

plot(bc_final,which=1)
plot(bc_final,which=2)

plot(predict(bc_final),Delta$bc,
      xlab="predicted",ylab="actual")

attach(Delta)## extra
plot(exp(predict(bc_final)),exp(Delta$bc),
      xlab="model Vf [m/hr]",ylab = "observed Vf [m/hr]",xlim=(c(0, 20)),ylim =
(c(0,20)))
text(exp(predict(bc_final)),exp(Delta$bc), labels=ID, cex= 0.7,pos = 4) ## extra
abline(a=0,b=1)
detach(Delta)## extra

#Ucinitial_bc_final_reduced<-lm(Ucinitial_bc ~ C0 + h + Elevation + VegAmb +
SpeciesInDom + Samb_submerged +
      #DominantAmbient + OrganicMatter + NDVI, data=Delta)
#anova(Ucinitial_bc_final_reduced,Ucinitial_bc_final) #F.test model comparison

cor.test(Delta$Cbackground,Delta$Elevation)

```

ProQuest Number: 28730854

INFORMATION TO ALL USERS

The quality and completeness of this reproduction is dependent on the quality and completeness of the copy made available to ProQuest.



Distributed by ProQuest LLC (2021).

Copyright of the Dissertation is held by the Author unless otherwise noted.

This work may be used in accordance with the terms of the Creative Commons license or other rights statement, as indicated in the copyright statement or in the metadata associated with this work. Unless otherwise specified in the copyright statement or the metadata, all rights are reserved by the copyright holder.

This work is protected against unauthorized copying under Title 17, United States Code and other applicable copyright laws.

Microform Edition where available © ProQuest LLC. No reproduction or digitization of the Microform Edition is authorized without permission of ProQuest LLC.

ProQuest LLC  
789 East Eisenhower Parkway  
P.O. Box 1346  
Ann Arbor, MI 48106 - 1346 USA